

# An Independent Planet Search In The Kepler Dataset

## I. A hundred new candidates and revised KOIs

Aviv Ofir<sup>1,2</sup> and Stefan Dreizler<sup>1</sup>

<sup>1</sup> Institut für Astrophysik, Georg-August-Universität, Friedrich-Hund-Platz 1, 37077 Göttingen, Germany.

<sup>2</sup> e-mail: avivofir@astro.physik.uni-goettingen.de

Received XXX; accepted YYY

### ABSTRACT

**Aims.** We start a project to re-analyze the entire public *Kepler* dataset, searching for planetary transits using a different processing pipeline than the one used by the *Kepler* Mission

**Methods.** The SARS pipeline was tried and tested extensively by processing the entire *CoRoT* mission data. In this first paper of the series we use this pipeline to search for (additional) planetary transits only in a small subset of stars - the *Kepler* Objects of Interest (KOIs), which are already known to include at least one promising planet candidate.

**Results.** Despite the fact that KOIs represent less than 1% of the *Kepler* dataset we are able to significantly update the overall statistics of planetary multiplicity: we find 84 new transit signals on 64 systems on these light curves (LCs) only, nearly doubling the number of transit signals in these systems. 41 of the systems were singly-transiting systems that are now multiply-transiting, significantly reducing the chances of false positive in them. Notable among the new discoveries are KOI 435 as a new 6-candidate systems (where only Kepler-11 was known before), KOI 277 which includes two candidates in a 6:7 period commensurability and with anti-correlated TTVs – all but validating the system, KOIs 719 and 1574 that have small planet candidates ( $1.29R_{\oplus}$  and  $2.05R_{\oplus}$  respectively) in the habitable zone of their host star, and KOI 1843 that exhibits the shortest period (4.25hr) and among the smallest ( $0.68 R_{\oplus}$ ) of all planet candidates. We are also able to completely reject 11 KOIs as eclipsing binaries based on photometry alone, update the ephemeris for five KOIs and otherwise discuss a number of other objects, bringing the total of new signals and revised KOIs in this study to over a hundred. We discuss sub-optimal fitting of multi-transiting systems by the *Kepler* Mission that does not take Kepler's third law into account, causing the error on the  $d/R_*$  parameter to be overestimated by 3.8 (median factor). Interestingly a large fraction, about  $\sim 1/3$ , of the newly detected candidates participate in period commensurabilities.

**Conclusions.** Our results strengthen previous analyzes of the multi-transiting ensemble, and only stress the great importance of this dataset. Nevertheless, we conclude that despite the phenomenal success of the *Kepler* mission, parallel analysis of the data by multiple teams is required to make full use of the data.

**Key words.** methods: data analysis – stars: variables: general – stars: planetary systems – occultations – binaries: eclipsing

### 1. Introduction

The *Kepler* mission goal is to determine the frequency of Earth-like planets around Sun-like stars, and in a wider sense – the distribution of planets of all types around a variety of host stars (Borucki *et al.* 2010 and references therein). *Kepler* had already produced a large number of milestone results (e.g. see introduction of Batalha *et al.* 2012 (hereafter B12) for a complete list), its importance to exoplanet studies is immense now and it is expected to be even larger in the future.

The previous list of over 1200 *Kepler* candidates (Borucki *et al.* 2011b) was severely incomplete. At the time, we were able - with very crude half-manual tools - to identify many more candidates in the then-public dataset, and we had suspected that the candidates list can be significantly enlarged using no additional data. Even citizen scientists that were just using their eyes to look through the huge database were able to find several such missed signals (Fischer *et al.* 2012, Lintott *et al.* 2012). Indeed, the *Kepler* team recently almost doubled the number of candidates using improved detection tools (and only slightly more data) (B12). We therefore tried to check for the completeness of the updated *Kepler* candidate list – and here we report that we are able to find a significant number of very good candidates that were missed by the *Kepler* team.

The *Kepler* pipeline processes the raw pixels transmitted from the spacecraft meticulously to produce the outstanding results achieved so far. This pipeline is progressively perfected, and together with the accumulating data had produced lists of growing length from 705 (Borucki *et al.* 2011a) to 1235 (Borucki *et al.* 2011b) to 2321 (B12) transiting planets candidates. Still, the fact remains that the analysis of the raw data and subsequent transit searches, as it is done by the *Kepler* team is to date almost the only analysis of this data set (The very recent work by Huang *et al.* 2012, hereafter H12, is the only exception – more below). This is in sharp contrast to *Kepler*'s older but smaller sibling, the *CoRoT* space mission, where the calibrated LCs are distributed to a number (up to 10) different teams and each team tries its own tools set to detect the most and best candidate signals, which are then individually approved or rejected in a common discussion. We believe that this latter approach allows more completely surveying the dataset for transiting planets.

In this paper series we apply this approach to the *Kepler* dataset and re-analyze it entirely using our own toolset. So far, very few attempts to do so are known: the Planet Hunters crowd-sourcing search (Fischer *et al.* 2012, Lintott *et al.* 2012) (which did not re-process the data) and the HATNet team (H12) who found four and 16 good periodic signals, respectively, that were not identified by the *Kepler* pipeline in the entire dataset. In this

first paper of the series we use a little-changed *CoRoT*-oriented pipeline to detrend all the data, and we search for additional transit-like signals only on a subset of less than 1% of all the detrended LCs - the *Kepler* KOIs (Kepler Objects of Interest). All KOIs have already at least one promising transit candidate in them, they passed a battery of tests for false positives (Wu *et al.* 2010), and the detection of a reliable second (or third, etc.) signal in the same light curve dramatically reduces the remaining chances of false positives so that nearly all multi-transiting light curves are indeed of planetary origin (Lissauer *et al.* 2012, Fabrycky *et al.* 2012a). Also, the true distribution of single- versus multi- transiting planets systems is, for itself, of interest to the understanding planet formation theory (Figueira *et al.* 2012). Other papers in this paper series are expected present the application of the same analysis to the entire *Kepler* dataset (which is > 100 times larger than just the KOIs) or to highlight particular systems.

The paper is organized in the following way: on §. II we describe our pre-processing and detection pipeline and also discuss the fitting of multi-transiting systems. On §IV we give our new detections, on §. V we discuss other KOIs that are determined to be eclipsing binaries or otherwise revised or noted, and we conclude on §. VI. Appendix A includes the remaining graphical fits of systems with new detected candidates not presented earlier, and Appendix B has additional graphical content related to the other KOIs.

## 2. SARS processing of Kepler light curves

### 2.1. Algorithm

We process the raw Q0-Q6 public *Kepler* photometry using a simple adaptation of the SARS pipeline (Ofir *et al.* 2010) that was designed for *CoRoT* and is almost exactly identical to it. The SARS pipeline was tried and tested extensively by processing the entire *CoRoT* mission data with it, and participation on the detection of transiting exoplanets and brown dwarfs *CoRoT* -12b, -13b, -14b, -15b, -16, -17b, -18b, -19b, -20b, -21b, -22b, -23b, -24 b & c (Gillon *et al.* 2010, Cabrera *et al.* 2010, Tingley *et al.* 2011, Bouchy *et al.* 2011, Ollivier *et al.* 2012, Csizmadia *et al.* 2011, Hébrard *et al.* 2011, Guenther *et al.* 2012, Deleuil *et al.* 2012, Pätzold *et al.* 2012, Moutou *et al.* 2011 and Rouan *et al.* 2012, Alonso *et al.* 2012, respectively]. In short, the SARS pipeline consists of these steps: the removal of all long-term variability with a median filter, the selection of a subset of stars that are intrinsically constant to serve as a "learning set" from which systematic effect (three pairs in this case) are deduced, and the removal of these effects from all stars.

On the differences side, the Kepler version of the SARS pipeline has the ability to account for various discontinuities and anomalies in the data since they are pre-tabulated (such as the monthly Earth-point). This is done by calculating the long-term median filter separately for each continuous section (see also Ofir *et al.* 2012). Also, the very long light curves are naturally divided to single-quarter length, so they are SARS-processed by quarter and channel and no division to smaller blocks is required.

### 2.2. Statistical comparison with PDC

The Pre-search Data Conditioning element of the *Kepler* pipeline was recently updated (Smith *et al.* 2012) and is now called PDC-MAP. This upgrading was the most significant element in the near-doubling in the number of KOIs reported in B12. We compare the SARS results to this data. We note that

the SARS pipeline aims squarely at detecting transiting planets and thus does not attempt to preserve intrinsic stellar variability. Having said that, it is possible to SARS-detrend variable stars by iteratively applying SARS to the residuals of some model or smoothed data, as demonstrated by Ofir *et al.* (2009), but this should probably be done manually for each target.

The process described above is actually not (yet) optimized for *Kepler* and is far from perfect in the simplest sense that it has known bugs. Notably, the after-discontinuity transients are frequently poorly corrected and residuals remain. These are then usually modeled-out by the pipeline simply as the next transits signal, but since this is not a good model residuals sometimes remain and artifact are sometimes injected into the LC. When manifested, this particular bug reduced significantly our ability to detect long period signals. Promising solutions to this and other problems already exist and they will be validated and then incorporated in the future.

Still, we can show that the SARS-based pipeline compares well with the *Kepler* processing. In Ofir *et al.* (2010) the Detection Power metric was defined as a function of standard deviation and the number of data points  $DP = \frac{\sqrt{N}}{\sigma}$  (where  $N$  is the number of surviving data points and  $\sigma$  is measured after long-term variability is removed) so that differently processed light curves of the same object can be compared for signal detectability potential even if the number of the data points in each is different due to different outlier rejection technique. We calculated this metric for each light curve in each quarter of both the PDC-MAP and the SARS LCs after applying identical filtering to both. In figure 1 we plot the distribution of  $\frac{DP_{SARS}}{DP_{PDC}}$ : it is easy to see that for the vast majority of light curves (typically ~ 95% of them) the SARS processed LCs have a higher Detection Power than PDC-MAP processed LCs (we believe, but not yet checked, the rest are mostly variable stars). The median ratio is in the range of 1.06 to 1.09, which may seem underwhelming, but as we pointed out in Ofir *et al.* 2010 - the main difference is not the magnitude of the noise but its color (or lack thereof) (Pont *et al.* 2006), and in Ofir *et al.* (2010) we observed a significant improvement in signal detectability even when both the above performance figures were lower. We note that these results were achieved using three pairs of effect (i.e., six effects) - less than the eight vectors used by the *Kepler* pipeline as cotrending basis vectors, so better results are obtained despite the fact that we use fewer decorrelation vectors.

### 2.3. Candidates detection and selection

Once SARS is done and the detrended LCs are obtained, they are searched for transit-like features using the standard BLS technique (Kovács *et al.* 2002). We note that the very first cut of significant signals is done based on the signal to noise ratio (SNR) of the highest periodogram peak, and not by the SNR of the proposed signal. This is done because we think that at this early stage we should not yet try to characterize the signal, but only to detect periodicity. Therefore, for detection purposes the correct question to ask is not "how significant is the signal (relative to the noise)", but "how significant is the folding at this particular period relative to other periods".

Detected signals (periodogram peak SNR > 20) are first fitted with a trapezoidal model using a 5000 steps Markov Chain Monte Carlo (MCMC) procedure. The result of this quick fit is used to define a good starting point for the slower but more accurate fit using the Mandel & Agol (2002) formalism, again using 5000 MCMC steps. The best fitting linear (i.e., no TTVs) model

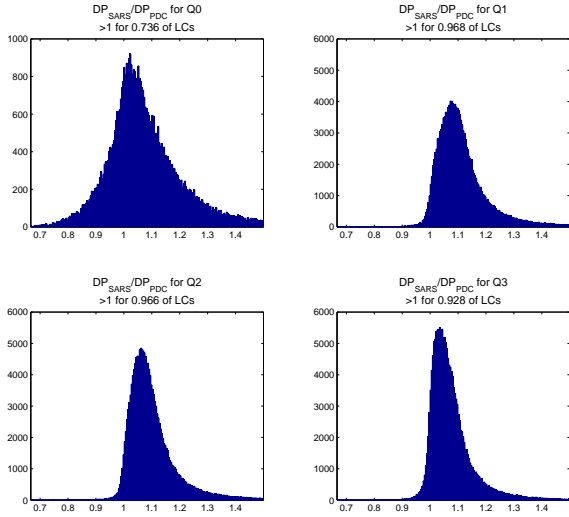


**Fig. 1.** The distribution of the ratio of Detection Power metric (see text for definition)  $\frac{DP_{SARS}}{DP_{PDC}}$  for quarters 0 through 3 (quarters 4,5 and 6 are very similar to Q1 and Q2). The anomalously short Q0 is exceptionally underperforming but there too SARS has higher DP than PDC for  $\sim 3/4$  of the data. For the sake of clarity we present only the range between  $2/3$  and  $1.5$  (representing a performance difference of 50% in each direction).

is then subtracted from the data and a new BLS search is initiated for possible other signal(s) in the data. All detected signals are manually inspected and must pass some standard tests, such as: not being associated with a systematic error, no odd/even difference, generally plausible shape (when the SNR is high enough), transit duration not far longer than the maximal one expected from a central transit of F, G or K dwarfs, individual transits must not be too different (especially if they are in a single quarter), no in-phase centroid motion and that the period is correct (detection of harmonics or sub harmonics). We also add another test used at the *CoRoT* science team<sup>1</sup> to help separate low-amplitude signals from noise that we dub the “half-half test”: a true signal, even if barely detectable using the entire LC, should also produce a visible signature (i.e., a significant local peak in the periodogram) independently on the first half of the data and on the second half. On the other hand, low amplitude “signals” that arise from a single (or a few) ill-corrected systematic effect(s) would very likely not produce such coordinated local peaks in the two halves.

Lastly, once selected the systems undergo more manual processing were we sometimes added manual breaks in obvious discontinuities that are particular to each target. This in turn allows changing the long-term filter from a median filter (which is good at absorbing discontinuities) with a Savitzky Golay (SG) filter. The SG filter has poor discontinuities behavior, but since at this stage these are already known and the filtering is thus done on continuous sections only - we can now enjoy the SG filter’s superior smoothing over the median filter. This also means that all the signals presented below – including some very shallow signals – were observed independently after applying two different filtering techniques, and are thus less likely to be an artifact of imperfect filtering (indeed a few candidate signals not presented below failed this last test). As a final “sanity check” we checked for the presence of some (but not all) of the newly detected

signals in the *Kepler* provided PDC data and nearly all of those checked were indeed found. The very shallowest new signals are probably where the SARS pipeline is absolutely required to extract the signals, and thus these are sometimes not found on the PDC data.

## 2.4. Modeling multi-transiting systems

The final model for each system is computed simultaneously for all detected components: an N-body Keplerian model gives the three-dimensional positions of all targets at the times of the data points. This information feeds a light curve generator based on the Mandel & Agol (2002) formalism, which itself is corrected for *Kepler*’s finite integration time (Kipping 2010). The best-fitting light curve is found using a 50,000-step MCMC chain, which also allows for the determination of all associated errors.

Importantly, the above procedure was born in the context of searching for circumbinary planets (Ofir 2008) and therefore our model assumes *two* central bodies, around which other bodies may revolve. For a low-enough mass ratio  $q = \frac{m_2}{m_1+m_2} \rightarrow 0$  these central bodies can just as well be the host star and the first (eastest) detected planet. At that point fitting the next planet in a circular orbit requires just  $P$  and  $T_{mid}$  - and does *not* require the next-planet’s scaled semi-major axis  $a/R_*$  because this can be deduced from Kepler’s third law  $P^2 \propto a^3$ . Obviously, this assumes that the two (or more) planet candidates orbit the same star, which is a non-trivial assumption given *Kepler*’s large pixels and PSF. However, if this fit succeeds, and if none of the signals shows in-phase centroid motion, then the single-host assumption is more likely than invoking another host star at a special configuration to reproduce all the above. Moreover, since the star-planet separation during transit is no longer a free parameter, the transit duration is completely fixed by the period ratios. This also means that constraints on the orbital eccentricity can be made from photometry alone in multi-transiting systems (Ragozzine & Holman 2010). To be precise, the fitted “ $a/R_*$ ” are actually  $d/R_*$  – the instantaneous scaled distances during transit which may be different from  $a/R_*$  for eccentric orbits. Therefore, the above constraints are degenerate if the candidates have similar eccentricity *and* have similar direction of the argument of periastron vector.

The above approach is in contrast to the fit by *Kepler*’s Data Validation module (Wu *et al.* 2010) where each planet is fitted individually, and therefore each candidate is fitted with its own  $d/R_*$ . These redundant degrees of freedom - one per planet from the second planet onwards - are probably the reason for the *Kepler* pipeline’s larger error estimates on  $d/R_*$ . The B12 errors on  $d/R_*$  are 3.8 times (median value) larger than our own (see Figure 2), despite the fact the B12 also used quarters 7 and 8 for model fitting (i.e., about 30% more data points).

Other than the above subject of fitting multi-transiting systems, we give the following notes on the fitting process and results:

- While the default fit for each planet is circular, cases were no good fit was found have one of their eccentricity parameters ( $e \sin \omega$ ) fitted too. This happened for some of the KOI 719 candidates. The limb darkening parameters were computed for each star based on their KIC  $T_{eff}$  and  $\log(g)$  values from Claret (2000) for the V band, and were not allowed to vary during the MCMC optimization. While these limb darkening coefficients are not very accurate, this is of minor importance since the bulk of the objects are shallow and the fits for them

<sup>1</sup> original idea by Juan Cabrera

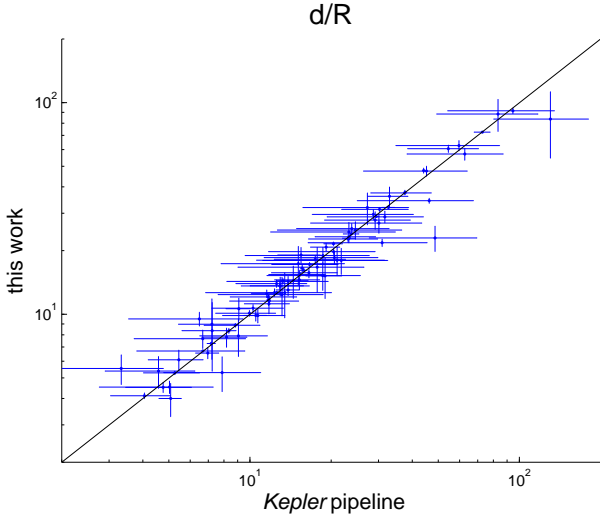


**Fig. 2.** The fitted values of  $d/R_*$  for the sample of KOIs presented here, which are all part of multi-transiting systems by definition. The consistency of the  $d/R_*$  fits between the *Kepler* pipeline and this work is evident over about 2 orders of magnitude, but the associated errorbars on each axis are significantly different – by a factor 3.8 (median value)

are therefore almost insensitive to changes in these parameters.

- The derived radii for the previously known candidates were checked for consistency with the published B12 values. This is also a check that the SARS pipeline does not affect the signals more than the *Kepler* pipeline. As a group, our values are typically slightly lower (7% lower on median) than the B12 radii, however this difference is almost always unimportant (less than  $3\sigma$  for 3/4 of the sample). This small difference is despite the fact that (currently) we do not correct for the changing contamination levels across different quarters. We suspect that this effect can be attributed to the interaction of the long-term filter with the transit signal. In this case it is possible to follow Ofir *et al.* (2009) and effectively nullify this interaction by iterative filtering and fitting.
- On some cases the filtering was imperfect, and as a result the out-of-transit LC directly adjacent to the transit is not at zero flux decrement, but slightly higher. This is actually the same phenomenon from the previous item, and the iterative approach will solve this too.
- The monotransits in our sample were given an initial period of one day longer than the span of the data and a large initial period error ( $\Delta P = 1\text{d}$ ) before the start of the fitting process.

### 3. New candidates in known KOIs

#### 3.1. Overview

In this section we give a case-by-case description of the newly detected signals. The models shown here are not from the serial identification during detection, but from a simultaneous solution of all identified signals (see §2.4). In total we find 84 new transit-like signals. These signals are found in 64 systems, of them 41 were singly-transiting systems that are now multiple. On 48 systems a single new signal was found, 13 systems now have two new signals, two have additional three, and in one system (KOI 435) four new transit signals were identified. Notable specific entries are (details below):

- KOI 435 is a new six-candidate system. The only other system with 6 transiting planets known to date was Kepler-11 (Lissauer *et al.* 2011). KOI 505 is a new five-candidate system, bringing the total to 9.
- The two signals in the KOI 277 system show anti-correlated TTVs, all but confirming these candidates as real planets.
- KOI 1843 has a new extremely small ( $0.68 R_\oplus$ ) and extremely short period (4.25hr) planet candidate.
- In KOI 246 we detected a single transit event that may be compatible with the radial velocity (RV) signature of what the *Kepler* team believed to be a non-transiting planet.
- Two of the new signals in KOI 719 show possible detection of orbital eccentricity from photometric data alone.
- We find an additional transit signal in the light curve of a confirmed planetary system Kepler-27 (KOI 841).

We note that our comments on period commensurability are given when the periods ratio is within 5% of the said value. The objects are ordered by KOI number and the complete list is given in Table 1. Physical sizes for the new candidates, as well as their physical semi-major axes and equilibrium temperatures, were calculated using the B12 technique and assumed values for flux redistribution factor and Bond albedo (i.e.,  $f = 1$  and  $A_b = 0.3$ , respectively) and these are tabulated in Table 2. Notable on this list are:

- 5 candidates have newly detected planets in the Habitable Zone (HZ) ( $273 \leq T_{eq} \leq 373$ ).
- 37 candidates have sizes similar to Earth or smaller ( $r_p \leq 1.25R_\oplus$ )
- Of particular interest are two of the candidates on KOIs 719 and 1574 that are both quite small ( $1.29R_\oplus$  and  $2.05R_\oplus$  respectively) and in the HZ of their host star. To date, The only confirmed planet with measured radius in the HZ of another star was the  $2.4R_\oplus$  Kepler-22b (Borucki *et al.* 2012).

#### 3.2. KOI 179

In this 20.7d single candidate object we find a single transit-like event over 22hr long of with a depth  $\sim 40\%$  larger than 179.01 (see Figure A.1).

#### 3.3. KOI 239

A previously single candidate with a new 3.62d signal that is within a few percents of the 2:3 period commensurability of KOI 239.01. (see Figure A.2).

#### 3.4. KOI 241

A previously single candidate with two new periodic signals (see Figure A.3). Both of the new signals are near period commensurability with KOI 241.01: a 1:4 interior commensurability (to 1.5%) and a 9:4 exterior commensurability (to 0.5%) respectively for the inner and outer new candidates, creating a resonant chain.

#### 3.5. KOI 246

B12 describes this object as having a single transiting planet candidate with a period of about 5.4d. We detected two new signals in this system: a periodic signal with  $P \approx 9.6\text{d}$  and a monotransit

(see Figure 3). Unpublished results<sup>2</sup> indicated that the *Kepler* team had not only detected the same second periodic signal in the extended photometry available to them, but also detected a third planet by its radial velocity signal. The association of this RV signal with the montransit we detect is non-trivial without the RV data, but on the one hand the duration of single transit ( $< 10\text{hr}$ ) is short relative to the a central transit at the minimum period of this planet ( $P > 449\text{d}$ ) and the size of this star - and this implies that the orbit is probably eccentric - as is the RV data of the additional planet. On the other hand, the montransit is significantly shallower than KOI 246.01 while the RV amplitude of the third RV planet is much higher than for KOI 246.01. Therefore, if the montransit and third RV signal come from the same object, its composition is radically different from that of KOI 246.01. This may be similar to what is observed in the KOI 277 system (below).

### 3.6. KOI 260

In this double-transiting system we detect another signal with a period between the two previously detected planet candidates (Figure A.4).

### 3.7. KOI 271

The two previously known planet candidates in this system are in 5:3 period commensurability. We detect a new signal interior to both and within 2% of the 1:2 period commensurability with the closer one, KOI 271.02 (see Figure A.5).

### 3.8. KOI 277 - An exceptionally strong candidate

We detect a second signal interior to the previously known singly-transiting planet candidate with period of 13.85d, i.e. in a 6:7 inner period commensurability with KOI 277.01 (Figure A.6). The planets' periods are so close that they are actually interacting and show anti-correlated TTVs (Figure 4), just like the confirmed systems Kepler-25 through -32 (Steffen *et al.* 2012, Fabrycky *et al.* 2012b).

We then checked that such a system can indeed be long-term stable. For a long-term dynamical stability in two-planet systems the separations of the semimajor axes of the two planets must exceed about 3.5 times the mutual Hill radius for coplanar and circular orbits (Marchal & Bozis 1982). Assuming planetary masses scaling with the planetary radius (see Table 2) according to  $M_p = M_\oplus (R_p/R_\oplus)^{2.06}$  the separation is 4.3 Hill radii and the system is therefore expected to be stable. We checked that using the hybrid symplectic integrator within the *Mercury* package (Chambers 1999), which we have run with a constant time step of 0.1 days, i.e. less than 1% of the orbital period of the inner planet, for over more than  $10^8$  orbital periods. During that time there was no close encounter, i.e. closer than 3 Hill radii.

We also used a *Mercury* run over a shorter time (100 years) at a higher time resolution to estimate the TTV signal. While the period of the TTV modulation is mainly determined by the nearly 6:7 mean motion resonance, the amplitude depend on the planetary masses. From the mass ratio obtained with the scaling relation, the amplitude ratio should be quite different, which is not what is observed. The newly discovered inner planet is therefore suspected to have a significantly higher density than

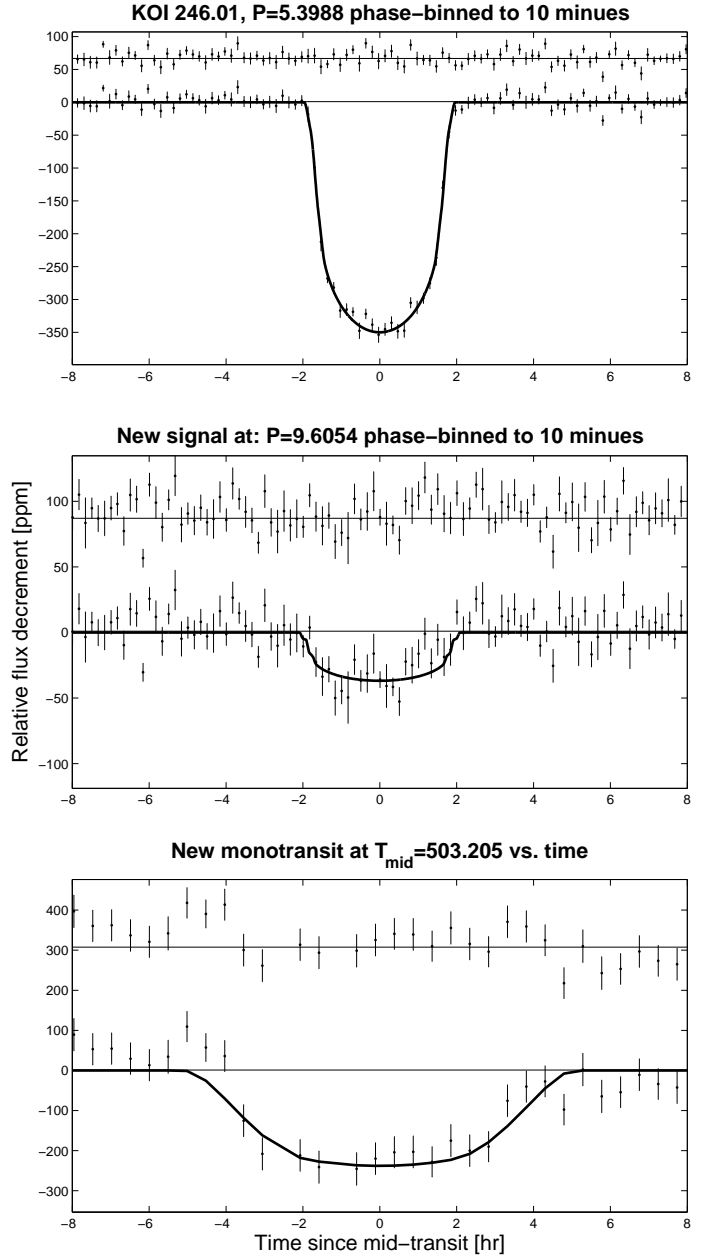


**Fig. 3.** Previously known (designated by their KOI number) and new signals in the KOI 246 LC. Periodic signals are shown binned and phased to the best-fit period, while montransits are given simply as relative flux vs. time. Note that due to the large variety of signals the time spanned by the shown window may be different for different candidates on the same system.

the outer planet. A more detailed investigation of the TTV is possible, but beyond the scope of this paper.

The detection of anti-correlated TTVs in this system in a stable configuration make this system extremely likely to be a bona-fide system with two transiting planets. When one adds our multi-transit fit technique, false positive scenarios become virtually impossible. An all-stellar false positive scenario should include a quadruple system of two EBs that are all very tightly bound and affecting each other. Such a system, in just the right geometrical arrangement, can (maybe) produce the observed transit signals and the anti-correlated TTVs by some momentum exchange. However, such exchanges are accompanied by

<sup>2</sup> Presented at the First Kepler Science Conference (December 2011) by G. Marcy

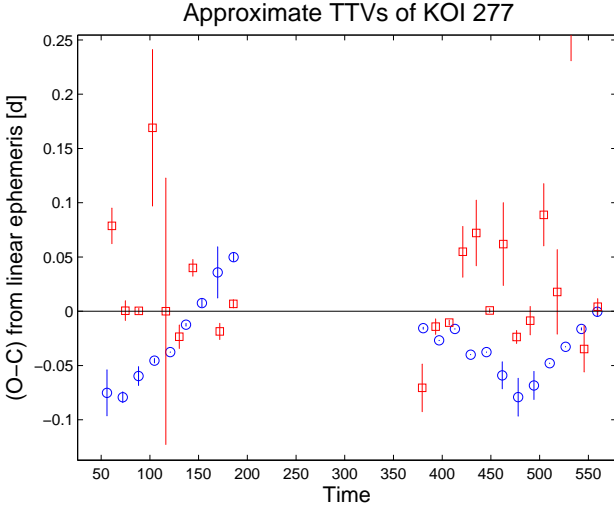


**Fig. 4.** The observed-calculated times of mid transit for KOI 277.01 (blue circles) and the newly detected 13.85d signal (red squares). We note two extremely imprecise (error > 0.1d) timings of the new signal are slightly beyond (above) the shown region. While the anti-correlation of the TTVs is visible, we note that this timing analysis is preliminary (see text).

changes in the system’s eccentricities and relative inclination, which should produce observable changes on the duration and/or depth of the observed transits. Such a detailed calculation is beyond the scope of this paper. We only note that this scenario is easily testable both by detailed LC analysis as above and by relatively low precision RV to detect the motion of the two EBs around each other (they should be quite tightly bound, or they wouldn’t have caused the observed TTVs). Finally, we note that the TTVs calculation is from the serial detection pipeline, not the global N-body Keplerian fit, and therefore it is – strictly speaking – not fully consistent with it, and we label it “preliminary”. Finally, we note that a manual break was added between cadences 23371 and 23372 for this object.

On the very last day of the work on this paper the KOI 277 system, with its two planets, was published by the Kepler team as confirmed and with the Kepler-36 name (Carter *et al.* 2012). Our analysis is thus an independent discovery and confirmation of this system.

### 3.9. KOI 285

We detect a second signal in this system with a period just lower of the outer 1:2 period commensurability with KOI 285.01 (see Fig. A.7). We also detected a third signal with a period of 49.3d. A manual break was added on cadence number 14601 for this object.

### 3.10. KOI 289

We detect an extremely shallow (27ppm) but significant second signal with a period of 1.47d (see Figure A.8).

### 3.11. KOI 295

A second, 10.1d signal is detected in this previously singly-transiting 5.3d system (Figure A.9). A manual break was added between cadences 17496 and 17497 for this object.

### 3.12. KOI 316

This was a double-transiting system with periods of 15.77d and 157.06d, i.e. - within 5% of the 1:10 period commensurability. We detect a new signal interior to these two (Figure A.10) with a period of 7.3d.

### 3.13. KOI 321

We detect a second planet outside this previously single-transiting system (Figure A.11). The new planet has a radius of only 60% of the first one, which itself is all but a confirmed planet as it was already RV followed-up by the *Kepler* team<sup>2</sup>nd its RV signal measured - making the second candidate all but validated without any additional measurement.

### 3.14. KOI 330

We detect a second planet candidate interior to the previously singly-transiting candidate (Figure A.12).

### 3.15. KOI 339

Two planet candidates with near-identical transit depths were known in this system, and we detect a third signal with slightly shallower transit and a longer (35.86d) period (Figure A.13).

### 3.16. KOI 408

We add a fourth candidate interior to the existing three (Figure A.14).

### 3.17. KOI 435

This system was known to contain a single periodic signal with  $P_1 \approx 20.55$ d and a depth of about 1500ppm. The published candidates table (B12) also included a second signal - KOI 435.02 - a monotransit with a depth of > 8000ppm that should have been quite easy to spot, but unfortunately the time of mid transit is  $T_{mid,2} = 2455490.27$  which is about a month after the end of the publicly available data. We therefore cannot model this candidate. On top of these two signals, we find four additional signals with periods of 3.93d, 33.04d, 66.30 and 9.92d (Figure 5). This is only the second six (candidate) transiting planets system, the first being the Kepler-11 system (Lissauer *et al.* 2011). We note that the 33.04d signal is within 0.5% of the 8:5 outer period commensurability with KOI 435.01. Manual breaks were added in cadences 22442 and 23990 for this object.

### 3.18. KOI 505

In this double-transiting (13.76d and 6.19d) system we detect three more signals with period of: 3.25d, 87.09d and 8.34d, where the latter is within 1% of the 3:4 period commensurability with KOI 505.02 (see Figure A.15). We note that the 8.34d signal was independently found by HATNet (H12). A manual break was added between cadences 6712 and 6718 for this object.

<sup>2</sup> a

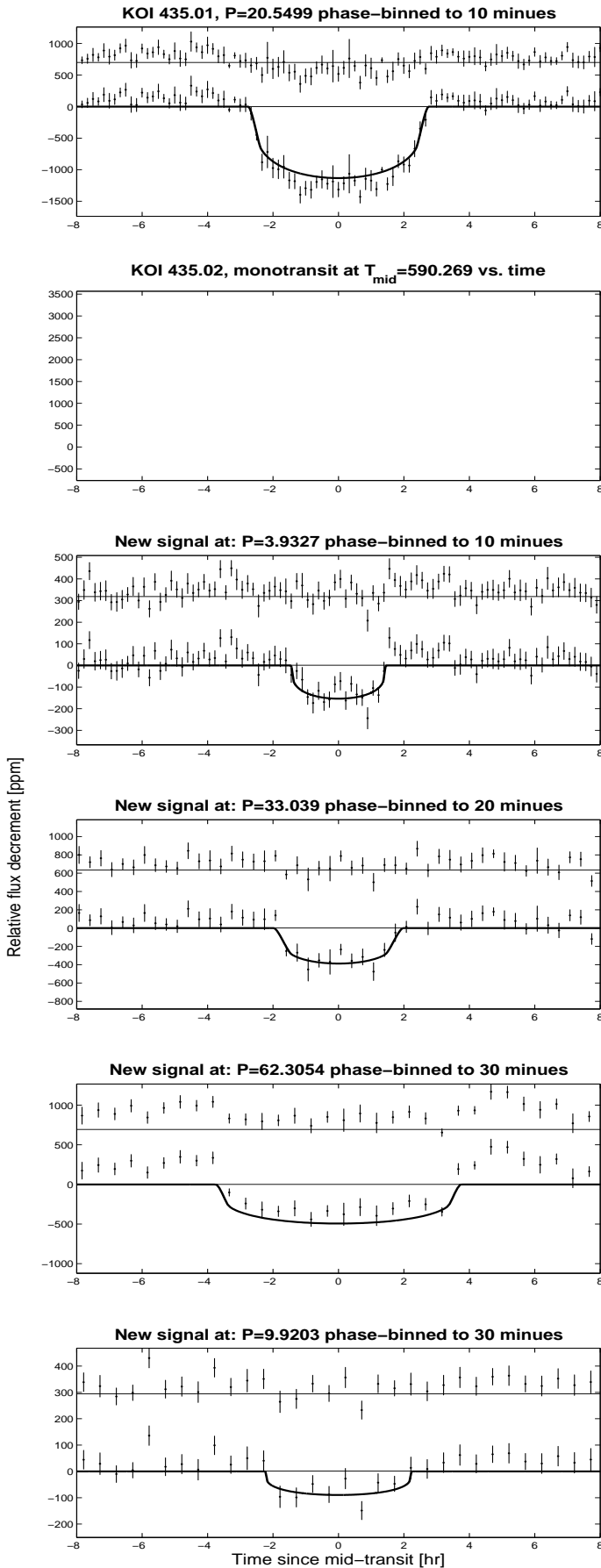


**Fig. 5.** Similar to Figure 3. Note the panel of KOI 435.02 is intentionally empty (see text).

### 3.19. KOI 509

We detect a third signal in this previously double-transiting system with a period of 39.59d, or within 1.5% of the 7:2 period commensurability with KOI 509.02 (Figure A.16).

### 3.20. KOI 510

We detect a fourth signal in this previously triple-transiting system with a period of 35.12d, or within 4% of the 5:2 period commensurability with KOI 509.03 (Figure A.17).

### 3.21. KOI 564

A planet candidate interior to the previously known two is detected with a period of 6.21d (see Figure A.18). The larger-than-usual error bars on KOI 564.02 were caused by a particularly unfortunate timing of one of the three events shortly after a discontinuity in the data that affected the filtering.

### 3.22. KOI 582

We detect a 9.94d signal in this system, in addition to the previously known 5.94d and 17.74d signals. The new planet candidate appears to be in a double period commensurability: within 0.4% of the 5:3 ratio exterior to KOI 582.01, and within 2% of the 4:7 ratio interior to KOI 582.02 (see Figure A.19).

### 3.23. KOI 584

This shallow candidate (detected to  $9.8\sigma$ ) lies interior to the two previously known planet candidates in this system (Figure A.20). An even shallower transit-like signal about half as deep as the first one was detected at phase 0.59 of the new 6.47d signal. This possible secondary eclipse is very close to the noise level – if not below it – and thus its very detection is much less robust. Still, we wish to point out that the proposed signal will need to be checked for binarity when more data becomes available. A manual break was added on cadence number 1386 for this object.

### 3.24. KOI 593

We detect the third planet candidate in this system with a period of 51.06d, between the two previously known candidates (Figure A.21).

### 3.25. KOI 597

We detect the third planet candidate in this system within 2% of the 3:1 period commensurability with KOI 597.02 (Figure A.22). Manual breaks were added on cadence numbers 1173, 1796 for this object.

### 3.26. KOI 623

We detect the fourth and outermost candidate in this very compact system (see Figure A.23).

### 3.27. KOI 624

We detected a candidate in a short period of 1.31d (Figure A.24) in addition to the previously known KOIs 624.01 and 624.02.

### 3.28. KOI 627

We detect the second candidate in this previously single-candidate system (Figure A.25).

### 3.29. KOI 671

We detect two additional planet candidates, both in between the two previously known planet candidates. The resulting compact system (4 planet candidates within  $P \approx 16d$ ) appears to be in a resonant chain of 4:7, 2:3 and 2:3 (from the inside out) period commensurabilities.

### 3.30. KOI 710

We detect a shallow signal ( $8.8\sigma$ ) in this previously singly-transiting system (Figure A.27).

### 3.31. KOI 717

A very short period planet candidate ( $P=0.9d$ ) is detected in this previously singly transiting system (Figure A.28).

### 3.32. KOI 719

This system experienced a dramatic transformation from our re-analysis of the KOIs. We detect no less than three additional signals in this previously singly-transiting system with periods of 4.16d, 45.09d, and 28.12d (see Figure A.29). The last two signals appear to be longer than can be explained by a circular orbit. This can be either because these three planets orbit another star in the *Kepler* aperture or because the orbits are not circular. Since none of the signals show in-phase centroid motion, which severely limits the possible configurations of any contaminating star, we opt to test the eccentricity scenario, and so the  $e \sin \omega$  parameter was allowed to float for these two signals (Barnes 2007). The resultant  $e \sin \omega$  values have large uncertainties but they are significantly non zero (see Figure 6):  $0.45 < e \sin \omega < 0.8$  for the 45d signal, and  $0.3 < e \sin \omega < 0.75$  for the 28d signal. Interestingly, within the large error bars the planets seem to be synchronized in their  $e \sin \omega$  factor. Moreover, the 45d planet candidate has very interesting physical parameters: at  $1.29R_{\oplus}$  and  $T_{eq} = 354K$  this is one of the most Earth-like exoplanet candidates known – both in size and in being inside the habitable zone.

### 3.33. KOI 780

We detect a second transit-like signal in the data that is very short: it lasts on the order of  $0.5hr$  despite the relatively long period of 7.24d (see Figure A.30).

### 3.34. KOI 841 = Kepler-27

In this confirmed system of planets (Steffen *et al.* 2012) we detect, on top of the previously known KOI 841.01 ( $P=15.3d$ ) and KOI 841.02 ( $P=31.3d$ ) another signal with a period of 6.55d (Figure A.31). This is most likely a third planet in the system.

### 3.35. KOI 856

We detect a shallow second marginal signal to  $6.86\sigma$ . This significance level is lower than the  $7.1\sigma$  threshold used by the

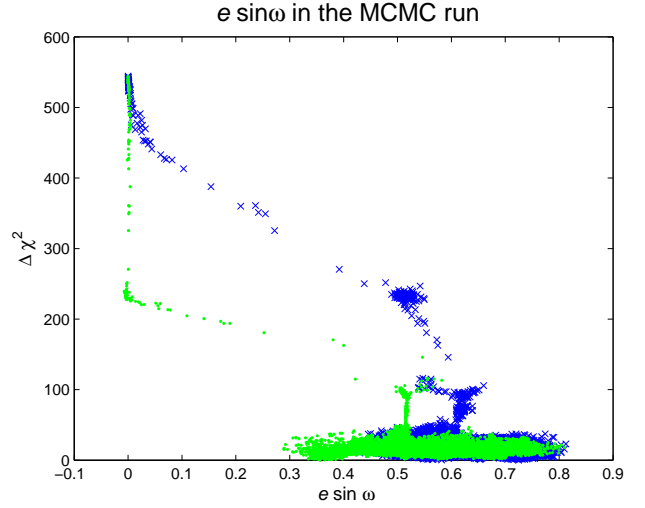


**Fig. 6.** The steps of the  $e \sin \omega$  parameters during the MCMC run for KOI 719 (blue squares for the 45d signal, green dots for the 28d signal). The final values have large errors but they are clearly nonzero.

*Kepler* team, but we chose to point it out as it looks quite problems-free, despite the low formal error. Note the previously known candidate KOI 856.01 is also noted in §4.

### 3.36. KOI 1060

We detect a fourth signal in the system, exterior to the known three (Figure A.33).

### 3.37. KOI 1069

The additional  $P=8.70d$  signal we detected in this previously singly-transiting system is very strong, with depth  $> 3.5$  times the depth of KOI 1069.01 (Figure A.34). We check that this signal appears neither in the detected binaries nor in the list of false positives. This strong signal, together with the candidates detected by the Planet Hunters project, showcase why parallel analyses of the same data are absolutely required.

### 3.38. KOI 1082

We detect two candidate planets in addition to the previously known candidate. The two are both interior and smaller than KOI 1082.01 (Figure A.35).

### 3.39. KOI 1108

We detect two candidate planets with period of 1.47d and 4.15d in addition to the previously known single candidate (Figure A.36). The 4.15d signal is about 1% from 9:2 period commensurability with KOI 1108.01.

### 3.40. KOI 1413

We detect (Figure A.37) a second signal in the system, marginally deeper than KOI 1413.01, and with a period about twice as long.

**3.41. KOI 1536**

This system is known to contain a 3.74d transit candidate and we detect a second signal about twice as deep and with a period of about 79.48d (see Figure A.38).

**3.42. KOI 1574**

This is a particularly long-periods system: on top of the known periodic signal at  $P=114.7d$ , we detect two separate events separated by 191.5d. The pattern of data points seemed, to the eye, different enough to believe that these are two separate monotransits (and one of these signals was also identified by H12). However, when the signals were modeled in detail it turned out that they are statistically identical, so the suggested model now includes a second periodic signal (Figure A.39) in an outer 5:3 period commensurability with 1574.01 to better than 0.2%. The new planet candidate has a radius of just over 2 Earth radii and an equilibrium temperature within the habitable zone of  $T_{eq} = 281K$  - making it one of the most Earth like planet candidates known.

**3.43. KOI 1593**

We detect an additional transit signal outside the known 1593.01 with a period of 15.38d (Figure A.40).

**3.44. KOI 1599**

We detect a second transit candidate interior to KOI 1599.01 with a period of 13.61d, or within 0.01% of the 2:3 resonance with KOI 1599.01 (Figure A.41).

**3.45. KOI 1601**

We detect the second planet candidate in this previously singly-transiting system. The new signal is about 1% off the 1:6 period commensurabilities with KOI 1601.01 (see Figure A.42).

**3.46. KOI 1650**

We detect only two events of a second signal suggesting a period of 100.8d in this previously single-candidate system (see Figure A.43).

**3.47. KOI 1681**

This system was known to contain a planet candidate with a period of 6.94d. We detect two new transit signals with periods of 1.99d and 3.53d (Figure A.44) – the latter is with 2% of the 1:2 period commensurabilities with KOI 1681.01.

**3.48. KOI 1830**

We detect a deep, long-period (198.7d) transit signal as the second signal in this system (see Figure A.45).

**3.49. KOI 1831**

we detect an additional planet candidate in an orbit significantly interior to the previously known two (see Figure A.46).

**3.50. KOI 1843**

This system was known to host two planet candidates with periods of 4.19d and 6.36d. We detect an additional and extreme transit signal with a period of 0.176d (4.25hr) and depth of 120ppm (Figure 7). Interestingly, the short period couples with the long *Kepler* cadence duration to create a seemingly unphysical duty cycle of  $> 22\%$ . Importantly, the host star is relatively cool and small with  $T_{eff} = 3673K$  and radius of  $0.52 R_{\odot}$  (KIC values). We plan to analyze this system in detail and attempt to fully validate it in a future paper, but this tantalizing signal implies that the newly detected signal is from a planet the with the shortest known period, shorter even than post common envelope planets (Charpinet *et al.* 2011) and with a radius of  $0.68 R_{\oplus}$  – among the smallest exoplanets known.

**3.51. KOI 1870**

We detect a 0.5% deep monotransit about 12hr long with no associated centroid motion in addition to the known 7.96d KOI 1870.01 (Figure A.47).

**3.52. KOI 1871**

We detect a periodic signal with a period of 32.38d in addition to the previously known KOI 1871.01 (Figure A.48).

**3.53. KOI 1875**

We detect a very short period (0.54d) signal in addition to the  $P=9.92d$  previously known KOI 1875.01.

**3.54. KOI 1955**

We detect two new signals in this previously double transiting system. One is significantly shallower and with significantly shorter period ( $P=1.64d$ ) than the known KOI 1955.01 and 1955.02. The second newly detected signal has a period of 26.23d - a 2:3 period commensurability with KOI 1955.02 to less than 0.5% (Figure A.50).

**3.55. KOI 1972**

We detect a second signal in this previously singly transiting system with a period of 1.23d (see Figure A.51).

**3.56. KOI 1986**

A second signal is detected in this previously singly transiting system with a period of 7.13d (see Figure A.52). We note that the local peak in the "half-half" test on the first half of the data exists, but very small.

**3.57. KOI 2004**

A second signal is detected in this previously singly transiting system with a period of 3.19d (see Figure A.53).

**3.58. KOI 2055**

We detect two more signals in this system with periods of 4.03d and 2.50d, or within 0.5% of the 8:5 period commensurability between them (Figure A.54), on top of the existing 2055.01.

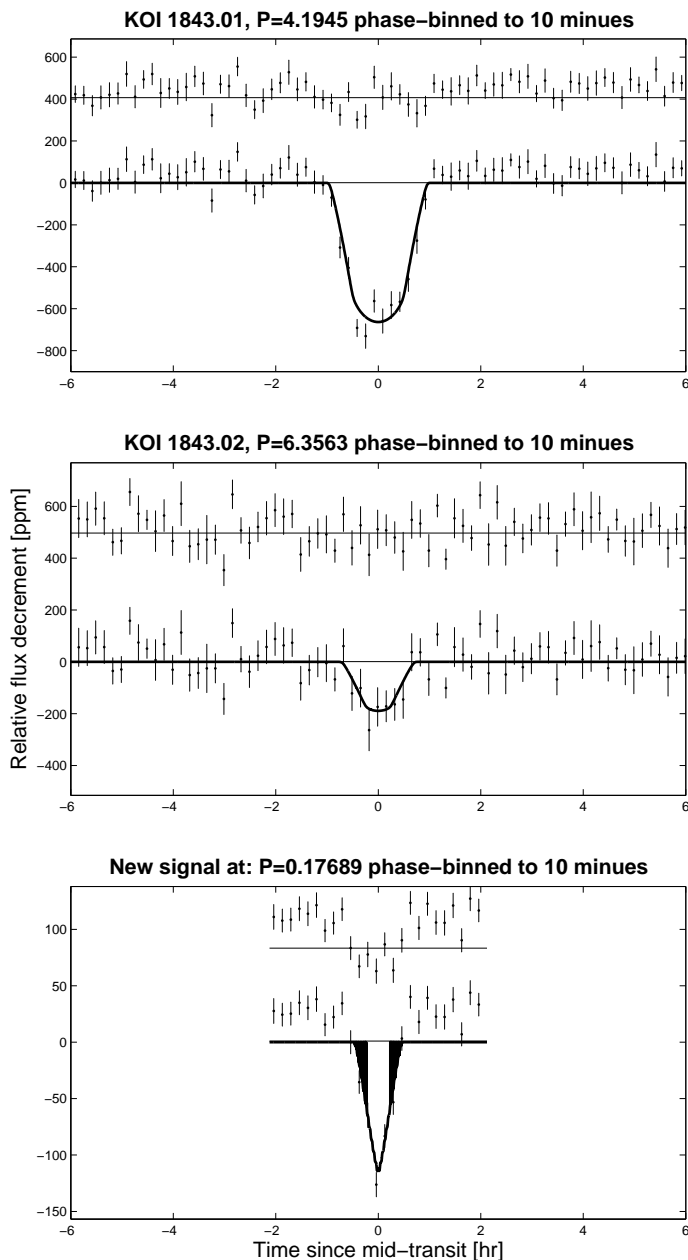


**Fig. 7.** Similar to Figure 3. Note that the large duty cycle of the new signal ( $> 22\%$ ) caused the mean of the LC to be actually different significantly from the mean of the out-of-transit points, despite the filtering of the data. Also, the triangle, or thick line, near ingress/egress is the model line fluctuating between the correct value and zero due to numerical problems. These effects will be taken into account on the planned future detailed study of this exceptional object.

### 3.59. KOI 2159

A second signal is detected with a period of 2.39d (Figure A.55).

### 3.60. KOI 2193

We detect a second signal outside of this previously singly transiting system with a period of 4.16d (see Figure A.56). The two signals are within 1% of the 7:4 period commensurability.

### 3.61. KOI 2195

We detect two signals with periods on both sides of the previously known KOI 2195.01: an inner  $P=6.85$ d within 3% of the 1:3 period commensurability with 2195.01, and an outer candidate with  $P=30.0922$  - or within 0.3% of the 3:2 period commensurability with 2195.01 (see Figure A.57) - creating a resonant chain.

### 3.62. KOI 2243

We detect a second signal with a period of 8.46d in this previously singly transiting system (Figure A.58).

### 3.63. KOI 2485

We detect two planet candidate with periods of 3.60d and 5.73d, or about 0.5% of the 5:8 period commensurability, in addition to the known 9.99d KOI 2485.01 (Figure A.59).

### 3.64. KOI 2579

We detect two planet candidate outside the known KOI 2579.01. The first has a period of 3.60d, or about 1% off the 3:4 period commensurability with KOI 2579.01. The second has a period of 10.30d (Figure A.60).

### 3.65. KOI 2597

We detect an additional planet candidate, interior to the previously known two, with a period of 5.61d (Figure A.61).

## 4. Notes about other KOIs

### 4.1. Overview

In this section we comment on a few of the other KOIs. Notably, we:

- Reject 11 KOIs as EBs based on close inspection of the LC.
- Correct the published ephemeris of for five KOIs.
- Suggest another interpretation to KOI 1401 as cause by stellar pulsations.
- Detect the secondary eclipse of KOIs 805, 1468 and identify it as consistent with a planetary secondary eclipse in an eccentric orbit.
- Confirm the second transit signal identified by Nesvorný *et al.* (2012) in the KOI 872 system.

### 4.2. KOI 225.01

We change the interpretation of KOI 225.01 from a planet candidate to an EB with double the period of KOI 225.01 since we detect significant differences between the odd and even events in this system (see Figure 8).

### 4.3. KOI 341.01

The true period of this candidate is half of the published period, i.e.  $P_{341.01} = 7.1706171$ d.

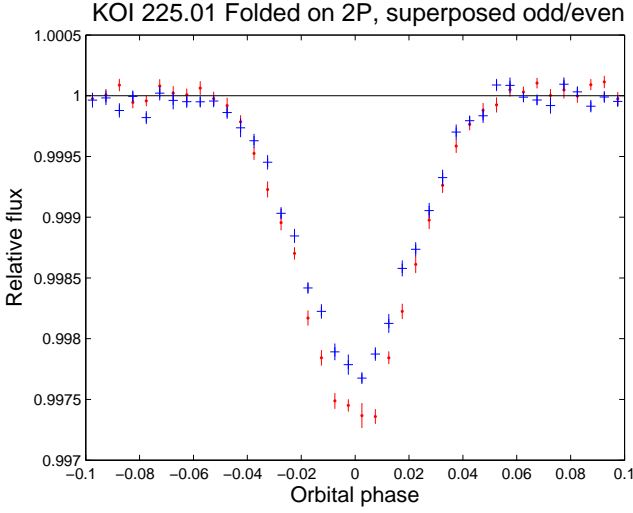


**Fig. 8.** Phase folded odd (red dots) and even (blue '+' signs) eclipsed of KOI 225.01 showing significant difference indicative of an EB with similar but not identical components.

#### 4.4. KOI 536.01

The true period of this candidate is half of the published period, i.e.  $P_{536.01} = 81.1697006d$ .

#### 4.5. KOI 741.01

This object has extremely deep eclipses ( $\sim 4\%$  deep) causing our processing pipeline, which is built to handle low-amplitude signals, to reject some of the in-transit points. Still we were able to detect a secondary signal with a depth of  $\sim 1000$  ppm to KOI 741.01, far larger than the  $(\frac{R_p}{R_*} \frac{R_s}{a})^2 \sim 40$  ppm maximal expected signal for a planetary secondary eclipse (assuming  $d/R_* = a/R_*$ , or circular orbit, and geometrical albedo of 1) showing that this object is an eccentric EB. Figure 9 shows *Kepler's* PDC LC since it clearly exhibits both the primary and secondary eclipses.

#### 4.6. KOI 743.01

This object has deep eclipses ( $\sim 1\%$  deep), but we were able to detect also a secondary eclipse to KOI 743.01 with a depth of  $\sim 1000$  ppm, far larger than the  $\sim 130$  ppm expected (calculated similarly to KOI 741.01) for a planetary secondary eclipse, showing that this object is an eccentric EB (see Figure B.1).

#### 4.7. KOI 805.01

This object has transit-like signals ( $\sim 1.6\%$  deep), but we were able to detect also a secondary eclipse near phase 0.6 to KOI 805.01 with a depth of  $\sim 140$  ppm (see Figure 10). The expected depth for a planetary secondary eclipse (calculated similarly to KOI 741.01) is  $141 \pm 5$  ppm. This means that the observed signal is consistent with a secondary eclipse of KOI 805.01 as an eccentric planet with a very high geometric albedo.

#### 4.8. KOI 856.01

This candidate shows  $> 1.3\%$  deep transit-like signals. We detect small but apparent in-phase centroid motion in the +X and +Y directions (Figure 11), the interpretation of which should be

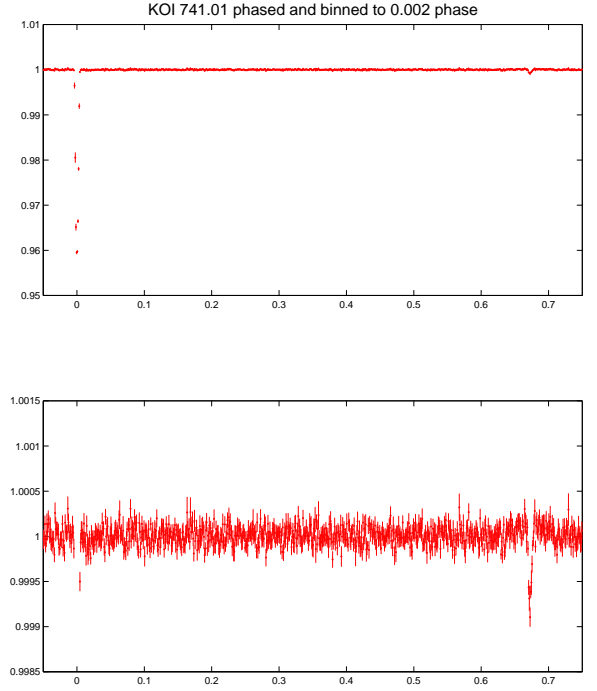


**Fig. 9.** Phase folded and binned *Kepler's* PDC LC of KOI 741.01. Top: showing the 741.01 signal at phase 0. Bottom: expanded scale of the same data, showing a secondary eclipse near phase 0.672.

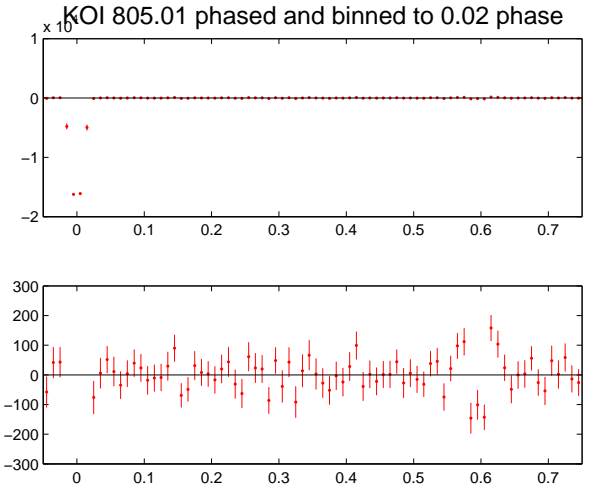


**Fig. 10.** Phase folded and binned LC of KOI 805.01 showing the secondary eclipse of this object, with depth that is consistent with a planetary interpretation of the transit signal.

done in a detailed analysis of the local stellar neighbors of KOI 856.

#### 4.9. KOI 872

A second transit signal was detected by Nesvorný *et al.* (2012). We confirm this detection, and note that we can do so only in

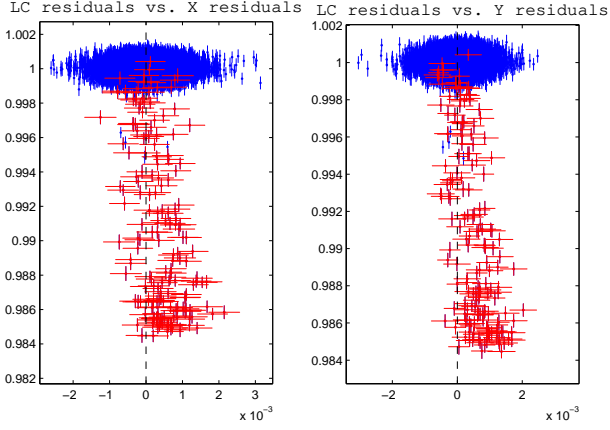


**Fig. 11.** The residuals of the LC model plotted vs. the residuals of the centroid of KOI 856.01, which were filtered in a similar way (i.e. - segmented smooth). In-transit points (red) are given with full error bars, and the other points (blue) are given with partial error bars for clarity

retrospect: for some yet unidentified reason the candidate was not promoted further in our pipeline.

#### 4.10. KOI 1003.01

This object has deep eclipses ( $\sim 1.9\%$  deep), but we were able to detect also a secondary eclipse to KOI 1003.01 with a depth of  $\sim 900$  ppm, much larger than the  $\sim 230$  ppm expected (calculated similarly to KOI 741.01) for a planetary secondary eclipse, showing that this object is an eccentric EB (see Figure B.1).

#### 4.11. KOI 1101.01

The true period of this candidate is four times the published period, i.e.  $P_{1101.01} = 11.390958d$ .

#### 4.12. KOI 1151.01

The true period of this candidate is twice the published period, i.e.  $P_{1151.01} = 10.4356212d$ .

#### 4.13. KOI 1152.01

This object has extremely deep eclipses ( $\sim 8.2\%$  deep), but we were able to detect also a secondary eclipse near phase 0.338 to KOI 1152.01 with a depth of  $\sim 6000$  ppm, far larger than the  $\sim 55$  ppm expected (calculated similarly to KOI 741.01) for a planetary secondary eclipse, showing that this object is an eccentric EB (see Figure B.3).

#### 4.14. KOI 1385.01

This object exhibits V-shaped eclipses about 5% deep. Fitting the data reveals a system with  $b = 0.9 \pm 0.005$  but  $R_2/R_1 = 0.2972 \pm 0.0034$ , i.e. - a grazing eclipse (The published *Kepler* fit is even 'worse' with  $b > 1$  directly). Such deep eclipses, and V-shaped suggesting significantly larger secondary radius, coupled with the KIC estimates for the properties of host ( $R_* = 0.84R_\odot$ ,  $T_{eff} = 5848K$ ,  $\log(g)=4.55$ ) leave little doubt that the secondary cannot

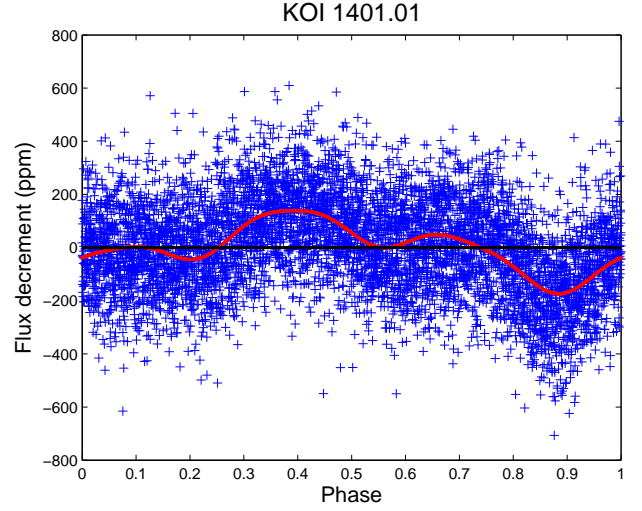


**Fig. 12.** KOI 1401.01 phased to the B12 orbital period. A transit-like feature appears near phase 0.88, and a similar-amplitude “hump” can be seen half a period offset from it. A two-sine fit with  $P_{1401.01}$  and  $P_{1401.01}/3$  is over plotted (solid red line).

be a planet, but is likely to be an EB on an eccentric and inclined orbit (due to the absence of a secondary eclipse).

#### 4.15. KOI 1401.01, KIC 9030447

This candidate appears on the B12 catalogue and so it was analyzed for this paper, but later we saw that it also appears on the list of *Kepler* eclipsing binaries (Slawson *et al.* 2011). Stellar variability in this star is dominated by pulsations at the KOI 1401.01 period and its second harmonic (i.e.  $P_1 = 0.56672d$  and  $P_2 = P_1/3$ ) that together create a transit-like signal, but also a “hump” about half a period later – which should not happen if the transit-like signal is from either planetary object or an EB. Practically all variability is explained by this two-periods pulsation model (see Figure 12). We therefore believe that KOI 1401.01 is caused by pulsations, rather than transits or eclipses.

#### 4.16. KOI 1419.01

We change the interpretation of KOI 1419.01 from a planet candidate to an EB with double the period of KOI 1419.01 since we detect significant differences between the odd and even events in this system (see Figure B.4). Note a manual break was added on cadence number 11108 for this object.

#### 4.17. KOI 1459.01

This object exhibits strong sine-like background variability that is almost, but not exactly, in-phase with the transit-like signal. We iteratively computed the power spectrum for the next-strongest frequency and then simultaneously fitted sines with all the previously found frequencies to the data with  $3\sigma$  iterative outlier rejection. It took only a single period of  $P_1 = 0.691758d$  and its near sub harmonic at  $P_2 = 1.38248d$  to all but remove the background and produce Figure 13, showing that this is an EB with twice the orbital period as suggested by B12.

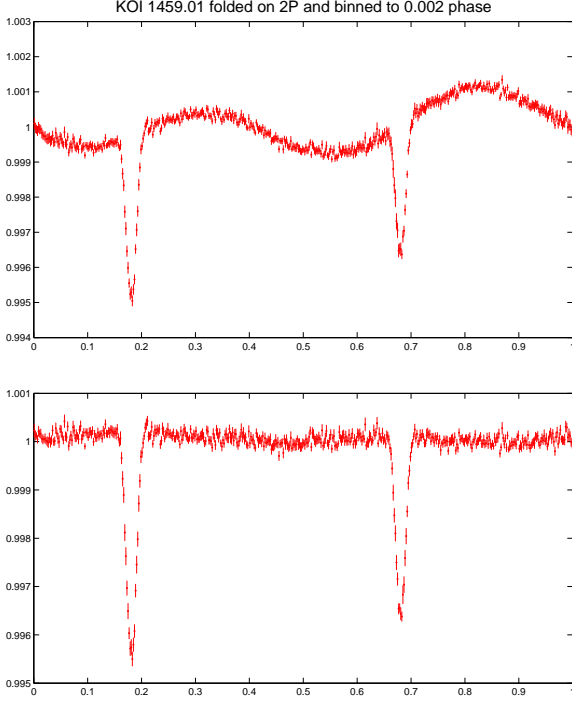


**Fig. 13.** The double-period phase folded LC of KOI 1459 before (top) and after (bottom) background subtraction.

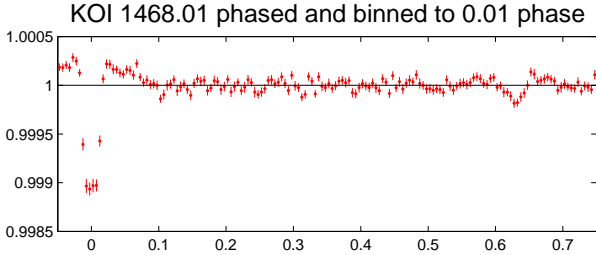


**Fig. 14.** Phase folded and binned LC of KOI 1468.01 showing the secondary eclipse of this object, with depth that is consistent with a planetary interpretation of the transit signal.

#### 4.18. KOI 1468.01

This object has transit-like signals ( $\sim 1000$  ppm deep), but we were able to detect also a secondary eclipse near phase 0.63 to KOI 1468.01 with a depth of  $\sim 18$  ppm (see Figure 14). The expected depth for a planetary secondary eclipse (calculated similarly to KOI 741.01) has fairly wide range: mostly in the 6 – 12 ppm range with  $\sim 20\%$  chance of being higher, even as high as 40 ppm. This means that the observed signal is consistent with a secondary eclipse of KOI 1468.01 as an eccentric planet with a high geometric albedo.

#### 4.19. KOI 1540.01

The long duration of this candidate signal caused us to look deeper into this candidate. The background variability is difficult to remove and requires some fine-tuning. We managed to achieve good filtering by using a Savitzky Golay filter with a  $3^{rd}$  degree polynomial and 1 day long window size with  $4\sigma$  itera-

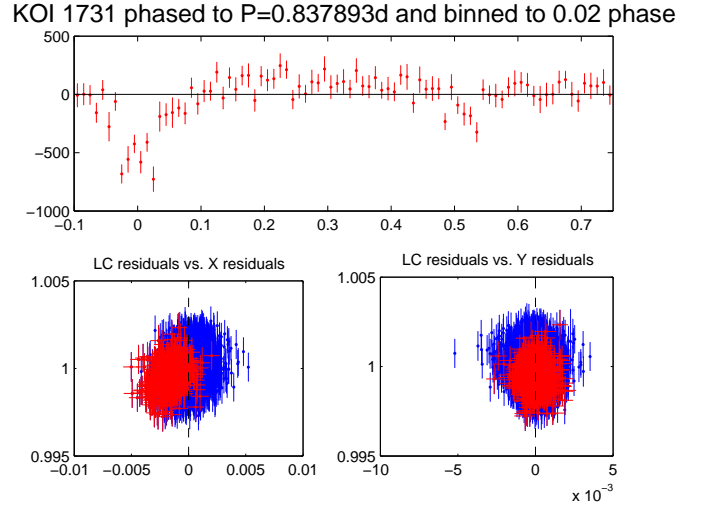


**Fig. 15.** top: phase-folded to  $P_2 \sim 0.84$ d and heavily binned to 0.02 phase LC of KOI 1731. Bottom: centroid motion of KOI 1731 in phase with  $P_2$ , similar to Figure 11.

tive rejection - applied for each continuous section separately. Once well filtered, the odd and even transit events were clearly different (Figure B.5), making this an EB at twice the published period for KOI 1540.01.

#### 4.20. KOI 1731.01

This object was observed on quarters 3 and 4 only, and the contamination levels rose by a factor of 3 (from  $\sim 8\%$  to  $\sim 24\%$ ) between the two data sets. We note that on top of the published  $\sim 2.6$ d transit-like signal we detect a second periodic transit-like signal with a period of  $P_2 = 0.837894$ d and of 500 ppm. This second signal, show very marginal secondary eclipse, slight out-of-transit variations and in-phase centroid motion (See Figure 15), where the level of the latter is unchanged between the two quarters. We conclude that there is a contaminating EB in the KOI 1731 aperture with short projected distance from the main target.

#### 4.21. KOI 2188.01

The true period of this candidate is  $2/5$  of the published period, i.e.  $P_{2188.01} = 2.69615$ d. When phased to this new period (see Figure 16) the transit signal seems somewhat deeper than the B12 value of 157 ppm and a possible secondary eclipse is also marginally detected.

#### 4.22. KOI 2269.01

We change the interpretation of KOI 2269.01 from a planet candidate to an EB with double the period of KOI 2269.01 since we detect significant differences between the odd and even events in this system (Figure B.6).

#### 4.23. KOI 2272.01

This object has a scaled semi major axis  $a/R_*$  that is consistent with the minimal value of  $a=1$ . On top of that, the transit duration is too long: it is somewhat too long for a central transit of a  $2.34R_\odot$  star (the KIC value for KOI 2272), and definitely

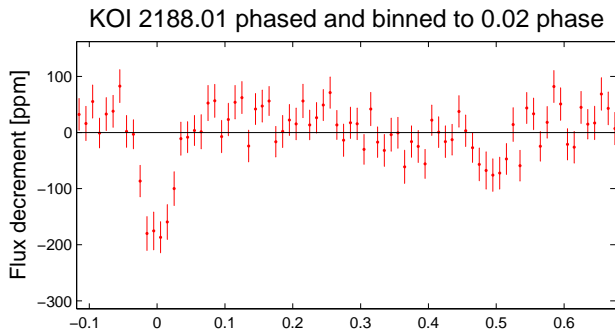


**Fig. 16.** Phase folded to  $2/5$  of the published period of KOI 2188.01, heavily binned to 0.02 phase.

too long for a high impact parameter transit such as this case ( $b$  is nonzero with  $> 4\sigma$  significance). The sum of these is that, as far as we can tell from the data, the secondary object in this system is all but touching the host’s surface, and it is not small relatively to the primary (causing the long transit signal). We conclude that it is more likely to be a contact binary in low inclination orbit, with possibly some dilution, than a transiting planet.

## 5. Discussion

In this paper we presented the discovery of 84 transit signals found only on a subset of less than 1% of the *Kepler* dataset - the Kepler Objects of Interest (KOIs). These signals were not detected by the *Kepler*’s processing pipeline in the publicly available Q0-Q6 data. We were able to achieve that with a pipeline that is optimized for *CoRoT*, and not for *Kepler*, and almost unchanged from it. Still, the very basic fact that this pipeline is simply different from the one used by *Kepler* team means that its sensitivities and biases are also different. Furthermore, we showed evidence that for the specific goal of transit searches the SARS pipeline may even be superior to *Kepler*’s PDC-MAP - helping to understand the significant number of new detections in such a small subsample of light curves. It is interesting to note that on previously known multi-transiting systems often the *order* in which signals are detected was different in the SARS pipeline relative to the published order - this is a hallmark of the different sensitivities of each pipeline.

In order to boost the confidence level in the newly detected signals we employ a very large array of tests for candidate selection: on top of the regular binarity and contamination tests we added the “half-half” test for false positives identification, required that signals are not effected by changing the long-term filter and thus are even less likely to be an artifact of data processing, and sometimes confirmed that they are present in *Kepler*’s PDC data too. This suite of tests exceeds the one used by the *Kepler* pipeline, helping to produce a clean catalogue.

We also presented an approach for the global fitting of multi-transiting systems that uses *Kepler*’s third law to reduce the number of degrees of freedom in the fitted model *if* one assumes that the multiple transit signals are all from the same host star. This assumption is anyhow taken by the *Kepler* team in subsequent steps (e.g., when estimating the physical size of the planets) but the assumption is not fully utilized, and we shows that doing so allows to significantly reduce the error on the  $d/R_*$  parameter by a factor of 3.8 .

The fact that additional transit candidates are found in the data of 41 systems that had only one previously known signal boosts significantly the chances that these systems are real planets since the false alarm rate of multi transiting planets is, intrinsically, very low. This is especially true to the KOI 277 system, which also exhibits anti-correlated TTVs in a dynamically stable configuration, all but validating the system. Also notable is the large number of planet candidates that are part of period commensurabilities, larger than the ones presented in Fabrycky *et al.* (2012a). We do not have a good explanation for why this happened - but near-resonant systems are particularly useful as they may allow for the full validation of their planetary nature using photometry alone.

In this paper we advocate for the parallel processing of the full data by other teams. However, in the near future the publicly available *Kepler* data will increase significantly - and with it the associated workload related to analyzing it, both in computer time and human time. We believe that the sheer volume of the work means that doing this re-analysis will be increasingly more difficult, and thus increasingly less possible for small groups of researches - but we hope that the results of this work will encourage others in this direction. For e.g., the *Kepler* pipeline has five primary modules: CAL, PA, PDC, TPS, and DV for: calibration, photometry, de-trending, transit search and signal validation, respectively. In this paper we presented our own versions of the PDC, TPS, and DV modules - and these change were productive. We therefore believe that an independent analysis matching the CAL and PA modules (that remain “unchallenged” to date) may also be productive.

Finally, since we were able to detect up to four additional transit signals in each of the presented systems, the chances of detecting more transiting systems - and even more multi-transiting systems - in the remaining  $> 99\%$  of the data are quite real.

## 6. Acknowledgements

A.O. acknowledges financial support from the Deutsche Forschungsgemeinschaft under DFG GRK

## References

- lonso *et al.* , In preparation.
- Barnes, J. W. 2007, *PASP*, 119, 986
- Batalha, N. M., Rowe, J. F., Bryson, S. T., et al. 2012, arXiv:1202.5852
- Borucki, W. J., Koch, D., Basri, G., et al. 2010, *Science*, 327, 977
- Borucki, W. J., Koch, D. G., Basri, G., et al. 2011a, *ApJ*, 728, 117
- Borucki, W. J., Koch, D. G., Basri, G., et al. 2011b, *ApJ*, 736, 19
- Borucki, W. J., Koch, D. G., Batalha, N., et al. 2012, *ApJ*, 745, 120
- Bouchy, F., Deleuil, M., Guillot, T., et al. 2011, *A&A*, 525, A68
- Cabrera, J., Bruntt, H., Ollivier, M., et al. 2010, *A&A*, 522, A110
- Carter, J. A., Agol, E., Chaplin, W. J., et al. 2012, arXiv:1206.4718
- Chambers, J. E. 1999, *MNRAS*, 304, 793
- Charpinet, S., Fontaine, G., Brassard, P., et al. 2011, *Nature*, 480, 496
- Claret, A. 2000, *A&A*, 363, 1081
- Csizmadia, S., Moutou, C., Deleuil, M., et al. 2011, *A&A*, 531, A41
- Deleuil, M., Bonomo, A. S., Ferraz-Mello, S., et al. 2012, *A&A*, 538, A145
- Fabrycky, D. C., Lissauer, J. J., Ragozzine, D., et al. 2012a, arXiv:1202.6328F
- Fabrycky, D. C., Ford, E. B., Steffen, J. H., et al. 2012b, *ApJ*, 750, 114
- Figueira, P., Marmier, M., Boué, G., et al. 2012, *A&A*, 541, A139
- Fischer, D. A., Schwamb, M. E., Schawinski, K., et al. 2012, *MNRAS*, 419, 2900
- Gillon, M., Hatzes, A., Csizmadia, S., et al. 2010, *A&A*, 520, A97
- Guenther, E. W., Díaz, R. F., Gazzano, J.-C., et al. 2012, *A&A*, 537, A136
- Hébrard, G., Evans, T. M., Alonso, R., et al. 2011, *A&A*, 533, A130
- Huang, X., Bakos, G. Á., & Hartman, J. D. 2012, arXiv:1205.6492
- Kipping, D. M. 2010, *MNRAS*, 408, 1758
- Kovács, G., Zucker, S., & Mazeh, T. 2002, *A&A*, 391, 369
- Lintott, C., Schwamb, M. E., Sharzer, C., et al. 2012, arXiv:1202.6007

- Lissauer, J. J., Fabrycky, D. C., Ford, E. B., et al. 2011, *Nature*, 470, 53  
Lissauer, J. J., Marcy, G. W., Rowe, J. F., et al. 2012, *ApJ*, 750, 112  
Mandel, K., & Agol, E. 2002, *ApJ*, 580, L171  
Marchal, C., & Bozis, G. 1982, *Celestial Mechanics*, 26, 311  
[Moutou et al. 2012] Moutou *et al.* ., In preparation.  
Nesvorný, D., Kipping, D. M., Buchhave, L. A., et al. 2012, *Science*, 336, 1133  
Ofir, A. 2008, *MNRAS*, 387, 1597  
Ofir, A., Deeg, H. J., & Lacy, C. H. S. 2009, *A&A*, 506, 445  
Ofir, A., Alonso, R., Bonomo, A. S., et al. 2010, *MNRAS*, 404, L99  
Ofir, A., Gandolfi, D., Buchhave, L., et al. 2012, *MNRAS*, 423, L1  
Ollivier, M., Gillon, M., Santerne, A., et al. 2012, *A&A*, 541, A149  
ätzold *et al.* ., In preparation.  
Pont, F., Zucker, S., & Queloz, D. 2006, *MNRAS*, 373, 231P  
Ragozzine, D., & Holman, M. J. 2010, arXiv:1006.3727  
Rouan, D., Parviainen, H., Moutou, C., et al. 2012, *A&A*, 537, A54  
Slawson, R. W., Prša, A., Welsh, W. F., et al. 2011, *AJ*, 142, 160  
Smith, J. C., Stumpe, M. C., Van Cleve, J. E., et al. 2012, arXiv:1203.1383  
Steffen, J. H., Fabrycky, D. C., Ford, E. B., et al. 2012, *MNRAS*, 421, 2342S  
Tamuz, O., Mazeh, T., & Zucker, S. 2005, *MNRAS*, 356, 1466  
Tingley, B., Endl, M., Gazzano, J.-C., et al. 2011, *A&A*, 528, A97  
Wu, H., Twicken, J. D., Tenenbaum, P., et al. 2010, *Proc. SPIE*, 7740,

**Table 1.** Results of the global fit for each system for both the previously known and new signals. Notes: (1) Negative period designat the best-fitting period that reproduces the observed transit duration/shape of a non-periodic monotransit. (2) The  $\frac{d}{R_*}$  is computed from the final  $\frac{d_1}{R_*}$  for the first signal, times the Keplerian factor  $(\frac{P_1}{P})^{\frac{2}{3}}$  - all directly from the MCMC distributions.

KOI	New signal	Period <sup>(1)</sup> [d]	Epoch [BJD-2454900]	depth [ppm]	$\frac{r}{R_*}$	$\frac{d}{R_*}$ <sup>(2)</sup>	i [degrees]	$e \cos \omega$
KOI 179.01		20.7404 ± 0.00011	75.7964 ± 0.0014	994	0.028 ± 0.00013	15.788 ± 0.067	NaN ± NaN	0 (fixed)
KOI 179	+	-384 ± 95	239.503 ± 0.0034	1794	0.03914 ± 0.00087	110 ± 18	89.737 ± 0.012	0 (fixed)
KOI 239.01		5.64071 ± 1.6e - 05	71.5539 ± 0.00074	1260	0.03599 ± 0.00082	9.85 ± 0.75	85.43 ± 0.57	0 (fixed)
KOI 239	+	3.6228 ± 9.3e - 05	315.963 ± 0.0037	141	0.01175 ± 0.00071	7.34 ± 0.56	84.26 ± 0.92	0 (fixed)
KOI 241.01		13.8214 ± 8.6e - 05	64.7923 ± 0.0018	739	0.02446 ± 0.00081	27.9 ± 2.6	89.13 ± 0.47	0 (fixed)
KOI 241	+	3.41058 ± 7.4e - 05	378.342 ± 0.0033	118	0.00956 ± 0.00042	11 ± 1	88.9 ± 1.2	0 (fixed)
KOI 241	+	30.9507 ± 0.0011	396.334 ± 0.005	243	0.0149 ± 0.0011	47.7 ± 4.5	89.22 ± 0.2	0 (fixed)
KOI 246.01		5.39876 ± 8e - 06	106.857 ± 0.00038	350	0.01917 ± 0.0001	7.27 ± 0.12	83.66 ± 0.17	0 (fixed)
KOI 246	+	9.60538 ± 0.00026	376.753 ± 0.0029	37	0.00638 ± 0.00027	10.68 ± 0.18	85.5 ± 0.13	0 (fixed)
KOI 246	+	-970 ± 50	503.204 ± 0.0059	238	0.02012 ± 0.00096	232.4 ± 8.2	89.7597 ± 0.0082	0 (fixed)
KOI 260.01		10.4958 ± 0.00012	105.784 ± 0.0033	92	0.01045 ± 0.0002	8.35 ± 0.21	83.95 ± 0.21	0 (fixed)
KOI 260.02		100.283 ± 0.00099	178.041 ± 0.002	316	0.01896 ± 0.00022	37.59 ± 0.96	88.688 ± 0.047	0 (fixed)
KOI 260	+	21.8701 ± 0.00026	379.472 ± 0.0023	93	0.01089 ± 0.00025	13.62 ± 0.35	86.16 ± 0.12	0 (fixed)
KOI 271.01		48.6309 ± 0.00035	105.545 ± 0.0018	331	0.01866 ± 0.00018	31.99 ± 0.45	88.552 ± 0.031	0 (fixed)
KOI 271.02		29.3924 ± 0.0002	142.072 ± 0.0015	320	0.01755 ± 0.00015	22.87 ± 0.32	88.201 ± 0.048	0 (fixed)
KOI 271	+	14.4364 ± 0.00021	305.487 ± 0.0024	81	0.01014 ± 0.00035	14.24 ± 0.2	86.334 ± 0.065	0 (fixed)
KOI 277.01		16.2293 ± 0.00015	104.668 ± 0.0029	453	0.02071 ± 0.00038	11.68 ± 0.67	86.56 ± 0.41	0 (fixed)
KOI 277	+	13.8538 ± 0.0016	379.475 ± 0.019	34	0.00588 ± 0.00063	10.51 ± 0.61	85.8 ± 0.68	0 (fixed)
KOI 285.01		13.7487 ± 8.8e - 05	112.28 ± 0.0014	404	0.01962 ± 0.00028	12.67 ± 0.53	86.79 ± 0.27	0 (fixed)
KOI 285	+	26.7234 ± 0.00069	268.003 ± 0.0034	125	0.01061 ± 0.00029	19.73 ± 0.82	88.17 ± 0.21	0 (fixed)
KOI 285	+	49.3612 ± 0.0042	264.716 ± 0.01	66	0.00766 ± 0.00045	29.7 ± 1.2	88.83 ± 0.17	0 (fixed)
KOI 289.01		26.6293 ± 0.00027	124.995 ± 0.0025	432	0.02105 ± 0.00032	16.53 ± 0.63	87.28 ± 0.17	0 (fixed)
KOI 289	+	1.47762 ± 5.3e - 05	377.687 ± 0.006	24	0.0063 ± 0.0014	2.405 ± 0.092	66.2 ± 1	0 (fixed)
KOI 295.01		5.31741 ± 1.7e - 05	104.875 ± 0.00087	275	0.01495 ± 0.0002	13.64 ± 0.56	88.77 ± 0.64	0 (fixed)
KOI 295	+	10.1057 ± 0.00015	371.68 ± 0.0026	99	0.01054 ± 0.00059	20.92 ± 0.86	87.67 ± 0.16	0 (fixed)
KOI 316.01		15.7708 ± 7.8e - 05	117.908 ± 0.0013	502	0.02091 ± 0.00021	19.77 ± 0.6	88.36 ± 0.16	0 (fixed)
KOI 316.02		157.05 ± 0.01	414.269 ± 0.0053	443	0.02158 ± 0.00063	91.5 ± 2.8	89.498 ± 0.023	0 (fixed)
KOI 316	+	7.30571 ± 5.8e - 05	313.172 ± 0.00099	193	0.01756 ± 0.00065	11.84 ± 0.36	85.35 ± 0.15	0 (fixed)
KOI 321.01		2.42632 ± 1e - 05	103.454 ± 0.001	163	0.01187 ± 0.0004	6.09 ± 0.68	84.8 ± 2.1	0 (fixed)
KOI 321	+	4.62325 ± 9e - 05	310.405 ± 0.0035	50	0.00675 ± 0.00042	9.4 ± 1.1	86.1 ± 1.1	0 (fixed)
KOI 330.01		7.97392 ± 0.0001	107.533 ± 0.0032	231	0.0139 ± 0.00059	10.6 ± 1.3	87.5 ± 1.5	0 (fixed)
KOI 330	+	1.88897 ± 5.7e - 05	314.441 ± 0.0046	41	0.00582 ± 0.00044	4.07 ± 0.49	83.9 ± 4.3	0 (fixed)
KOI 339.01		1.98035 ± 8.7e - 06	103.139 ± 0.0012	241	0.01531 ± 0.00033	4.52 ± 0.25	80.7 ± 1	0 (fixed)
KOI 339.02		12.834 ± 0.00026	71.3321 ± 0.007	230	0.01696 ± 0.00064	15.7 ± 0.86	86.7 ± 0.23	0 (fixed)

Continued on next page.

KOI	New signal	Period <sup>(1)</sup> [d]	Epoch [BJD-2454900]	depth [ppm]	$\frac{r}{R_s}$	$\frac{d}{R_s}$ <sup>(2)</sup>	i [degrees]	$e \cos \omega$
KOI 339	+	$35.863 \pm 0.0013$	$391.692 \pm 0.0058$	170	$0.01331 \pm 0.00076$	$31.2 \pm 1.7$	$88.53 \pm 0.14$	0 (fixed)
KOI 408.01		$7.38202 \pm 2.7e - 05$	$106.071 \pm 0.00093$	1396	$0.03746 \pm 0.00036$	$12.07 \pm 0.28$	$86.38 \pm 0.13$	0 (fixed)
KOI 408.02		$12.5609 \pm 9.3e - 05$	$99.7959 \pm 0.0019$	808	$0.02839 \pm 0.00048$	$17.2 \pm 0.4$	$87.48 \pm 0.1$	0 (fixed)
KOI 408.03		$30.825 \pm 0.00047$	$86.0153 \pm 0.0048$	652	$0.02668 \pm 0.00077$	$31.29 \pm 0.72$	$88.482 \pm 0.056$	0 (fixed)
KOI 408	+	$3.42817 \pm 5.3e - 05$	$312.184 \pm 0.0028$	164	$0.01343 \pm 0.00076$	$7.24 \pm 0.17$	$83.39 \pm 0.28$	0 (fixed)
KOI 435.01		$20.5499 \pm 9.9e - 05$	$111.945 \pm 0.0014$	1132	$0.037 \pm 0.0014$	$21.54 \pm 0.42$	$88.11 \pm 0.072$	0 (fixed)
KOI 435.02		$1e + 07 \pm 5.6e + 07$	$NaN \pm NaN$	-0	$0.17 \pm 0.51$	$280000 \pm 300000$	$NaN \pm NaN$	0 (fixed)
KOI 435	+	$3.93269 \pm 6.8e - 05$	$311.479 \pm 0.0018$	154	$0.01383 \pm 0.00066$	$7.15 \pm 0.14$	$84.01 \pm 0.19$	0 (fixed)
KOI 435	+	$33.039 \pm 0.00069$	$325.504 \pm 0.0029$	387	$0.0253 \pm 0.0014$	$29.56 \pm 0.57$	$88.227 \pm 0.041$	0 (fixed)
KOI 435	+	$62.3054 \pm 0.0011$	$361.307 \pm 0.0022$	494	$0.0247 \pm 0.0011$	$45.12 \pm 0.87$	$89.061 \pm 0.036$	0 (fixed)
KOI 435	+	$9.92025 \pm 0.00057$	$317.866 \pm 0.0082$	90	$0.01014 \pm 0.0009$	$13.26 \pm 0.26$	$87.24 \pm 0.47$	0 (fixed)
KOI 505.01		$13.7671 \pm 9.7e - 05$	$107.809 \pm 0.0016$	622	$0.02829 \pm 0.00067$	$18.12 \pm 0.71$	$87.17 \pm 0.14$	0 (fixed)
KOI 505.02		$6.19552 \pm 7.5e - 05$	$67.7119 \pm 0.0032$	222	$0.01521 \pm 0.0005$	$10.64 \pm 0.42$	$85.77 \pm 0.28$	0 (fixed)
KOI 505	+	$3.25059 \pm 3.3e - 05$	$313.737 \pm 0.0016$	209	$0.01529 \pm 0.00057$	$6.92 \pm 0.27$	$83.12 \pm 0.4$	0 (fixed)
KOI 505	+	$87.0897 \pm 0.0012$	$294.498 \pm 0.0024$	1053	$0.03394 \pm 0.00084$	$62 \pm 2.4$	$89.244 \pm 0.045$	0 (fixed)
KOI 505	+	$8.34808 \pm 0.0001$	$311.937 \pm 0.0018$	242	$0.01678 \pm 0.00063$	$12.98 \pm 0.51$	$86.24 \pm 0.21$	0 (fixed)
KOI 509.01		$4.16696 \pm 2.1e - 05$	$102.714 \pm 0.0013$	703	$0.02355 \pm 0.00031$	$11.55 \pm 0.44$	$88.85 \pm 0.82$	0 (fixed)
KOI 509.02		$11.4635 \pm 7.9e - 05$	$70.382 \pm 0.0017$	881	$0.02962 \pm 0.00067$	$22.68 \pm 0.86$	$88.1 \pm 0.13$	0 (fixed)
KOI 509	+	$39.5891 \pm 0.0014$	$299.132 \pm 0.0043$	414	$0.01837 \pm 0.00082$	$51.8 \pm 2$	$89.56 \pm 0.18$	0 (fixed)
KOI 510.01		$2.94034 \pm 2.3e - 05$	$102.902 \pm 0.0016$	403	$0.02081 \pm 0.00043$	$5.29 \pm 0.1$	$81.16 \pm 0.32$	0 (fixed)
KOI 510.02		$6.38905 \pm 4.8e - 05$	$108.472 \pm 0.002$	476	$0.02304 \pm 0.00053$	$8.87 \pm 0.18$	$84.58 \pm 0.17$	0 (fixed)
KOI 510.03		$14.627 \pm 0.00027$	$69.2401 \pm 0.0052$	322	$0.01988 \pm 0.00097$	$15.4 \pm 0.31$	$86.707 \pm 0.095$	0 (fixed)
KOI 510	+	$35.1183 \pm 0.00089$	$295.83 \pm 0.0036$	539	$0.028 \pm 0.0015$	$27.62 \pm 0.55$	$88.055 \pm 0.051$	0 (fixed)
KOI 564.01		$21.0547 \pm 0.00062$	$104.905 \pm 0.0082$	556	$0.02411 \pm 0.00051$	$14.35 \pm 0.39$	$86.81 \pm 0.14$	0 (fixed)
KOI 564.02		$127.861 \pm 0.0031$	$179.54 \pm 0.005$	2427	$0.05069 \pm 0.00059$	$47.8 \pm 1.3$	$89.032 \pm 0.04$	0 (fixed)
KOI 564	+	$6.2174 \pm 0.00017$	$313.408 \pm 0.0043$	134	$0.01261 \pm 0.00072$	$6.36 \pm 0.17$	$82.07 \pm 0.33$	0 (fixed)
KOI 582.01		$5.94508 \pm 3.1e - 05$	$103.468 \pm 0.0014$	740	$0.0256 \pm 0.00055$	$14.3 \pm 0.78$	$87.56 \pm 0.37$	0 (fixed)
KOI 582.02		$17.7389 \pm 0.00022$	$81.9806 \pm 0.0039$	476	$0.02335 \pm 0.00088$	$29.6 \pm 1.6$	$88.37 \pm 0.13$	0 (fixed)
KOI 582	+	$9.93964 \pm 0.00019$	$313.075 \pm 0.0025$	251	$0.01503 \pm 0.00067$	$20.1 \pm 1.1$	$88.2 \pm 0.27$	0 (fixed)
KOI 584.01		$9.92669 \pm 5.5e - 05$	$108.686 \pm 0.0013$	662	$0.0265 \pm 0.00044$	$12.51 \pm 0.52$	$86.32 \pm 0.25$	0 (fixed)
KOI 584.02		$21.2233 \pm 0.00025$	$103.374 \pm 0.0026$	506	$0.02366 \pm 0.00054$	$20.76 \pm 0.87$	$87.7 \pm 0.15$	0 (fixed)
KOI 584	+	$6.47027 \pm 0.00021$	$308.9 \pm 0.0051$	84	$0.00951 \pm 0.00079$	$9.41 \pm 0.39$	$85.03 \pm 0.42$	0 (fixed)
KOI 593.01		$9.99772 \pm 0.00011$	$104.784 \pm 0.0027$	495	$0.02291 \pm 0.00066$	$13.96 \pm 0.56$	$86.67 \pm 0.2$	0 (fixed)
KOI 593.02		$90.4109 \pm 0.0026$	$141.503 \pm 0.0058$	1104	$0.0348 \pm 0.001$	$60.6 \pm 2.4$	$89.213 \pm 0.05$	0 (fixed)
KOI 593	+	$51.065 \pm 0.0013$	$335.942 \pm 0.0042$	436	$0.0229 \pm 0.0012$	$41.4 \pm 1.7$	$88.776 \pm 0.071$	0 (fixed)
KOI 597.01		$17.3082 \pm 0.00022$	$109.939 \pm 0.0033$	480	$0.02174 \pm 0.00069$	$18.5 \pm 1.3$	$87.7 \pm 0.29$	0 (fixed)
KOI 597.02		$2.09221 \pm 3e - 05$	$66.0692 \pm 0.004$	166	$0.01274 \pm 0.00059$	$4.53 \pm 0.31$	$80.7 \pm 1.4$	0 (fixed)
KOI 597	+	$52.815 \pm 0.0023$	$309.16 \pm 0.006$	345	$0.01839 \pm 0.00094$	$39 \pm 2.7$	$88.91 \pm 0.14$	0 (fixed)
KOI 623.01		$10.3498 \pm 0.00016$	$107.059 \pm 0.0037$	95	$0.01037 \pm 0.00027$	$9.88 \pm 0.6$	$85.04 \pm 0.41$	0 (fixed)
KOI 623.02		$15.6776 \pm 0.00024$	$112.467 \pm 0.0041$	83	$0.00952 \pm 0.00027$	$13.03 \pm 0.79$	$86.35 \pm 0.32$	0 (fixed)
KOI 623.03		$5.59936 \pm 7.3e - 05$	$104.472 \pm 0.0033$	64	$0.0084 \pm 0.00023$	$6.56 \pm 0.4$	$82.63 \pm 0.63$	0 (fixed)

Continued on next page.

KOI	New signal	Period <sup>(1)</sup> [d]	Epoch [BJD-2454900]	depth [ppm]	$\frac{r}{R_*}$	$\frac{d}{R_*}$ <sup>(2)</sup>	i [degrees]	$e \cos \omega$
KOI 623	+	25.211 ± 0.0015	314.307 ± 0.008	41	0.00652 ± 0.00044	17.9 ± 1.1	87.43 ± 0.25	0 (fixed)
KOI 624.01		17.79 ± 0.0001	115.436 ± 0.0014	855	0.0264 ± 0.0005	28.9 ± 1.9	89.25 ± 0.42	0 (fixed)
KOI 624.02		49.5669 ± 0.00082	102.542 ± 0.0047	597	0.02591 ± 0.00082	57.3 ± 3.7	89.154 ± 0.079	0 (fixed)
KOI 624	+	1.31186 ± 5.7e - 06	312.735 ± 0.00049	225	0.01407 ± 0.00041	5.09 ± 0.33	83.5 ± 1.3	0 (fixed)
KOI 627.01		7.75196 ± 4.7e - 05	109.169 ± 0.0015	314	0.01696 ± 0.00052	13.6 ± 1.4	87.26 ± 0.68	0 (fixed)
KOI 627	+	4.16523 ± 9e - 05	314.963 ± 0.0022	102	0.00936 ± 0.00044	8.98 ± 0.91	86.8 ± 1.6	0 (fixed)
KOI 671.01		4.22866 ± 5.3e - 05	103.74 ± 0.003	134	0.01324 ± 0.00036	4.12 ± 0.13	77.13 ± 0.5	0 (fixed)
KOI 671.03		16.26 ± 0.00053	77.5278 ± 0.0097	98	0.01204 ± 0.00073	10.11 ± 0.32	84.61 ± 0.2	0 (fixed)
KOI 671	+	7.46647 ± 0.00026	312.176 ± 0.0043	82	0.01059 ± 0.00056	6.02 ± 0.19	81.11 ± 0.33	0 (fixed)
KOI 671	+	11.1317 ± 0.00051	312.329 ± 0.0071	67	0.00969 ± 0.0007	7.85 ± 0.25	83.14 ± 0.26	0 (fixed)
KOI 710.01		5.37515 ± 0.00014	103.929 ± 0.0071	112	0.01234 ± 0.0008	4 ± 0.72	76.4 ± 2.4	0 (fixed)
KOI 710	+	8.58569 ± 0.00037	371.469 ± 0.0067	84	0.0114 ± 0.0011	5.46 ± 0.98	79.8 ± 1.7	0 (fixed)
KOI 717.01		14.7074 ± 0.00019	108.79 ± 0.0029	230	0.01408 ± 0.00076	31.9 ± 5.5	89.04 ± 0.65	0 (fixed)
KOI 717	+	0.900351 ± 1.2e - 05	376.75 ± 0.0027	41	0.00605 ± 0.00057	4.96 ± 0.85	83.6 ± 4	0 (fixed)
KOI 719.01		9.03423 ± 2.7e - 05	104.013 ± 0.00074	558	0.02266 ± 0.00048	34.4 ± 1.2	88.904 ± 0.098	0 (fixed)
KOI 719	+	4.15976 ± 4.1e - 05	312.214 ± 0.00078	148	0.01048 ± 0.0002	20.54 ± 0.74	89.82 ± 0.21	0 (fixed)
KOI 719	+	45.904 ± 0.00048	329.076 ± 0.0015	325	0.018 ± 0.0011	101.8 ± 3.6	89.755 ± 0.033	0 (fixed)
KOI 719	+	28.1226 ± 0.00038	304.892 ± 0.0021	207	0.01316 ± 0.00087	73.4 ± 2.6	89.69 ± 0.11	0 (fixed)
KOI 780.01		2.33745 ± 9.6e - 06	104.76 ± 0.001	859	0.02861 ± 0.00037	6.705 ± 0.065	NaN ± NaN	0 (fixed)
KOI 780	+	7.24078 ± 8.3e - 05	309.698 ± 0.0017	473	0.121 ± 0.042	14.25 ± 0.14	85.63 ± 0.18	0 (fixed)
KOI 841.01		15.3349 ± 6.7e - 05	107.007 ± 0.0013	2839	0.05297 ± 0.00044	23.24 ± 0.062	NaN ± NaN	0 (fixed)
KOI 841.02		31.3309 ± 0.00014	86.4255 ± 0.0013	5020	0.0703 ± 0.0004	37.42 ± 0.1	NaN ± NaN	0 (fixed)
KOI 841	+	-1400 ± 550	487.916 ± 0.021	1160	0.0411 ± 0.0074	470 ± 130	89.886 ± 0.028	0 (fixed)
KOI 841	+	6.54629 ± 7.6e - 05	315.621 ± 0.0017	657	0.0264 ± 0.0011	13.176 ± 0.035	86.5 ± 0.1	0 (fixed)
KOI 856.01		39.749 ± 6.3e - 05	105.853 ± 0.00039	13882	0.13353 ± 0.00058	28.988 ± 0.036	NaN ± NaN	0 (fixed)
KOI 856	+	0.870579 ± 1.4e - 05	380.217 ± 0.0024	115	0.0151 <sup>+0.0062</sup> <sub>-0.0022</sub>	2.2692 ± 0.0028	64.34 ± 0.33	0 (fixed)
KOI 1060.01		12.1097 ± 0.00031	73.2107 ± 0.0065	194	0.01308 ± 0.00063	14.5 ± 1.5	87.78 ± 0.79	0 (fixed)
KOI 1060.02		4.75771 ± 0.00019	70.7138 ± 0.0098	108	0.00951 ± 0.00058	7.8 ± 0.81	87.1 ± 2.2	0 (fixed)
KOI 1060.04		8.1945 ± 0.00033	71.9266 ± 0.0077	153	0.0148 ± 0.0036	11.2 ± 1.2	85.15 ± 0.64	0 (fixed)
KOI 1060	+	20.4973 ± 0.0012	305.914 ± 0.0088	128	0.01082 ± 0.00084	20.6 ± 2.1	88.23 ± 0.54	0 (fixed)
KOI 1069.02		2.46693 ± 5.6e - 05	287.933 ± 0.0039	283	0.01549 ± 0.00083	9.51 ± 0.71	86.9 ± 1.2	0 (fixed)
KOI 1069	+	8.70385 ± 0.00011	421.123 ± 0.0011	995	0.02818 ± 0.00076	22 ± 1.7	89.1 ± 0.59	0 (fixed)
KOI 1082.01		6.50338 ± 0.00014	68.2658 ± 0.0056	371	0.0183 ± 0.0016	15.2 ± 3.3	87.6 ± 1.3	0 (fixed)
KOI 1082	+	1.1966 ± 1.8e - 05	313.216 ± 0.0028	186	0.0139 ± 0.0019	4.9 ± 1.1	80.9 ± 3.4	0 (fixed)
KOI 1082	+	4.09665 ± 8.9e - 05	311.896 ± 0.0033	236	0.0159 ± 0.0018	11.2 ± 2.4	85.9 ± 1.5	0 (fixed)
KOI 1108.01		18.9248 ± 0.00027	82.4986 ± 0.0037	542	0.02322 ± 0.00098	27 ± 2.8	88.41 ± 0.32	0 (fixed)
KOI 1108	+	1.47534 ± 2.2e - 05	312.685 ± 0.0025	119	0.00975 ± 0.00045	4.92 ± 0.51	86.3 ± 3.1	0 (fixed)
KOI 1108	+	4.15247 ± 7.9e - 05	312.574 ± 0.0027	179	0.01281 ± 0.00076	9.8 ± 1	86.2 ± 0.97	0 (fixed)
KOI 1413.01		12.6451 ± 0.00059	71.635 ± 0.012	113	0.01207 ± 0.00085	5.3 ± 0.99	80.2 ± 2	0 (fixed)
KOI 1413	+	21.5274 ± 0.0011	302.069 ± 0.0069	127	0.01343 ± 0.00092	7.6 ± 1.4	82.9 ± 1.3	0 (fixed)

Continued on next page.

KOI	New signal	Period <sup>(1)</sup> [d]	Epoch [BJD-2454900]	depth [ppm]	$\frac{r}{R_s}$	$\frac{d}{R_s}$ <sup>(2)</sup>	i [degrees]	$e \cos \omega$
KOI 1536.01		$3.74447 \pm 6.2e - 05$	$66.5558 \pm 0.0055$	59	$0.00821 \pm 0.00054$	$5.54 \pm 0.88$	$81.1 \pm 2$	0 (fixed)
KOI 1536	+	$79.4949 \pm 0.0056$	$355.839 \pm 0.014$	140	$0.0118 \pm 0.00095$	$42.5 \pm 6.8$	$88.98 \pm 0.31$	0 (fixed)
KOI 1574.01		$114.738 \pm 0.00064$	$98.1461 \pm 0.0018$	4751	$0.0627 \pm 0.00021$	$72.59 \pm 0.23$	$89.6571 \pm 7.1e - 15$	0 (fixed)
KOI 1574	+	$191.512 \pm 0.021$	$219.107 \pm 0.015$	614	$0.02238 \pm 0.00087$	$102.14 \pm 0.32$	$89.782 \pm 0.063$	0 (fixed)
KOI 1593.01		$9.69453 \pm 0.00027$	$115.466 \pm 0.0063$	497	$0.0231 \pm 0.0018$	$18 \pm 2.8$	$87.41 \pm 0.61$	0 (fixed)
KOI 1593	+	$15.3837 \pm 0.00089$	$287.433 \pm 0.0061$	458	$0.02 \pm 0.0015$	$24.5 \pm 3.8$	$88.66 \pm 0.72$	0 (fixed)
KOI 1599.01		$20.42 \pm 0.00071$	$73.0061 \pm 0.008$	367	$0.01973 \pm 0.00093$	$19.1 \pm 1.6$	$87.57 \pm 0.34$	0 (fixed)
KOI 1599	+	$13.6129 \pm 0.00027$	$305.419 \pm 0.0028$	330	$0.02012 \pm 0.00099$	$14.5 \pm 1.2$	$86.49 \pm 0.39$	0 (fixed)
KOI 1601.01		$10.3515 \pm 0.00033$	$66.7017 \pm 0.0088$	201	$0.0147 \pm 0.0013$	$9 \pm 2.8$	$84.8 \pm 2.2$	0 (fixed)
KOI 1601	+	$62.9135 \pm 0.0042$	$336.376 \pm 0.0085$	224	$0.0151 \pm 0.0014$	$29.9 \pm 9.5$	$88.51 \pm 0.75$	0 (fixed)
KOI 1650.01		$6.53177 \pm 0.0002$	$69.041 \pm 0.012$	582	$0.0266 \pm 0.0022$	$8.4 \pm 3$	$84 \pm 2$	0 (fixed)
KOI 1650	+	$100.829 \pm 0.014$	$351.042 \pm 0.022$	1175	$0.037 \pm 0.0032$	$52 \pm 19$	$89.05 \pm 0.34$	0 (fixed)
KOI 1681.01		$6.93938 \pm 0.0001$	$71.3245 \pm 0.0039$	585	$0.0217 \pm 0.0011$	$24.5 \pm 2.7$	$89.05 \pm 0.62$	0 (fixed)
KOI 1681	+	$1.99278 \pm 3.1e - 05$	$311.811 \pm 0.0021$	284	$0.0155 \pm 0.0012$	$10.6 \pm 1.2$	$87.2 \pm 1.3$	0 (fixed)
KOI 1681	+	$3.53109 \pm 8e - 05$	$310.96 \pm 0.0029$	302	$0.0165 \pm 0.002$	$15.6 \pm 1.7$	$87.69 \pm 0.99$	0 (fixed)
KOI 1830.01		$13.2268 \pm 9.1e - 05$	$75.2071 \pm 0.0015$	728	$0.02595 \pm 0.00059$	$25.4 \pm 1.5$	$88.59 \pm 0.22$	0 (fixed)
KOI 1830	+	$198.704 \pm 0.0023$	$288.227 \pm 0.0021$	1955	$0.04174 \pm 0.00089$	$154.5 \pm 9$	$89.792 \pm 0.039$	0 (fixed)
KOI 1831.01		$51.8036 \pm 0.00076$	$116.011 \pm 0.0042$	1041	$0.02877 \pm 0.00059$	$62.6 \pm 3.4$	$89.68 \pm 0.15$	0 (fixed)
KOI 1831.03		$34.2145 \pm 0.0014$	$81.7248 \pm 0.0093$	142	$0.0124 \pm 0.0013$	$47.5 \pm 2.6$	$89.02 \pm 0.11$	0 (fixed)
KOI 1831	+	$4.38508 \pm 9.8e - 05$	$379.199 \pm 0.003$	98	$0.00919 \pm 0.00058$	$12.08 \pm 0.66$	$87.39 \pm 0.71$	0 (fixed)
KOI 1843.01		<i>NaN ± NaN</i>	<i>NaN ± NaN</i>	664	<i>NaN ± NaN</i>	<i>NaN ± NaN</i>	<i>NaN ± NaN</i>	0 (fixed)
KOI 1843.02		$6.3563 \pm 1.5e - 05$	$70.4836 \pm 0.00053$	189	$0.0156058 \pm 8.7e - 19$	<i>NaN ± NaN</i>	$87.528 \pm 0.015$	0 (fixed)
KOI 1843	+	$0.176892 \pm 1.4e - 17$	<i>NaN ± NaN</i>	114	$0.01199 \pm 0.00015$	$1.9378 \pm 1.1e - 16$	$65.075 \pm 0.028$	0 (fixed)
KOI 1870.01		$7.96431 \pm 3.2e - 05$	$69.8156 \pm 0.001$	664	$0.02742 \pm 0.00067$	$21.78 \pm 0.88$	$87.79 \pm 0.13$	0 (fixed)
KOI 1870	+	$-530 \pm 100$	$537.107 \pm 0.0012$	6429	$0.07034 \pm 0.00079$	$360 \pm 60$	$89.963 \pm 0.017$	0 (fixed)
KOI 1871.01		$92.7245 \pm 0.0017$	$110.453 \pm 0.0043$	1052	$0.0309 \pm 0.002$	$88 \pm 15$	$89.57 \pm 0.18$	0 (fixed)
KOI 1871	+	$32.3763 \pm 0.00063$	$310.044 \pm 0.0026$	640	$0.0251 \pm 0.0016$	$43.8 \pm 7.5$	$89.04 \pm 0.29$	0 (fixed)
KOI 1875.01		$9.91711 \pm 0.00012$	$68.1427 \pm 0.0035$	367	$0.01863 \pm 0.00091$	$18 \pm 2.5$	$87.78 \pm 0.67$	0 (fixed)
KOI 1875	+	$0.538349 \pm 2.8e - 06$	$313.368 \pm 0.00079$	160	$0.01176 \pm 0.0006$	$2.58 \pm 0.36$	$78.4 \pm 7.3$	0 (fixed)
KOI 1955.01		$15.1701 \pm 0.0002$	$65.6673 \pm 0.0034$	188	$0.01544 \pm 0.00036$	$12.673 \pm 0.053$	$85.8671 \pm 7.1e - 15$	0 (fixed)
KOI 1955.02		$39.4615 \pm 0.0012$	$69.4458 \pm 0.0097$	157	$0.01273 \pm 0.00038$	$23.969 \pm 0.1$	<i>NaN ± NaN</i>	0 (fixed)
KOI 1955	+	$1.64423 \pm 3.5e - 05$	$313.028 \pm 0.0029$	35	$0.006 \pm 0.0003$	$2.881 \pm 0.012$	$73.92 \pm 0.55$	0 (fixed)
KOI 1955	+	$26.2335 \pm 0.00057$	$311.103 \pm 0.0033$	202	$0.022 \pm 0.0049$	$18.258 \pm 0.076$	$86.894 \pm 0.03$	0 (fixed)
KOI 1972.01		$17.7911 \pm 0.0002$	$82.2558 \pm 0.0032$	363	$0.0219 \pm 0.0012$	$23.1 \pm 3.4$	$87.72 \pm 0.4$	0 (fixed)
KOI 1972	+	$1.22623 \pm 2.9e - 05$	$313.382 \pm 0.003$	50	$0.00644 \pm 0.0004$	$3.89 \pm 0.57$	$83.6 \pm 4.4$	0 (fixed)
KOI 1986.01		$148.458 \pm 0.0026$	$84.3871 \pm 0.0046$	1411	$0.0445 \pm 0.004$	$84 \pm 29$	$89.37 \pm 0.18$	0 (fixed)
KOI 1986	+	$7.12775 \pm 0.00024$	$311.347 \pm 0.0067$	188	$0.015 \pm 0.0024$	$11 \pm 3.8$	$85.5 \pm 1.6$	0 (fixed)
KOI 2004.01		$56.1879 \pm 0.0014$	$79.3788 \pm 0.0068$	272	$0.01774 \pm 0.00089$	$36 \pm 3.9$	$88.63 \pm 0.19$	0 (fixed)
KOI 2004	+	$3.18895 \pm 8.1e - 05$	$379.044 \pm 0.0044$	67	$0.00889 \pm 0.00087$	$5.32 \pm 0.57$	$80.6 \pm 1.3$	0 (fixed)

Continued on next page.

KOI	New signal	Period <sup>(1)</sup> [d]	Epoch [BJD-2454900]	depth [ppm]	$\frac{r}{R_*}$	$\frac{d}{R_*}$ <sup>(2)</sup>	i [degrees]	$e \cos \omega$
KOI 2055.01		$8.67913 \pm 0.00014$	$66.0298 \pm 0.004$	437	$0.01985 \pm 0.001$	$15.2 \pm 2.3$	$87.64 \pm 0.92$	0 (fixed)
KOI 2055	+	$4.02581 \pm 0.00011$	$269.714 \pm 0.0031$	196	$0.01307 \pm 0.00074$	$9.1 \pm 1.4$	$86.5 \pm 1.8$	0 (fixed)
KOI 2055	+	$2.50465 \pm 6.4e - 05$	$267.01 \pm 0.0035$	146	$0.0119 \pm 0.001$	$6.65 \pm 0.99$	$83.8 \pm 1.9$	0 (fixed)
KOI 2159.01		$7.59683 \pm 0.00012$	$64.9479 \pm 0.0045$	102	$0.00991 \pm 0.0007$	$12.4 \pm 2.6$	$86.7 \pm 1.4$	0 (fixed)
KOI 2159	+	$2.39265 \pm 3.1e - 05$	$313.226 \pm 0.002$	75	$0.00981 \pm 0.00073$	$5.7 \pm 1.2$	$80.9 \pm 2.1$	0 (fixed)
KOI 2193.01		$2.36172 \pm 1.7e - 05$	$66.2386 \pm 0.0019$	502	$0.0251 \pm 0.0014$	$7.66 \pm 0.77$	$83.54 \pm 0.89$	0 (fixed)
KOI 2193	+	$4.1629 \pm 2.5e - 05$	$314.452 \pm 0.00084$	647	$0.057 \pm 0.034$	$11.2 \pm 1.1$	$84.87 \pm 0.76$	0 (fixed)
KOI 2195.01		$20.0541 \pm 0.00066$	$69.5794 \pm 0.0084$	234	$0.01621 \pm 0.00098$	$14.4 \pm 2.5$	$86.59 \pm 0.8$	0 (fixed)
KOI 2195	+	$30.0918 \pm 0.0014$	$322.778 \pm 0.0072$	188	$0.0149 \pm 0.001$	$18.9 \pm 3.3$	$87.31 \pm 0.58$	0 (fixed)
KOI 2195	+	$6.85035 \pm 0.00027$	$314.253 \pm 0.006$	99	$0.0103 \pm 0.00084$	$7 \pm 1.2$	$83.3 \pm 1.9$	0 (fixed)
KOI 2243.01		$5.18549 \pm 0.00014$	$65.3316 \pm 0.0079$	186	$0.0131 \pm 0.00085$	$7.9 \pm 1.6$	$85.2 \pm 2.5$	0 (fixed)
KOI 2243	+	$8.45812 \pm 0.00023$	$306.887 \pm 0.0034$	213	$0.0159 \pm 0.0012$	$11 \pm 2.2$	$85.4 \pm 1.4$	0 (fixed)
KOI 2485.01		$9.99119 \pm 0.0002$	$67.3913 \pm 0.0067$	386	$0.0206 \pm 0.0017$	$17.3 \pm 3.6$	$87.29 \pm 0.81$	0 (fixed)
KOI 2485	+	$3.60087 \pm 5.7e - 05$	$376.705 \pm 0.0025$	244	$0.0162 \pm 0.0015$	$8.8 \pm 1.8$	$84.8 \pm 1.6$	0 (fixed)
KOI 2485	+	$5.72691 \pm 0.00011$	$376.227 \pm 0.003$	269	$0.0176 \pm 0.0015$	$12 \pm 2.5$	$86 \pm 1.1$	0 (fixed)
KOI 2579.01		$2.72968 \pm 8e - 05$	$66.2773 \pm 0.0079$	114	$0.01047 \pm 0.00074$	$5.39 \pm 0.93$	$82.3 \pm 2.5$	0 (fixed)
KOI 2579	+	$3.59657 \pm 0.00016$	$313.922 \pm 0.0057$	104	$0.0107 \pm 0.0011$	$6.5 \pm 1.1$	$82.6 \pm 1.9$	0 (fixed)
KOI 2579	+	$10.3007 \pm 0.00049$	$304.827 \pm 0.0071$	154	$0.0134 \pm 0.0014$	$13.1 \pm 2.3$	$86.18 \pm 0.88$	0 (fixed)
KOI 2597.01		$8.00513 \pm 0.00031$	$71.712 \pm 0.01$	133	$0.0114 \pm 0.0012$	$12.7 \pm 3$	$86.6 \pm 1.5$	0 (fixed)
KOI 2597.02		$12.1305 \pm 0.00049$	$72.895 \pm 0.013$	144	$0.0117 \pm 0.001$	$16.7 \pm 4$	$87.6 \pm 1.2$	0 (fixed)
KOI 2597	+	$5.61365 \pm 0.00016$	$311.815 \pm 0.0041$	123	$0.0114 \pm 0.0012$	$10 \pm 2.4$	$85.4 \pm 1.7$	0 (fixed)

**Table 2.** Physical properties of the newly detected planet candidate. Notes: (1) Negative period designat the best-fitting period that reproduces the observed transit duration/shape of a non-periodic monotransit. (2) The  $\frac{d}{R_s}$  is computed from the final  $\frac{d}{R_s}$  for the first signal, times the Keplerian factor  $(\frac{P}{P_1})^{\frac{2}{3}}$  - all directly from the MCMC distributions.

Host star	Period <sup>(1)</sup> (d)	$r$ [ $R_{\oplus}$ ]	$a^{(2)}$ [AU]	$T_{eq}$ [K]
KOI 179	-384	4.09	1.004	251
KOI 239	3.6228	1.19	0.047	1175
KOI 241	3.41058	0.63	0.039	873
KOI 241	30.9507	0.97	0.170	418
KOI 246	9.60538	0.86	0.090	946
KOI 246	-970	2.72	1.954	203
KOI 260	21.8701	1.50	0.158	767
KOI 271	14.4364	1.40	0.125	866
KOI 277	13.8538	1.03	0.116	981
KOI 285	26.7234	1.77	0.184	746
KOI 285	49.3612	1.28	0.277	608
KOI 289	1.47762	0.69	0.025	1616
KOI 295	10.1057	1.22	0.093	880
KOI 316	7.30571	2.26	0.075	979
KOI 321	4.62325	0.82	0.054	1107
KOI 330	1.88897	0.79	0.030	1639
KOI 339	35.863	1.26	0.207	542
KOI 408	3.42817	1.27	0.043	1110
KOI 435	3.93269	1.19	0.047	1035
KOI 435	33.039	2.18	0.193	509
KOI 435	62.3054	2.13	0.294	412
KOI 435	9.92025	0.87	0.086	760
KOI 505	3.25059	1.52	0.041	1035
KOI 505	87.0897	3.37	0.366	346
KOI 505	8.34808	1.66	0.077	756
KOI 509	39.5891	1.62	0.218	462
KOI 510	35.1183	2.99	0.199	523
KOI 564	6.2174	1.17	0.065	906
KOI 582	9.93964	1.24	0.085	671
KOI 584	6.47027	0.78	0.064	805
KOI 593	51.065	2.32	0.270	468
KOI 597	52.815	1.94	0.265	491
KOI 623	25.211	0.84	0.160	703
KOI 624	1.31186	1.27	0.023	1469
KOI 627	4.16523	1.22	0.054	1270
KOI 671	7.46647	1.14	0.075	933
KOI 671	11.1317	1.05	0.098	817
KOI 710	8.58569	1.68	0.090	1135
KOI 717	0.900351	0.71	0.019	1901
KOI 719	4.15976	0.75	0.045	788
KOI 719	45.904	1.29	0.225	354
KOI 719	28.1226	0.95	0.162	416
KOI 780	7.24078	8.83	0.067	674
KOI 841	-1400	4.12	2.440	146
KOI 841	6.54629	2.65	0.068	873

*Continued on next page.*

Host star	Period <sup>(1)</sup> (d)	$r$ [ $R_{\oplus}$ ]	$a^{(2)}$ [AU]	$T_{eq}$ [K]
KOI 856	0.870579	1.46	0.018	1824
KOI 1060	20.4973	1.36	0.156	766
KOI 1069	8.70385	3.41	0.080	855
KOI 1082	1.1966	1.17	0.021	1359
KOI 1082	4.09665	1.33	0.048	902
KOI 1108	1.47534	0.74	0.023	1287
KOI 1108	4.15247	0.98	0.047	911
KOI 1413	21.5274	1.21	0.139	581
KOI 1536	79.4949	1.48	0.379	450
KOI 1574	191.512	2.05	0.634	281
KOI 1593	15.3837	1.94	0.121	679
KOI 1599	13.6129	2.15	0.111	737
KOI 1601	62.9135	1.35	0.299	401
KOI 1650	100.829	3.55	0.423	345
KOI 1681	1.99278	0.88	0.025	748
KOI 1681	3.53109	0.93	0.037	618
KOI 1830	198.704	2.64	0.565	220
KOI 1831	4.38508	0.76	0.050	890
KOI 1843	0.176892	0.68	0.005	1654
KOI 1870	-530	6.97	1.211	191
KOI 1871	32.3763	1.67	0.172	370
KOI 1875	0.538349	1.18	0.013	2157
KOI 1955	1.64423	0.69	0.028	1684
KOI 1955	26.2335	2.52	0.180	669
KOI 1972	1.22623	0.67	0.022	1671
KOI 1986	7.12775	2.68	0.071	1080
KOI 2004	3.18895	0.89	0.041	1153
KOI 2055	4.02581	1.13	0.047	994
KOI 2055	2.50465	1.02	0.035	1164
KOI 2159	2.39265	0.90	0.034	1229
KOI 2193	4.1629	3.54	0.043	695
KOI 2195	30.0918	1.74	0.198	644
KOI 2195	6.85035	1.20	0.074	1055
KOI 2243	8.45812	1.63	0.082	885
KOI 2485	3.60087	1.32	0.042	929
KOI 2485	5.72691	1.44	0.057	796
KOI 2579	3.59657	1.27	0.046	1277
KOI 2579	10.3007	1.59	0.092	899
KOI 2597	5.61365	1.30	0.064	1107

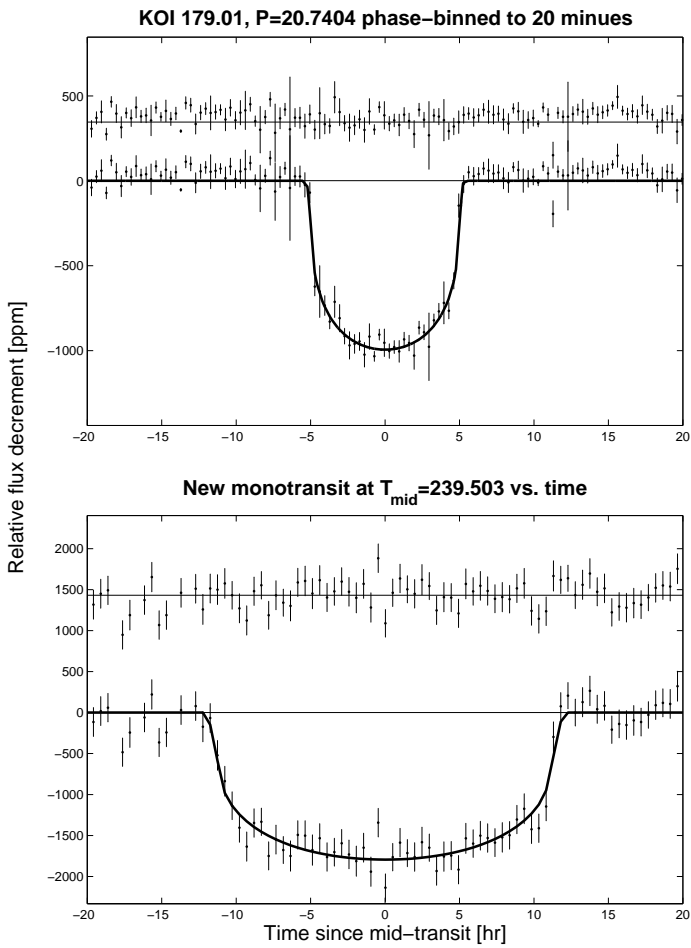


Fig. A.1. Similar to Figure 3.

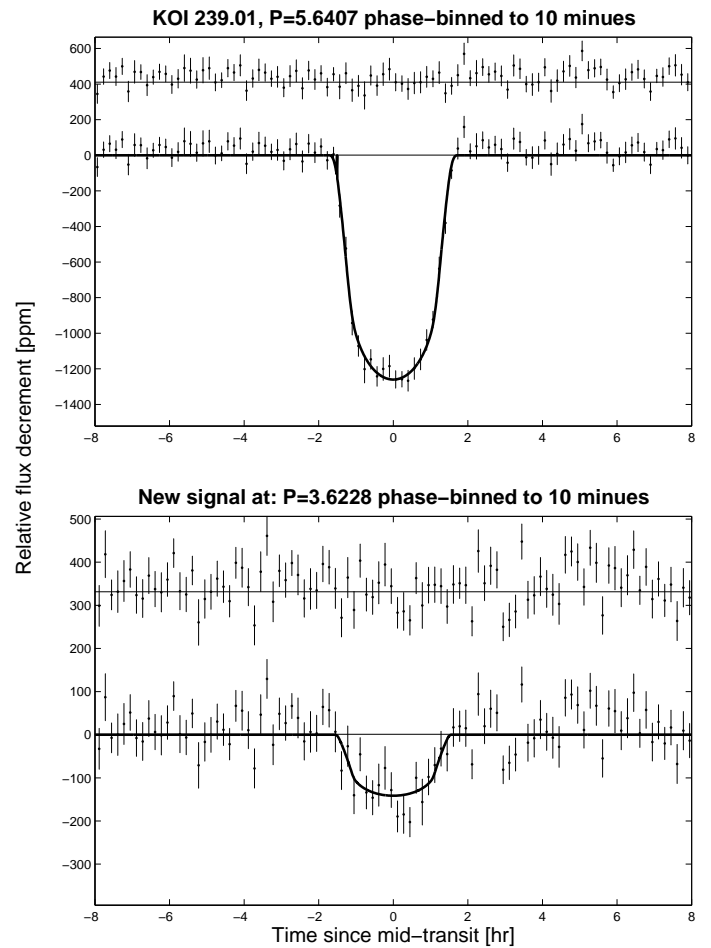


Fig. A.2. Similar to Figure 3.

### Appendix A: Appendix A

This appendix contain the figures representing the global fits for “regular” systems with new detections, where we have little/no special comments. The figures are given primarily to show the reality of te signals.

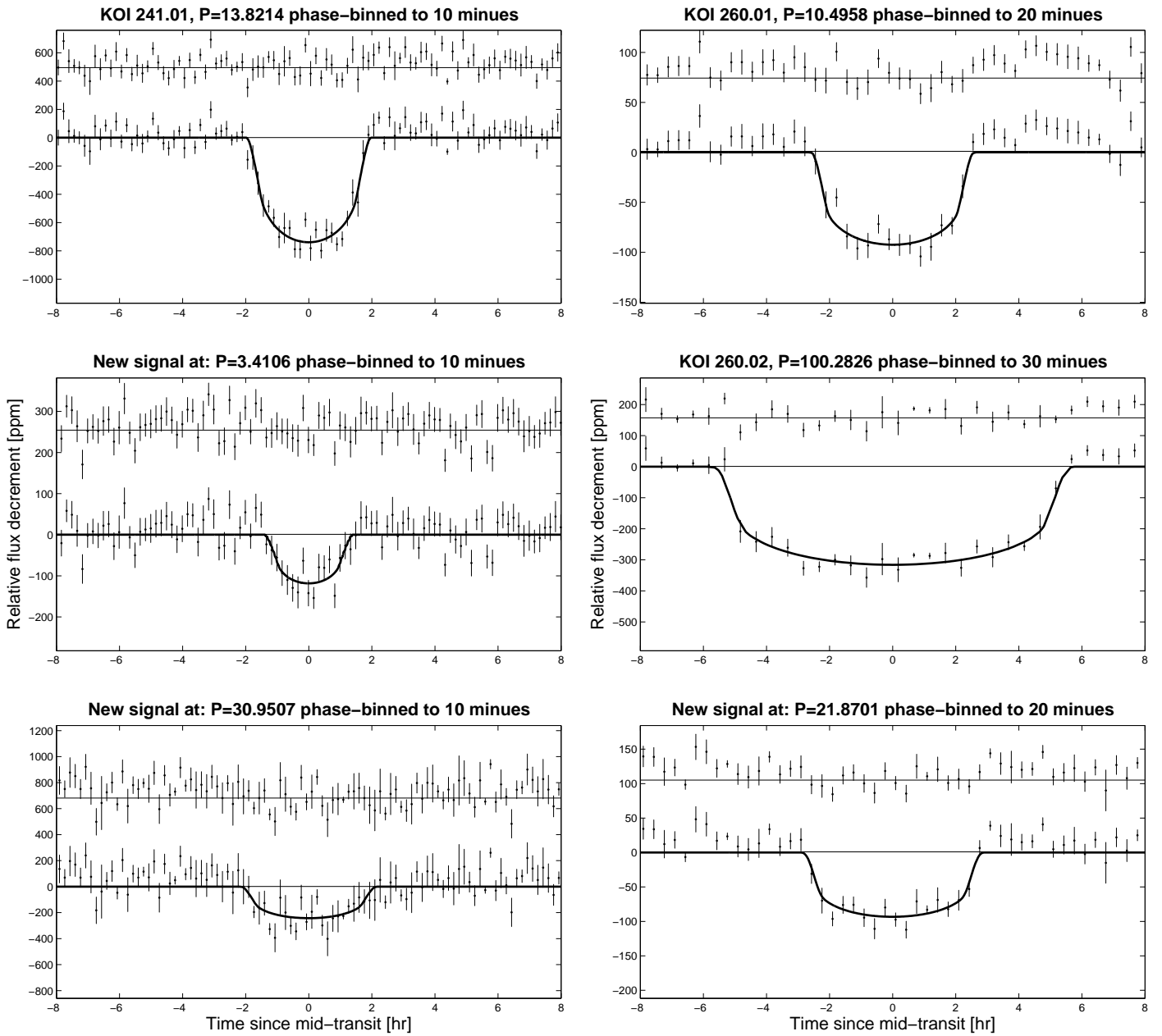


Fig. A.3. Similar to Figure 3.

Fig. A.4. Similar to Figure 3.

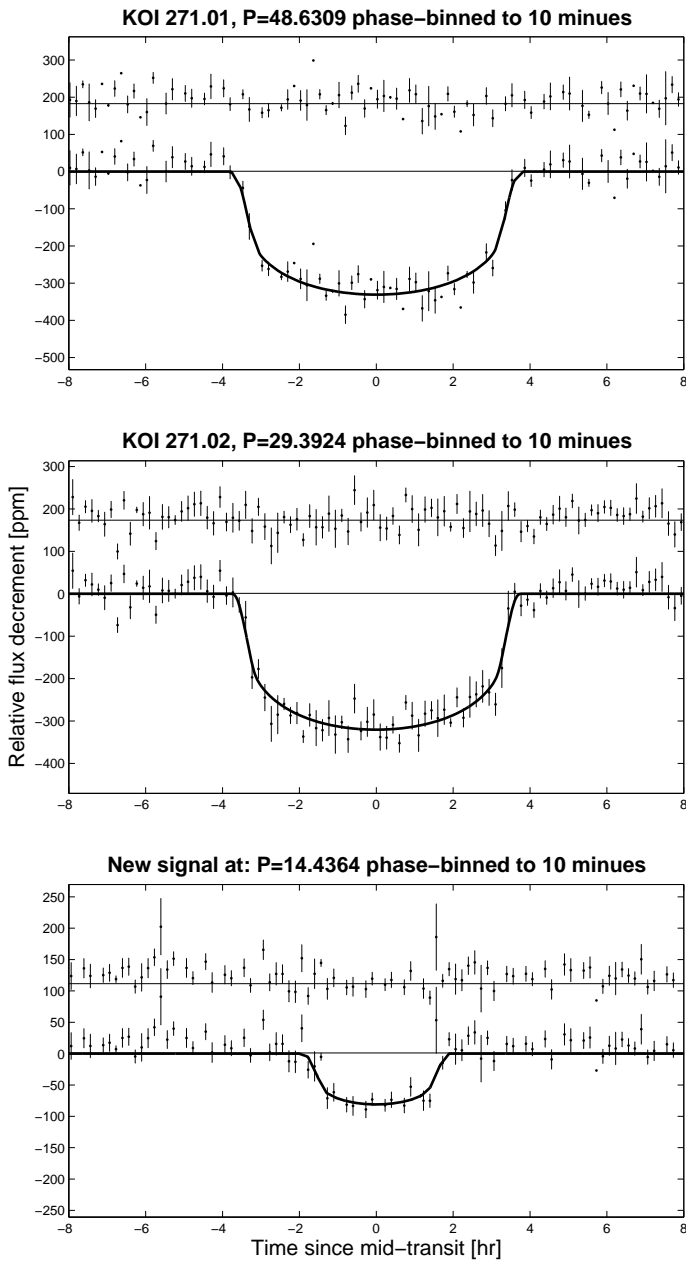


Fig. A.5. Similar to Figure 3.

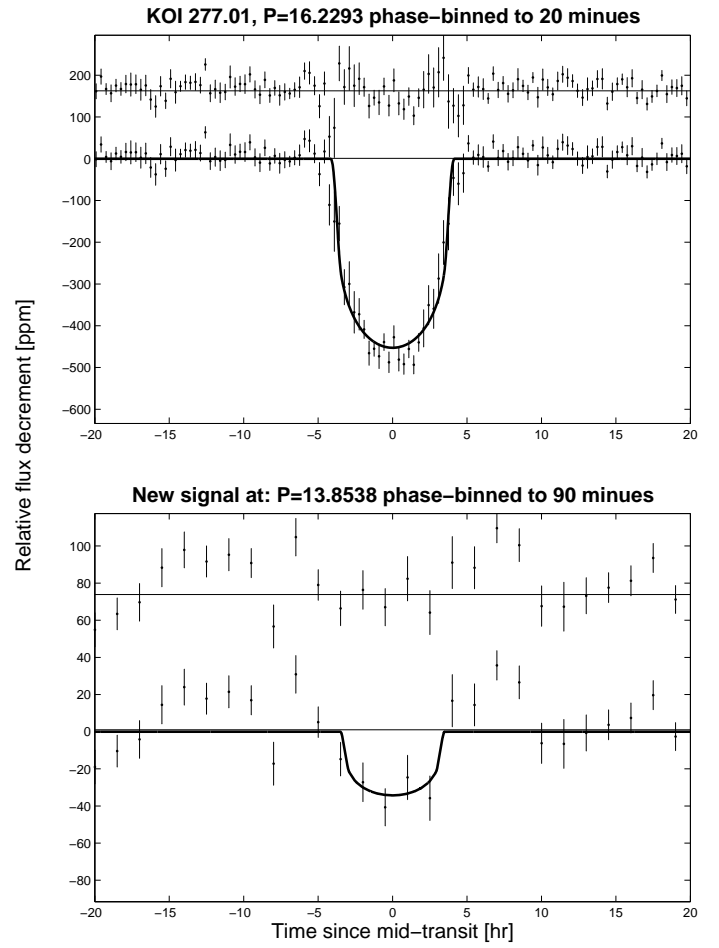


Fig. A.6. Similar to Figure 3.

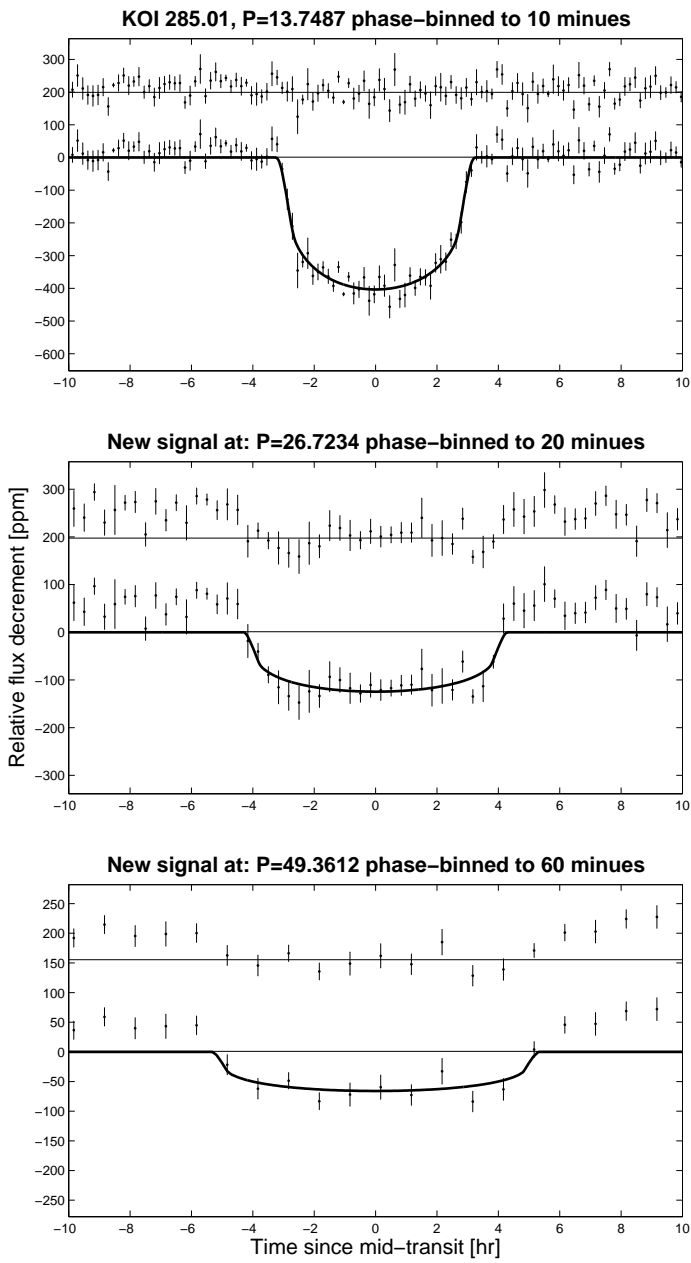


Fig. A.7. Similar to Figure 3.

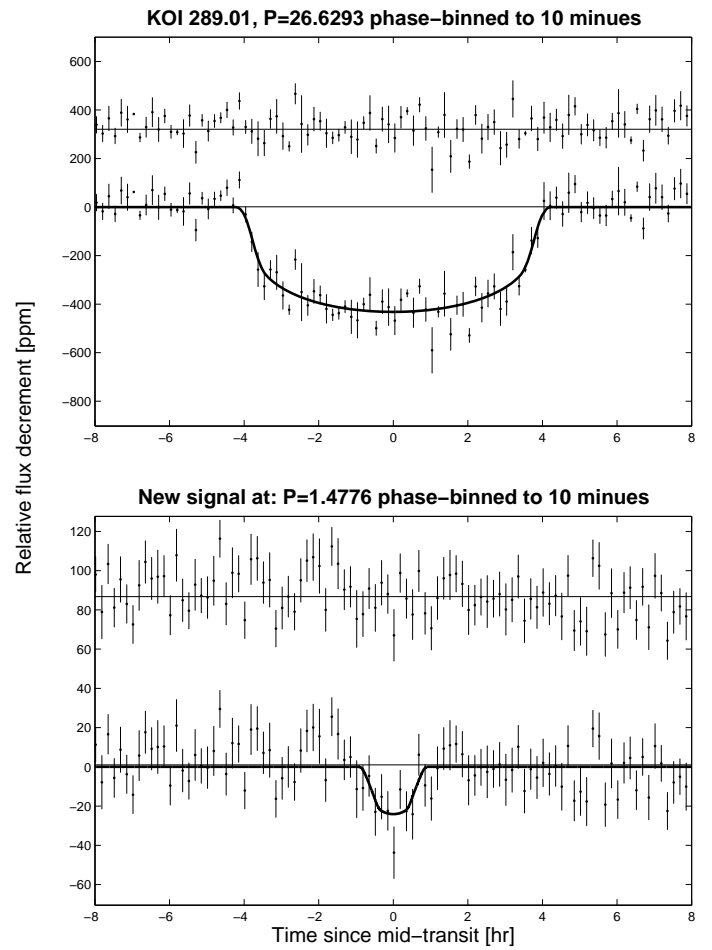


Fig. A.8. Similar to Figure 3.

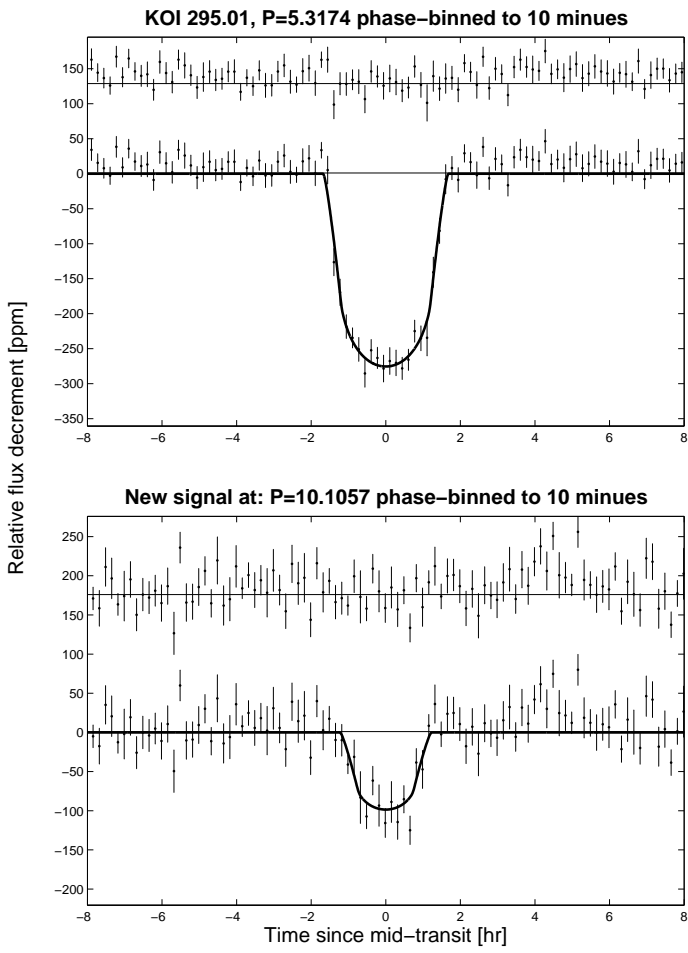


Fig. A.9. Similar to Figure 3.

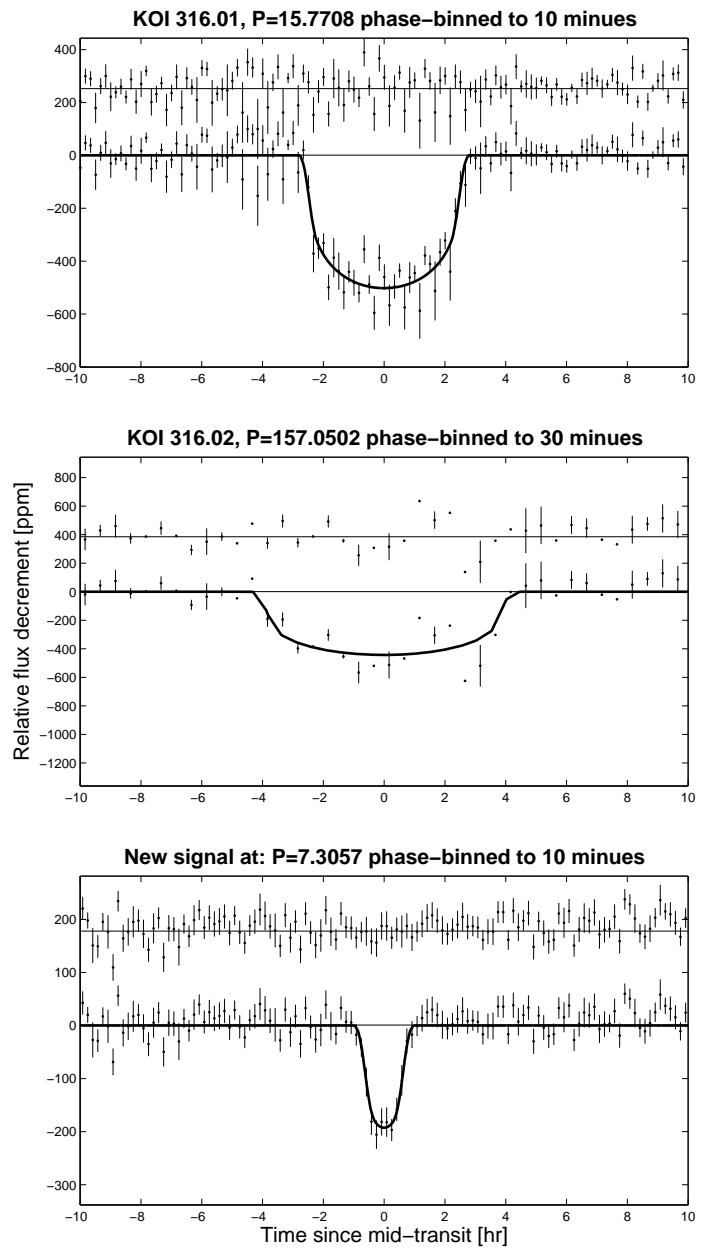


Fig. A.10. Similar to Figure 3.

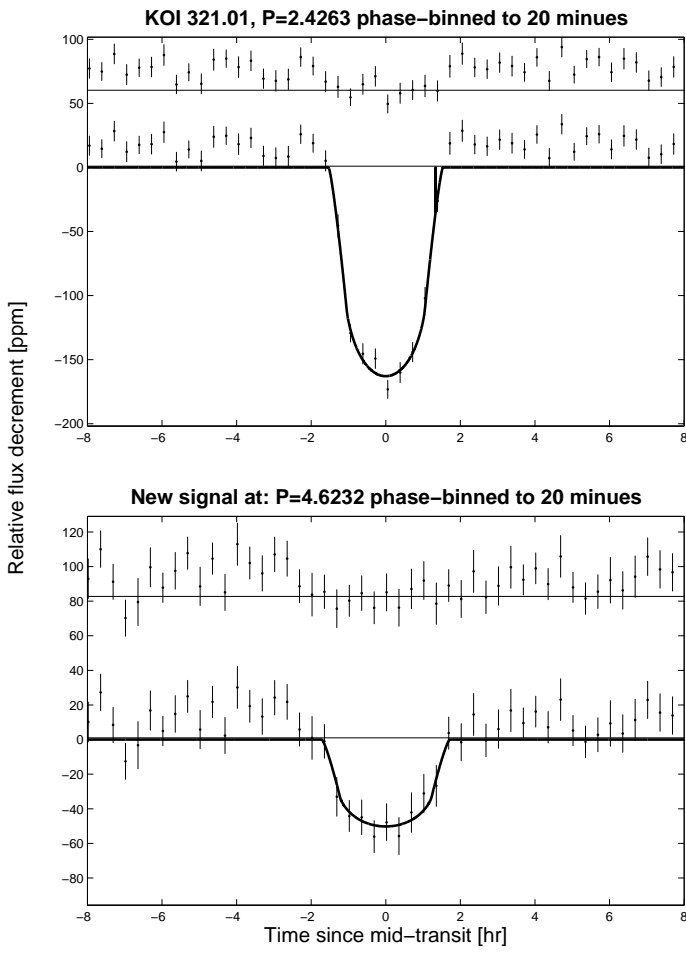


Fig. A.11. Similar to Figure 3.

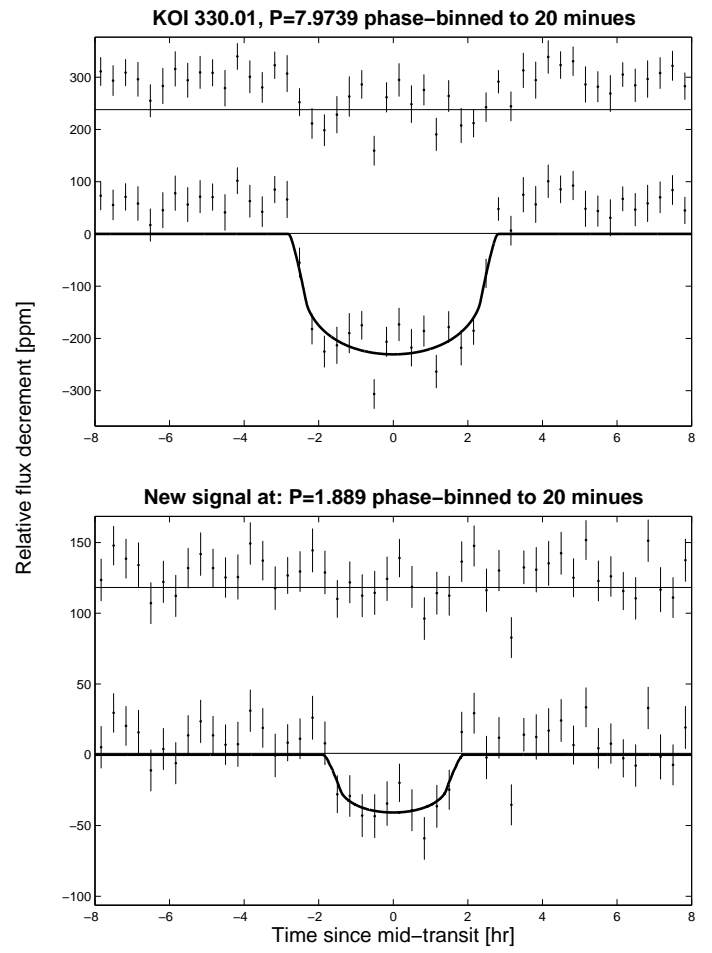
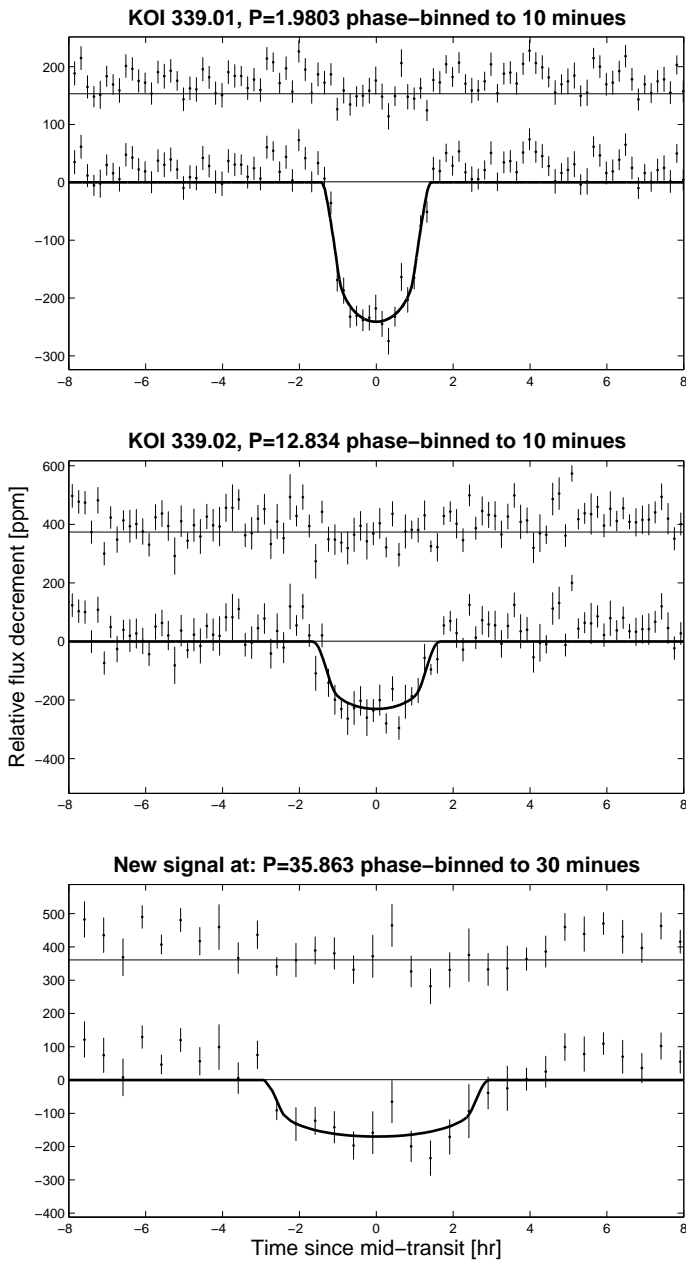
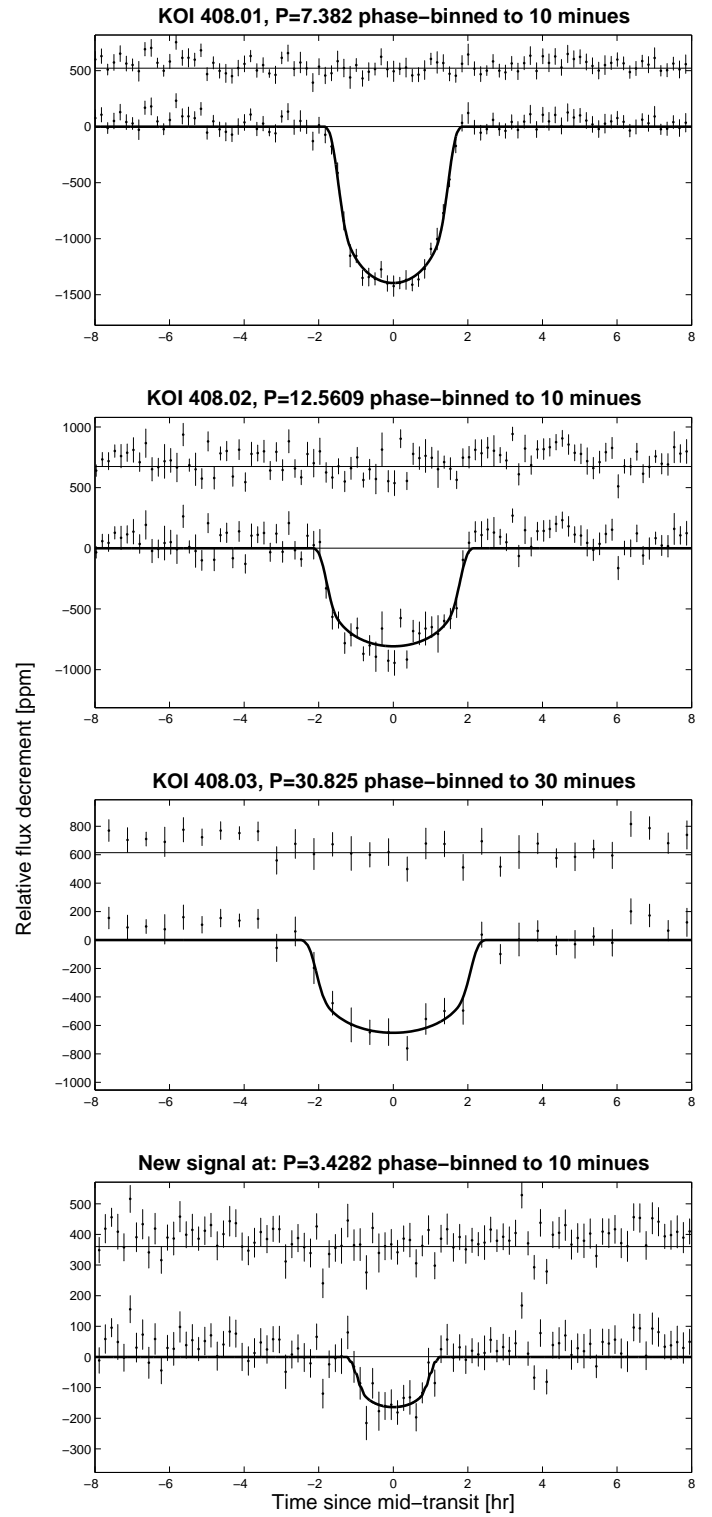


Fig. A.12. Similar to Figure 3.



**Fig. A.13.** Similar to Figure 3.



**Fig. A.14.** Similar to Figure 3.

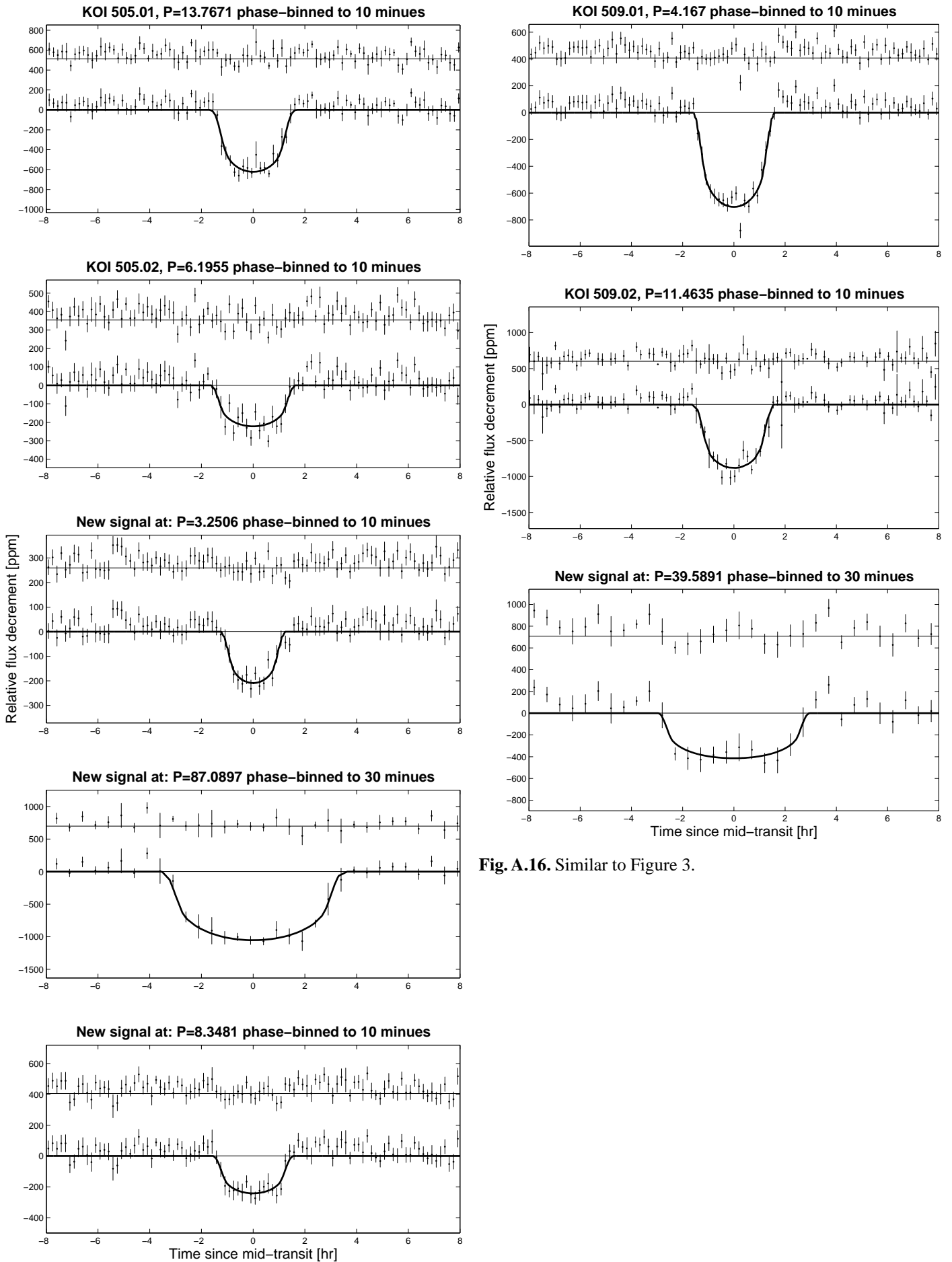


**Fig. A.16.** Similar to Figure 3.

**Fig. A.15.** Similar to Figure 3.

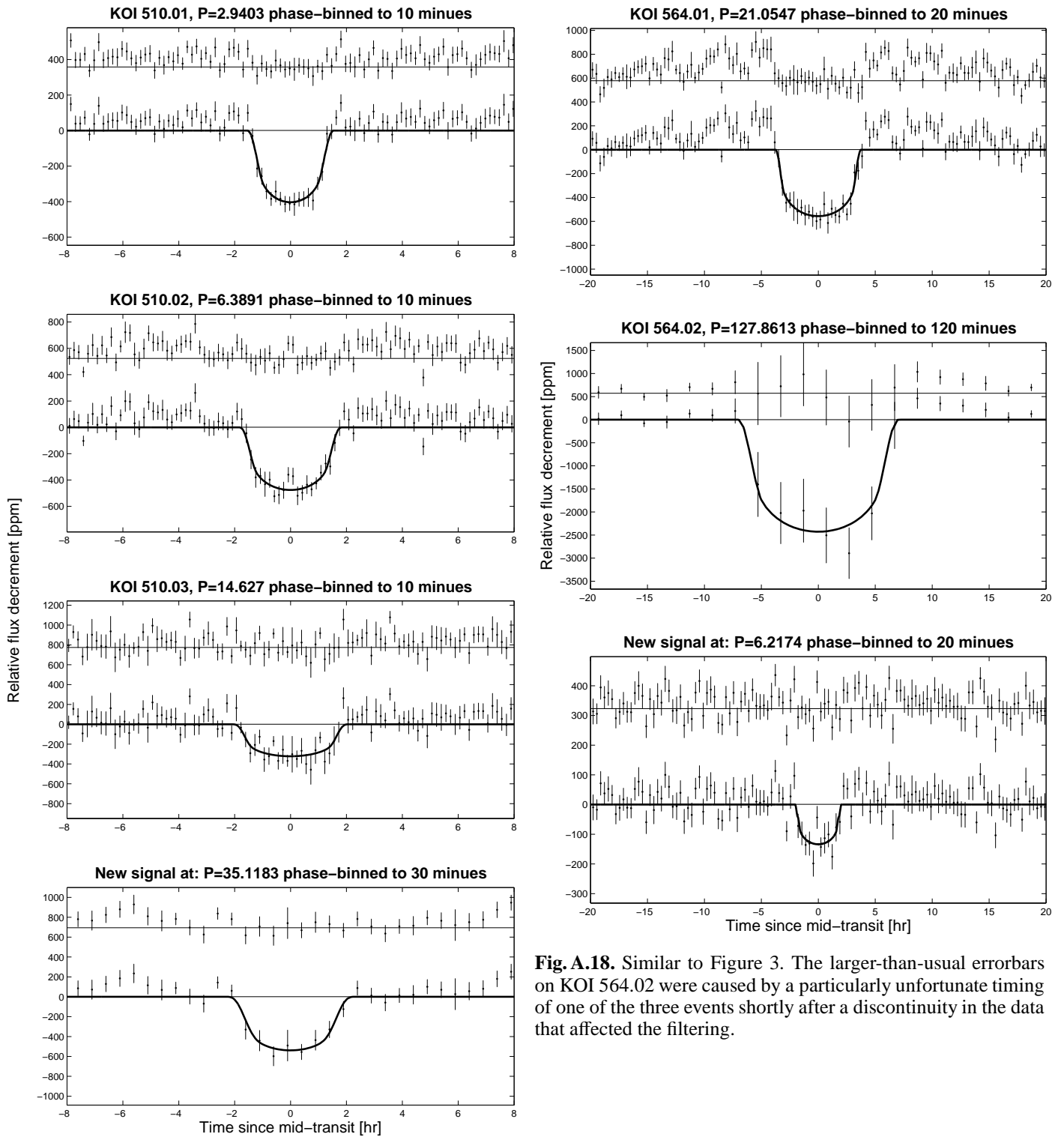


**Fig. A.17.** Similar to Figure 3.

**Fig. A.18.** Similar to Figure 3. The larger-than-usual errorbars on KOI 564.02 were caused by a particularly unfortunate timing of one of the three events shortly after a discontinuity in the data that affected the filtering.

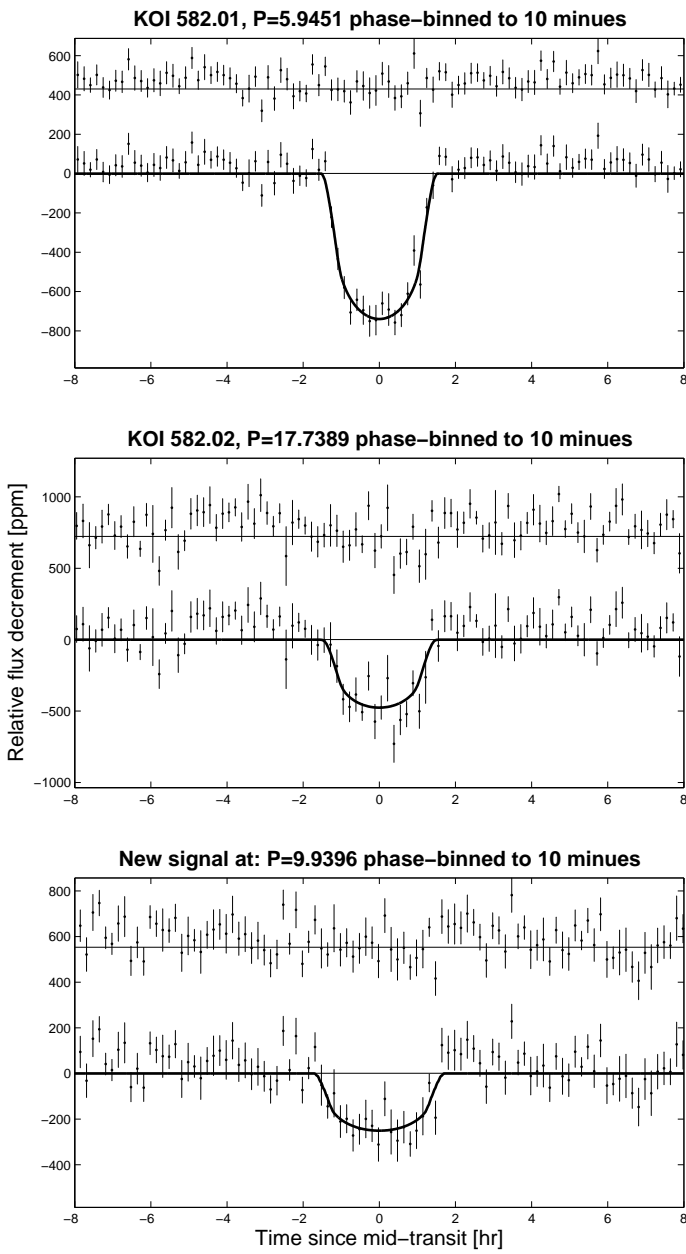


**Fig. A.19.** Similar to Figure 3.

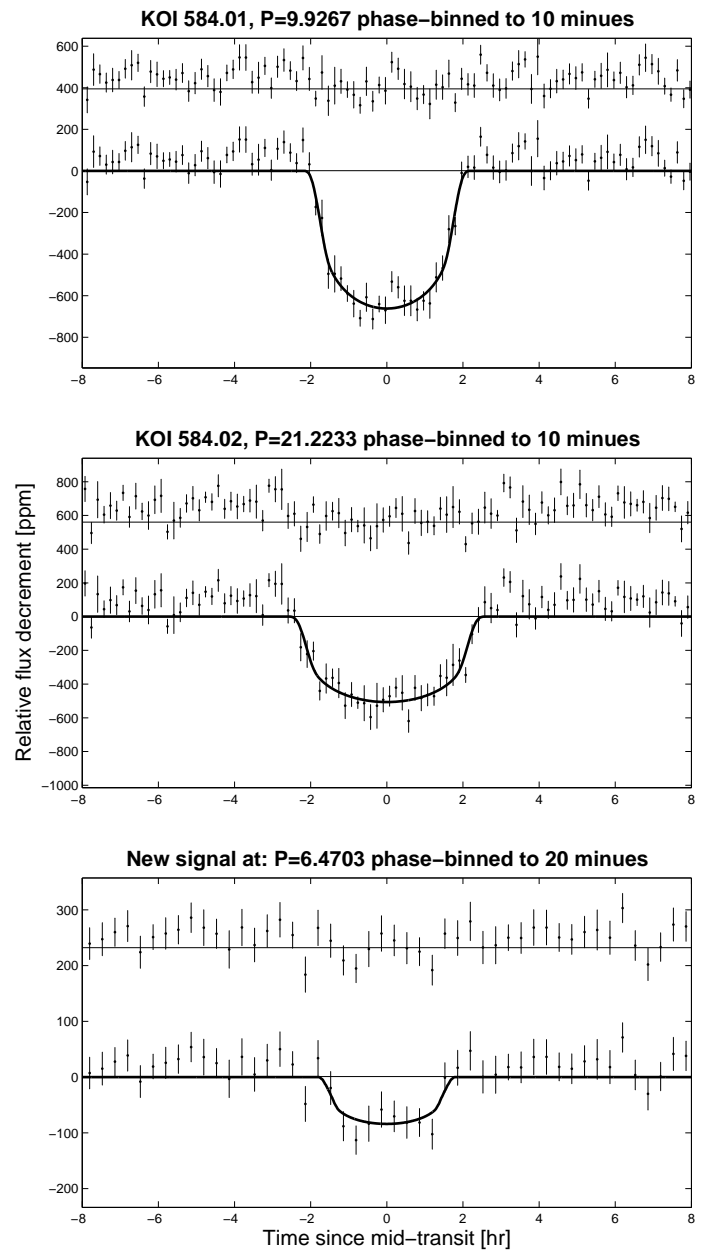


**Fig. A.20.** Similar to Figure 3. Note an even shallower, and thus much less robust, transit-like signal was detected at phase 0.59 (see text) relative to the new 6.47d signal.

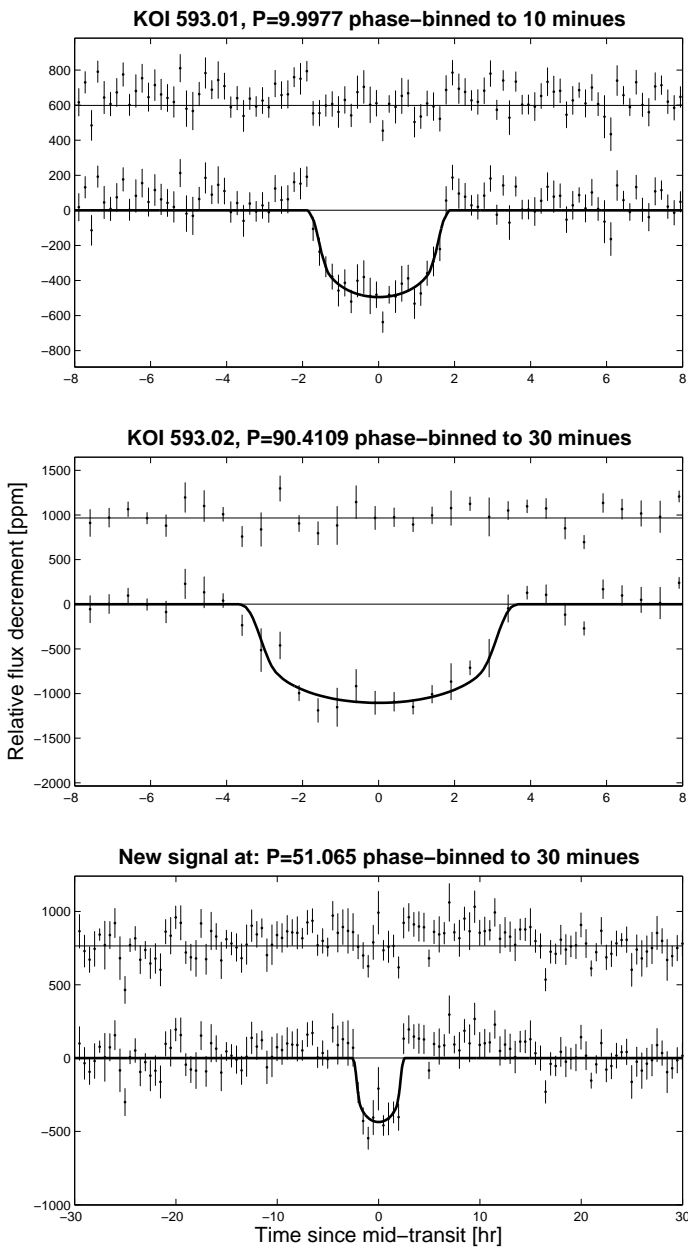


Fig. A.21. Similar to Figure 3.

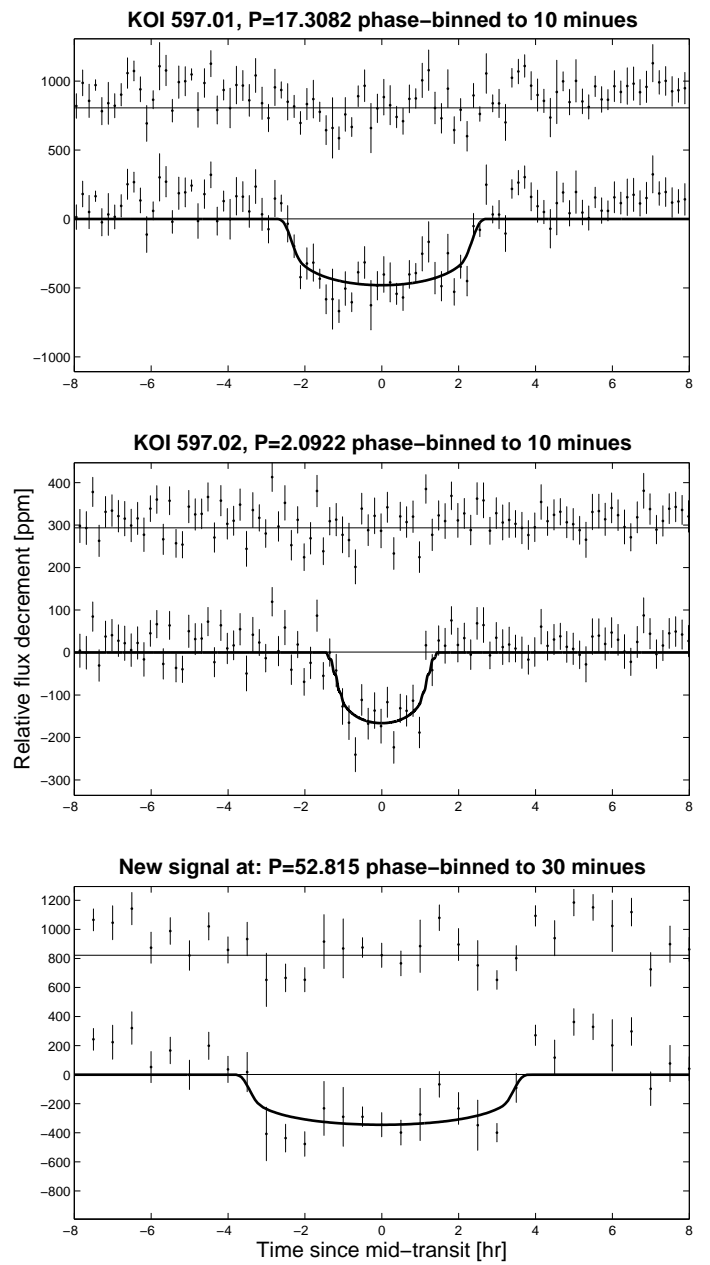
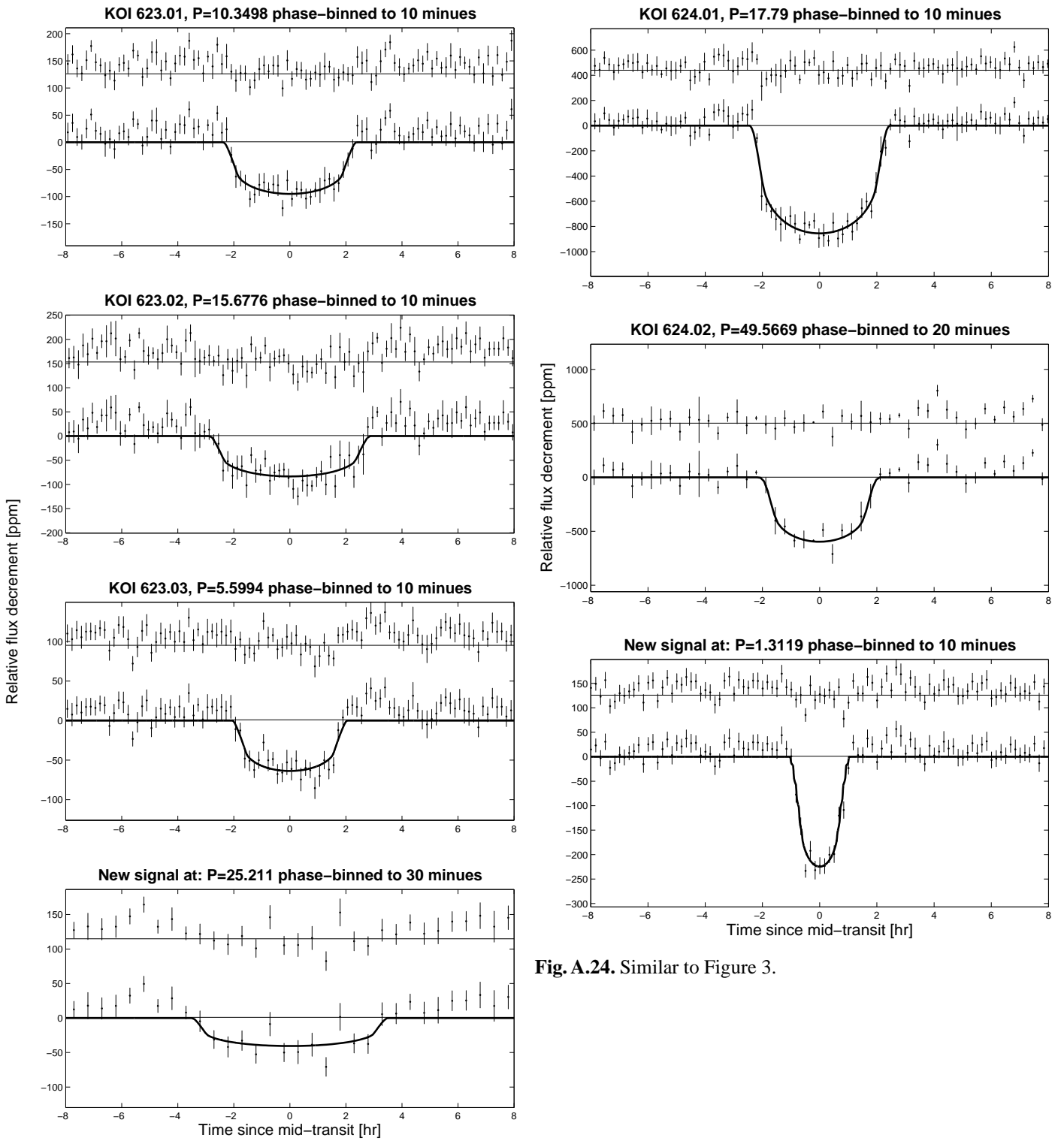


Fig. A.22. Similar to Figure 3.



**Fig. A.23.** Similar to Figure 3.

**Fig. A.24.** Similar to Figure 3.

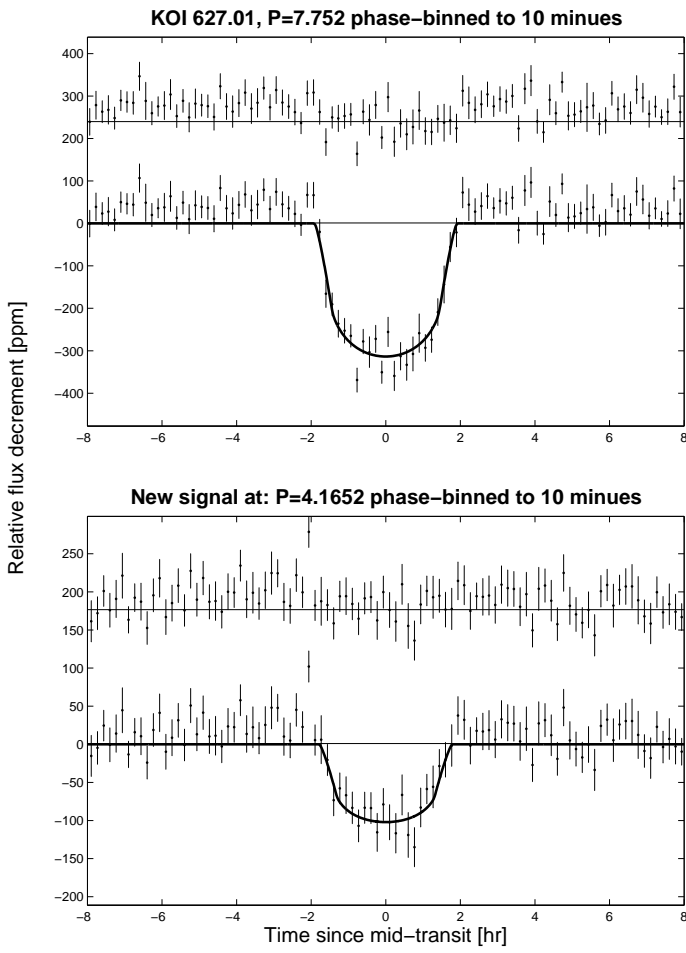


Fig. A.25. Similar to Figure 3.

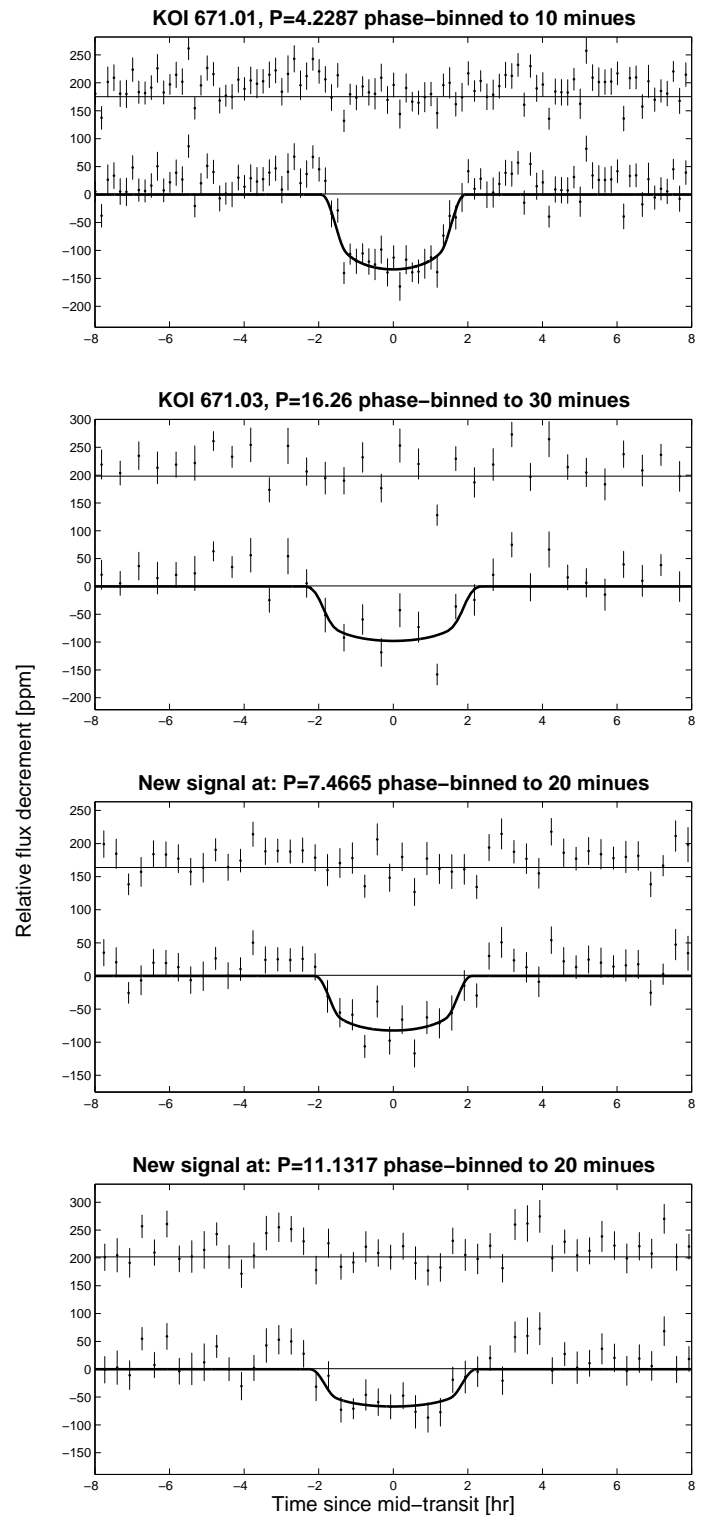


Fig. A.26. Similar to Figure 3.

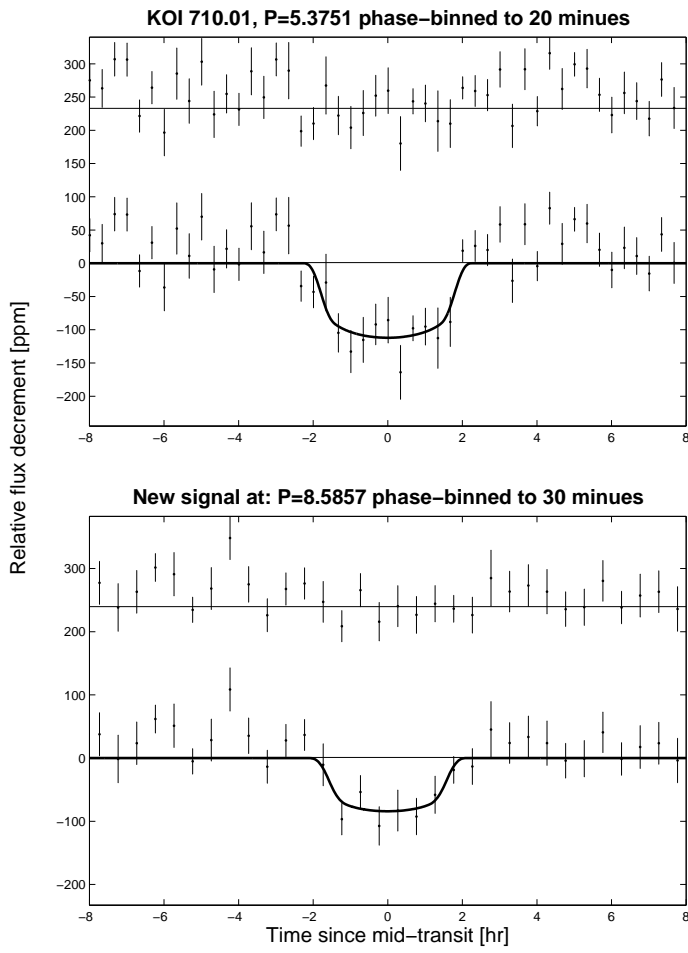


Fig. A.27. Similar to Figure 3.

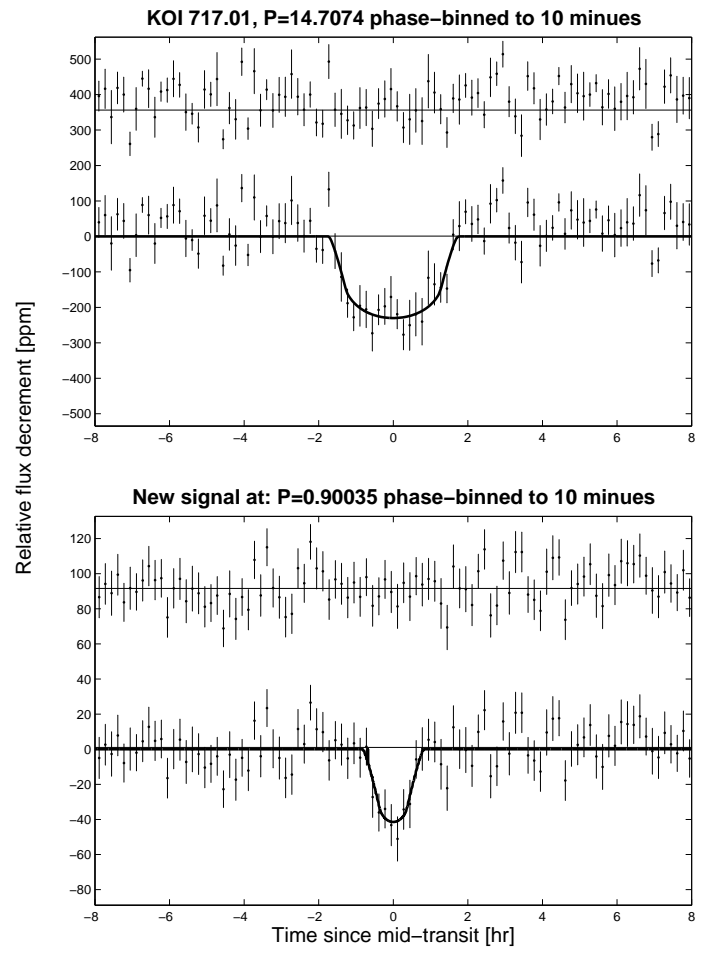
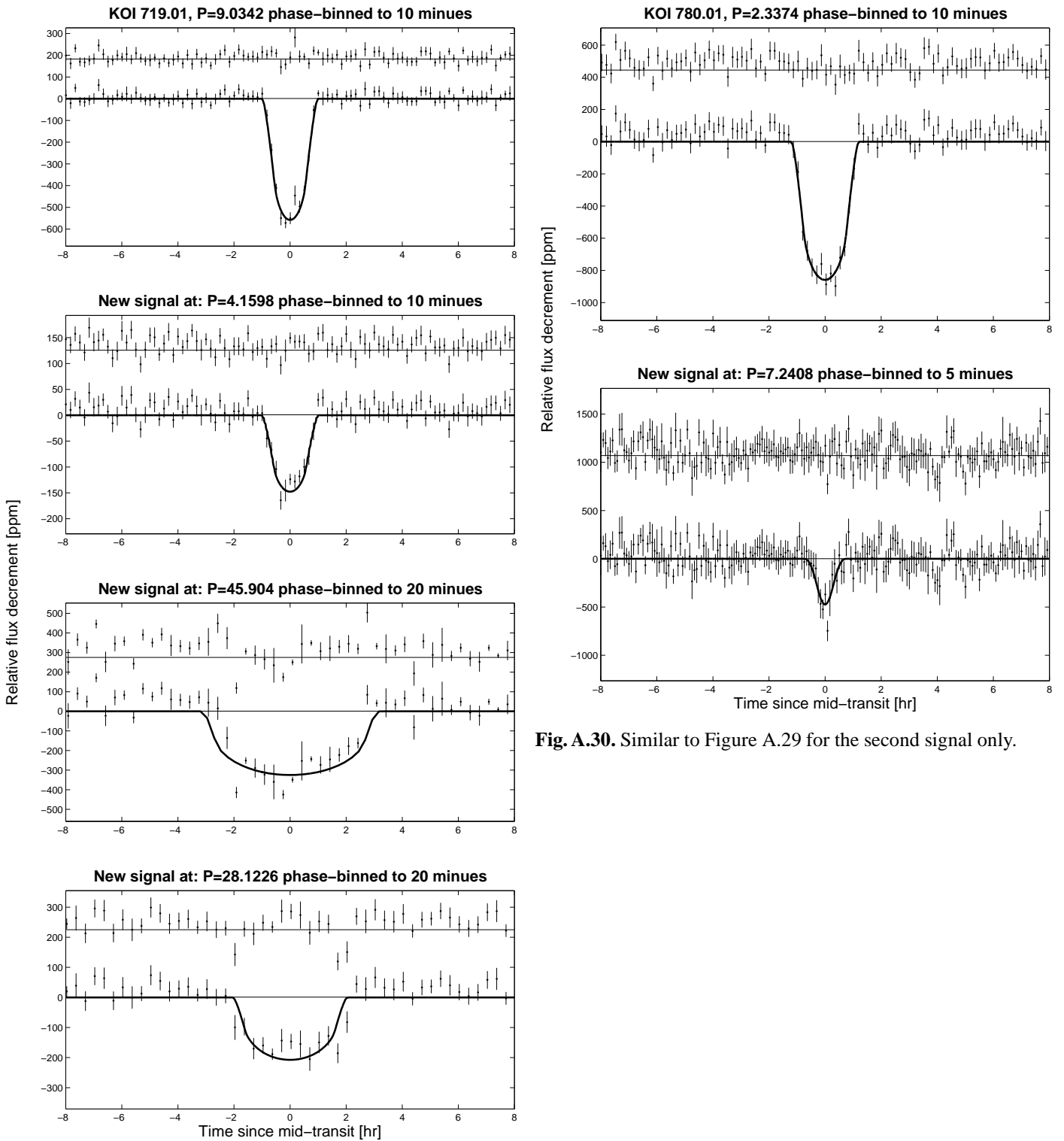
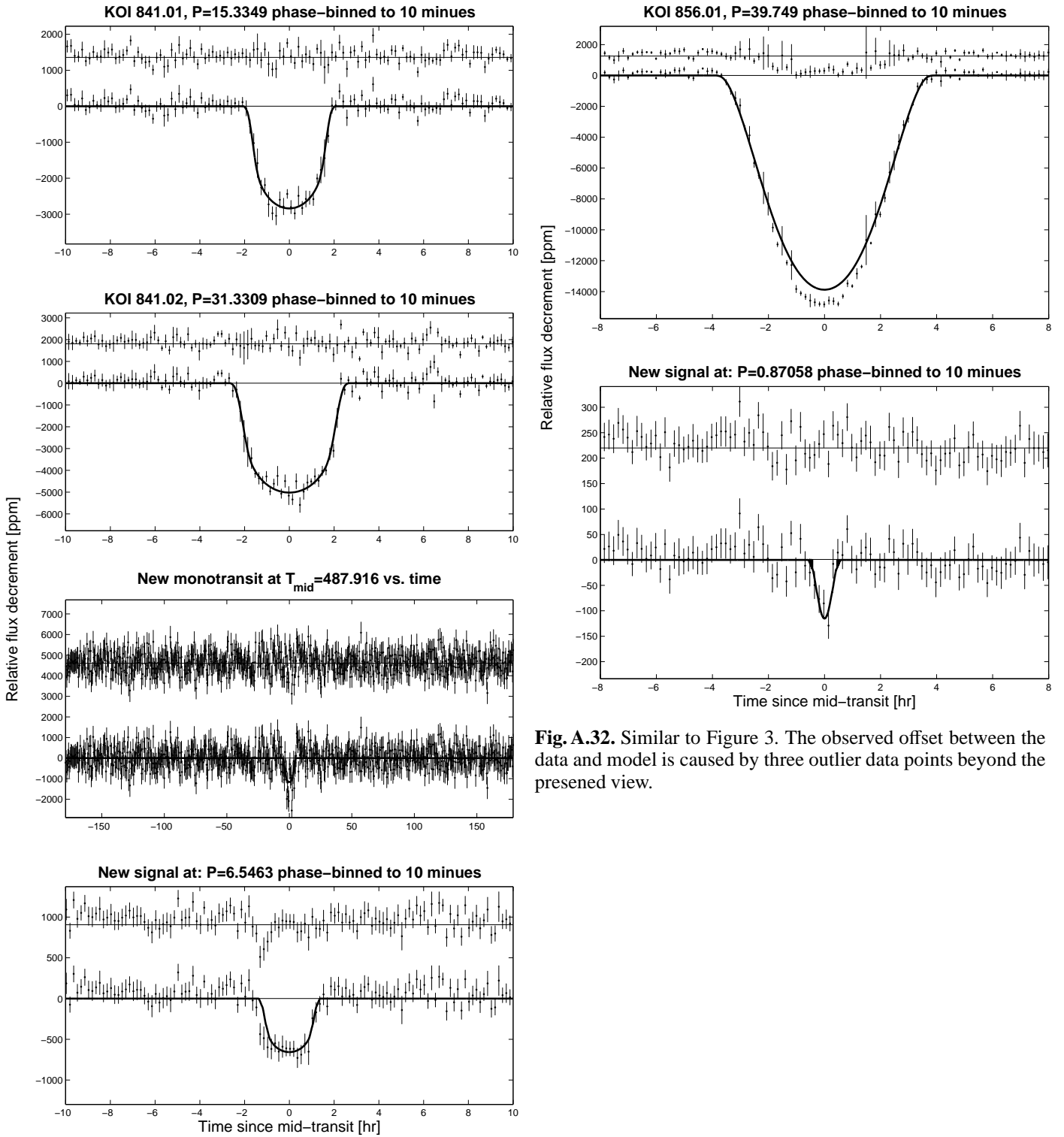


Fig. A.28. Similar to Figure 3.



**Fig. A.30.** Similar to Figure A.29 for the second signal only.

**Fig. A.29.** Similar to Figure 3. We note that this system apparently shows the effect of eccentricity by exhibiting too-long transits for two of the new signals (see text).



**Fig. A.32.** Similar to Figure 3. The observed offset between the data and model is caused by three outlier data points beyond the presented view.

**Fig. A.31.** Similar to Figure 3. We note that the 14.98d signal is probably not from the same system as the other signals (see text). The model shown here has its eccentricity parameter  $e \sin \omega$  allowed to vary simply to produce a good, albeit astrophysically meaningless, fit.

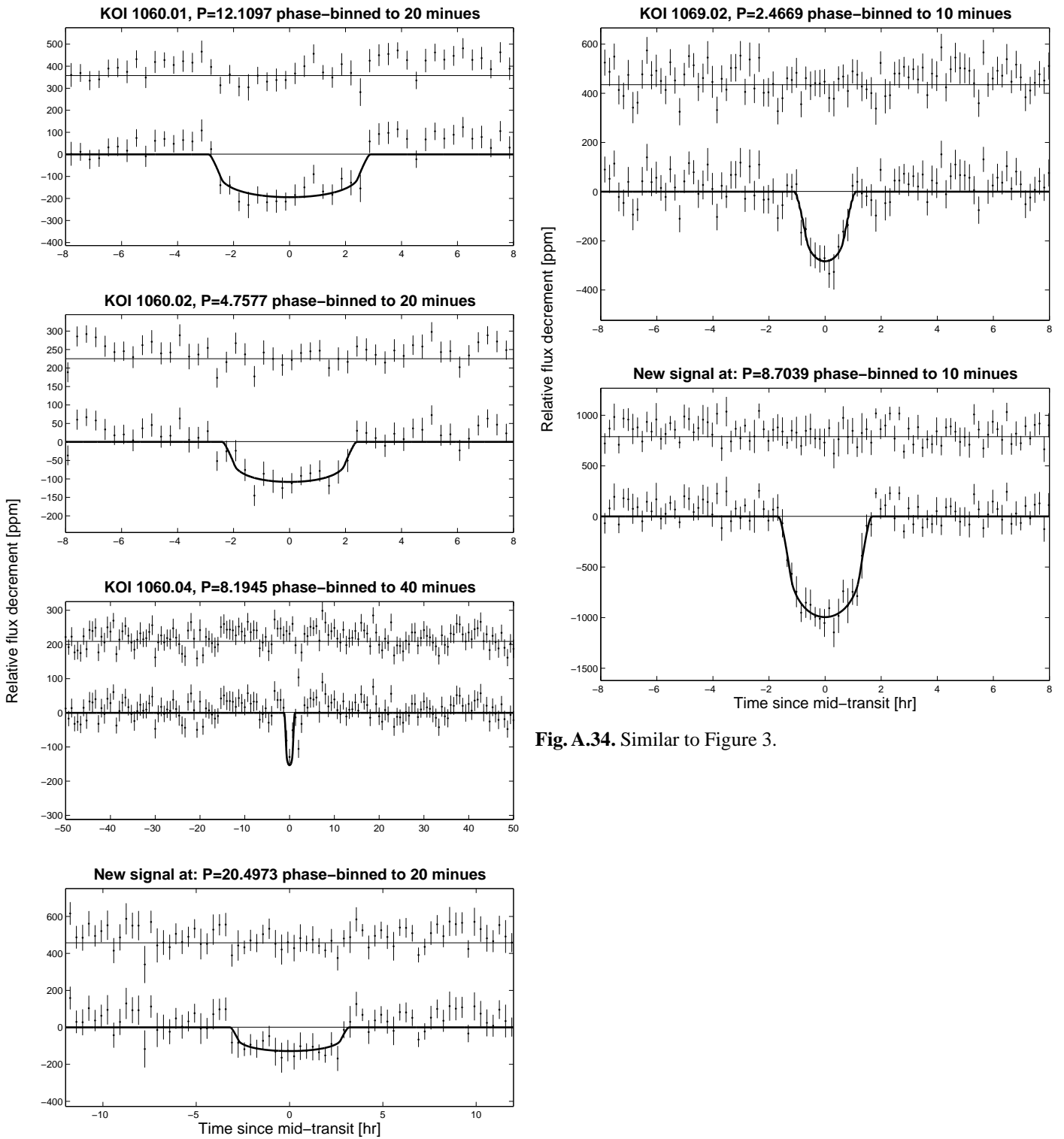


Fig. A.34. Similar to Figure 3.

Fig. A.33. Similar to Figure 3. We note the large window for KOI 1060.04, spanning about half the orbital period, was chosen to highlight the significance of this shallow signal.

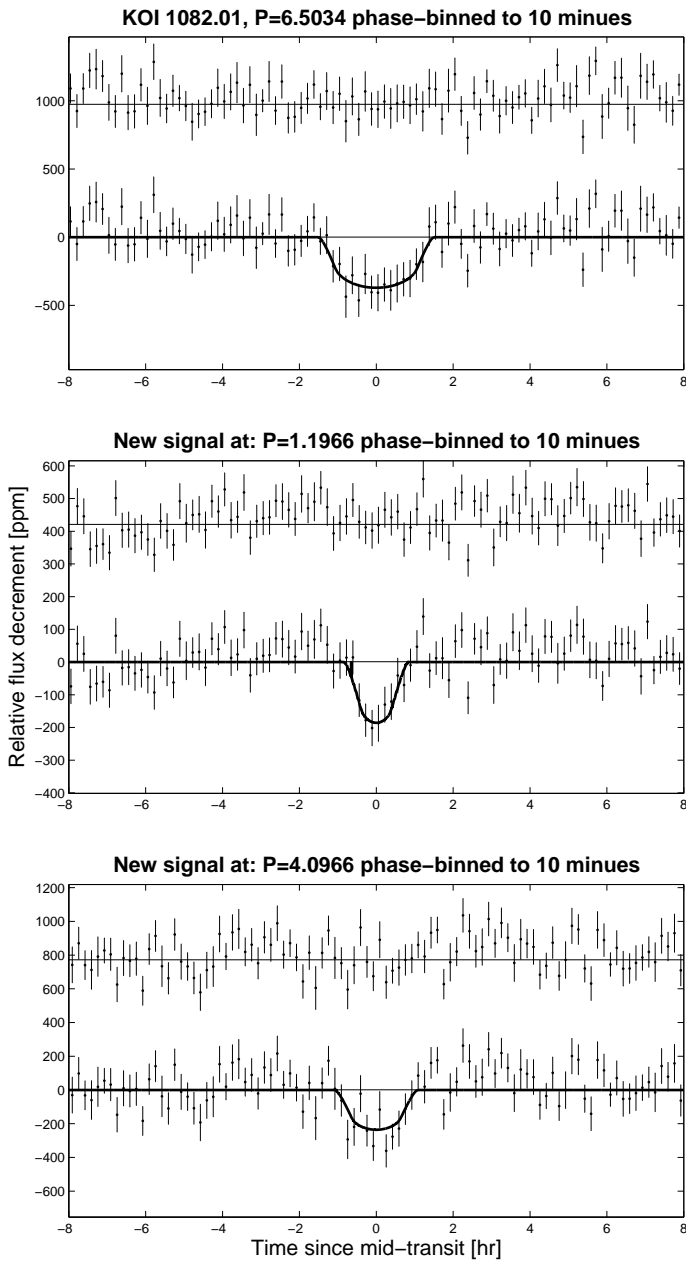


Fig. A.35. Similar to Figure 3.

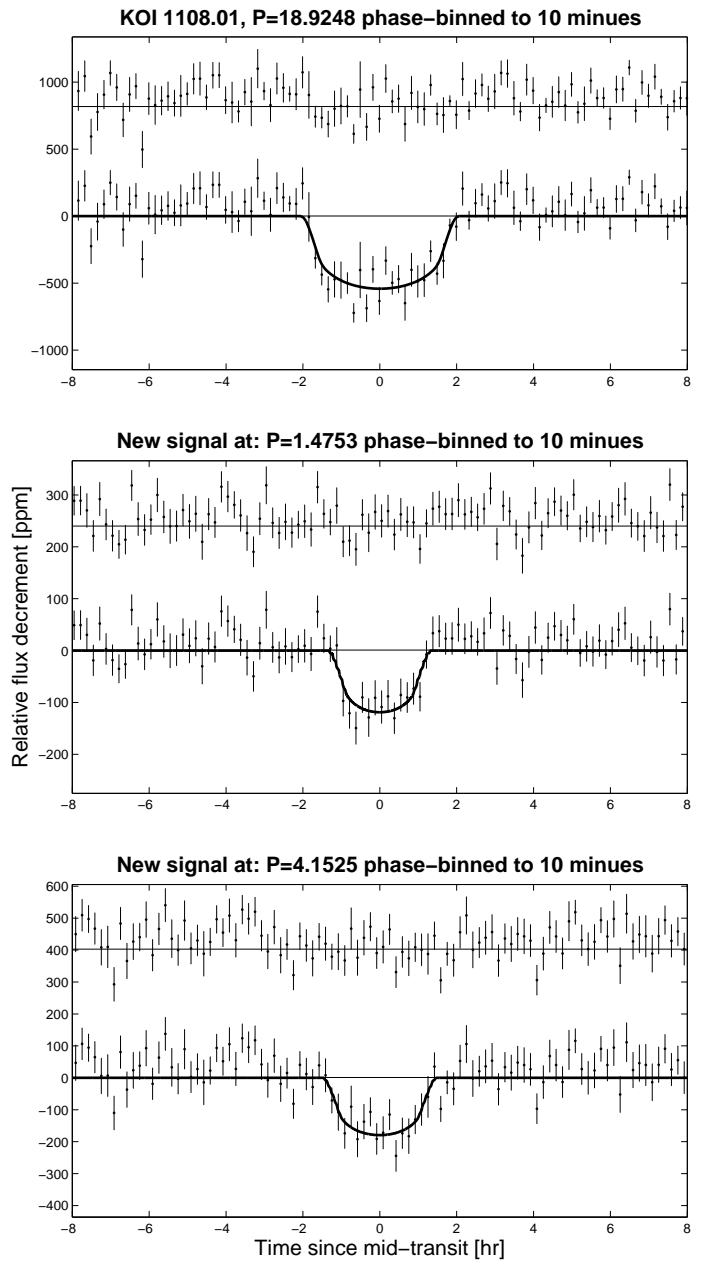


Fig. A.36. Similar to Figure 3.

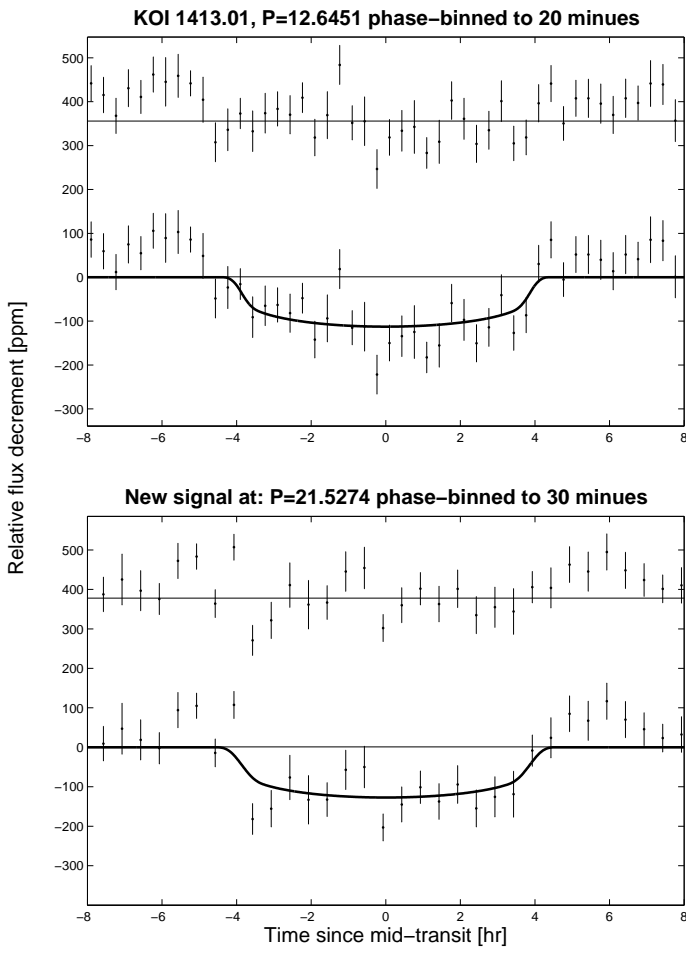


Fig. A.37. Similar to Figure 3.

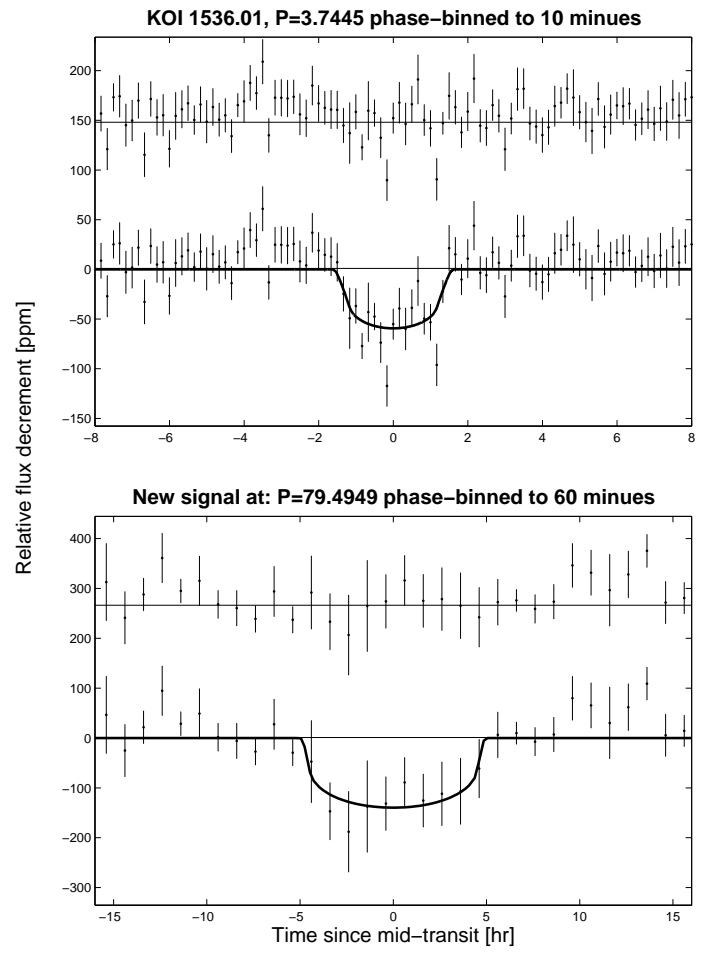


Fig. A.38. Similar to Figure 3.

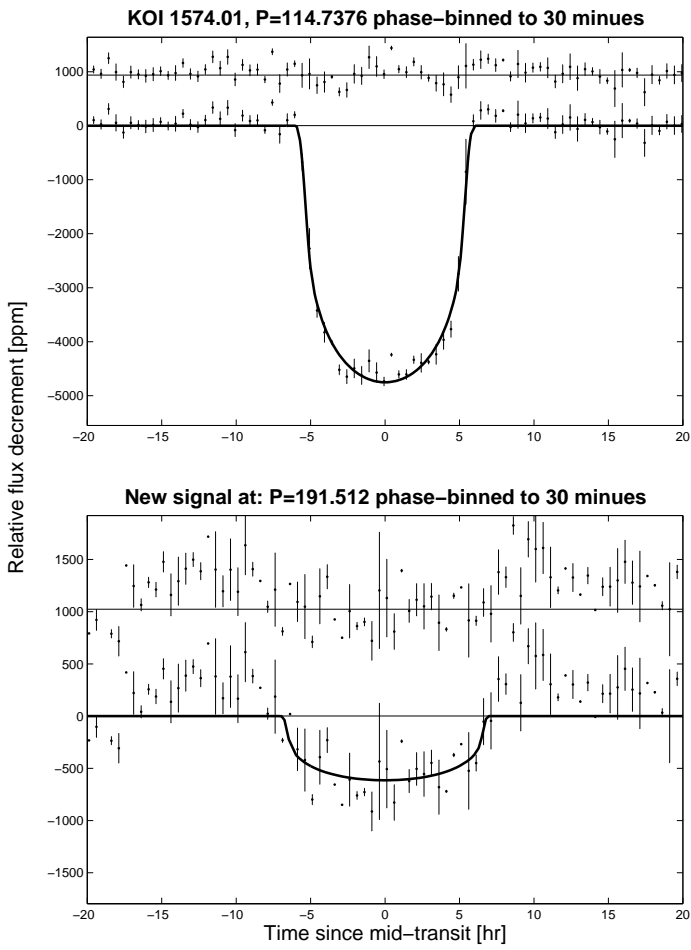


Fig. A.39. Similar to Figure 3.

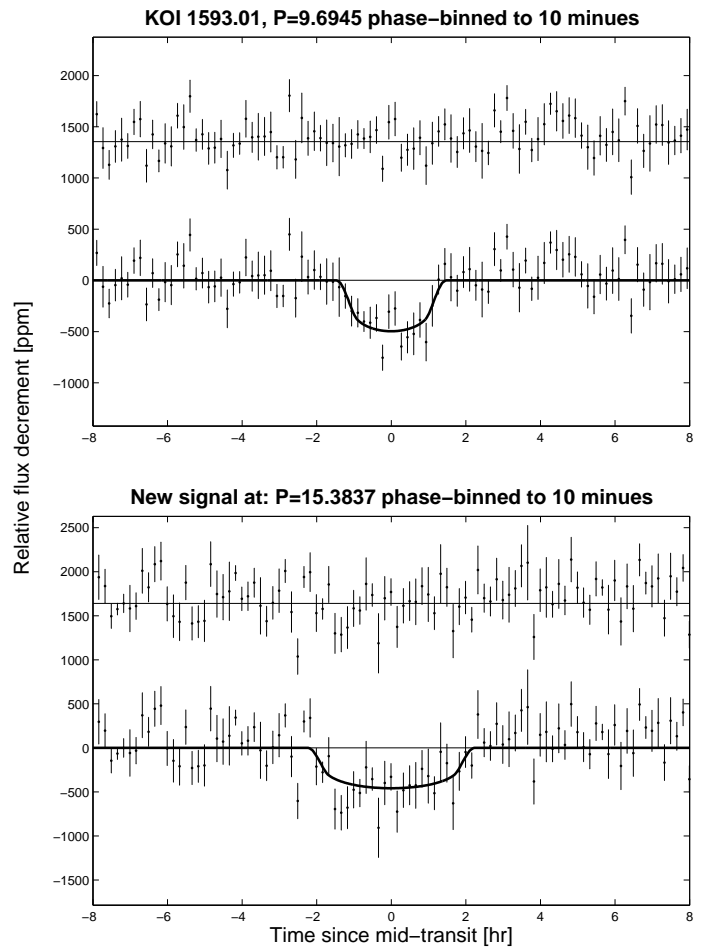


Fig. A.40. Similar to Figure 3.

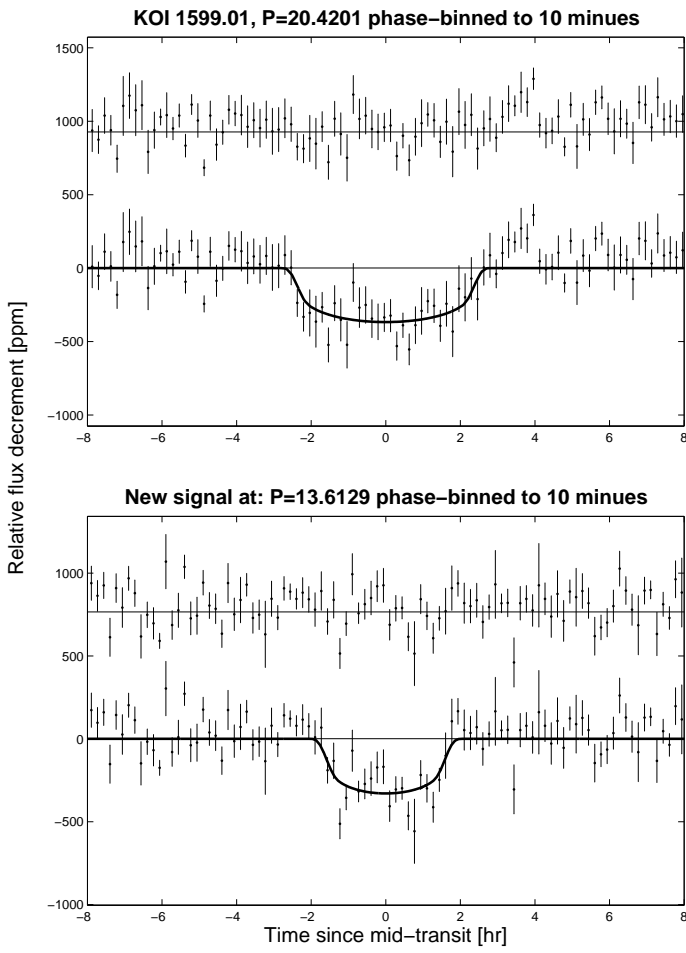


Fig. A.41. Similar to Figure 3.

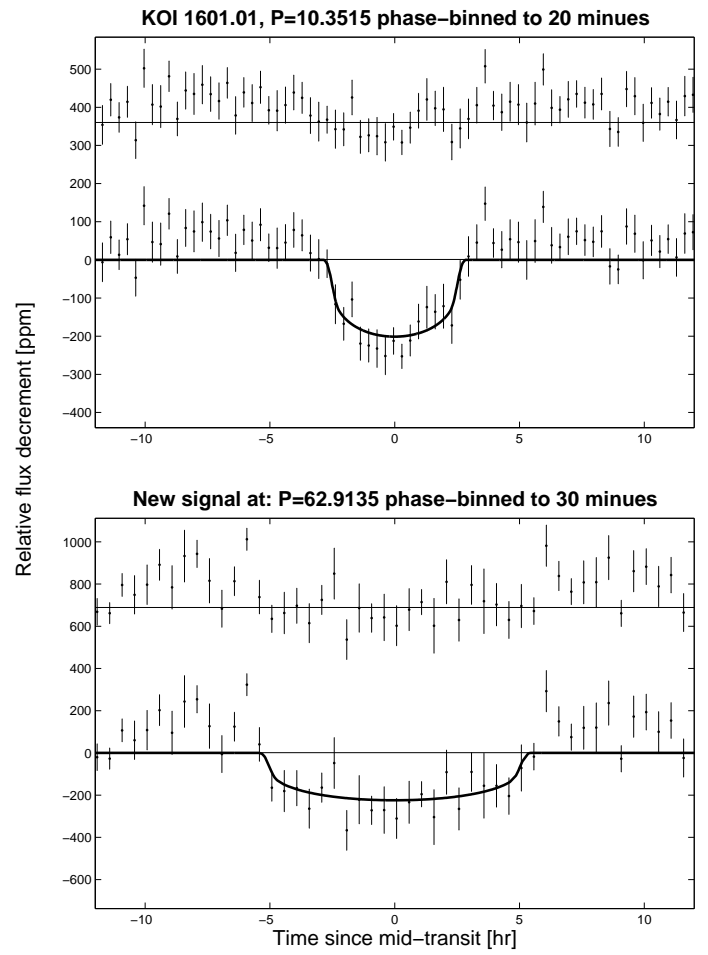


Fig. A.42. Similar to Figure 3.

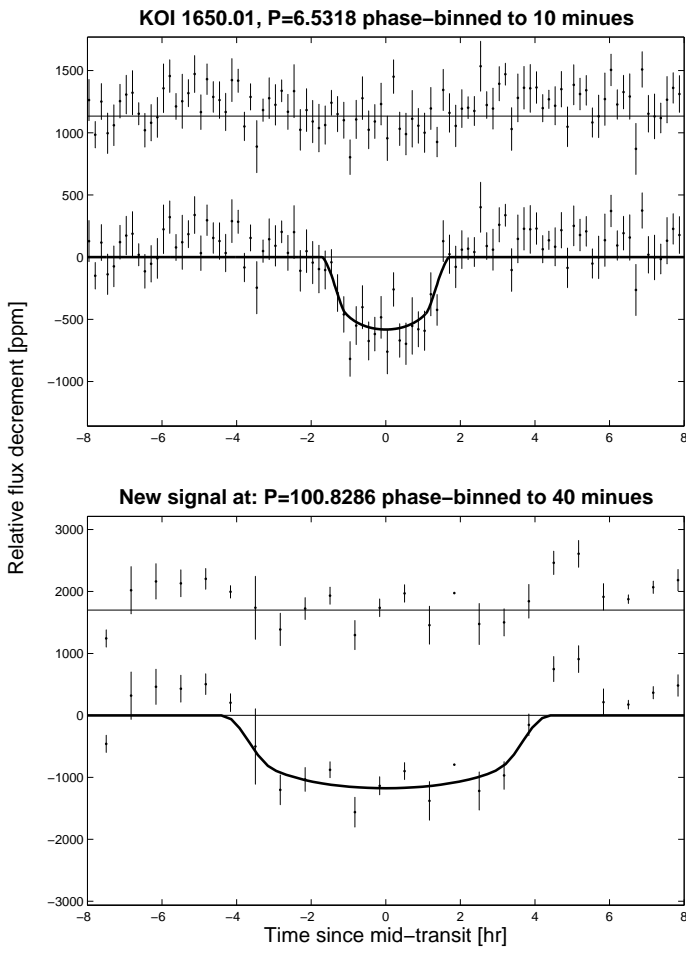


Fig. A.43. Similar to Figure 3.

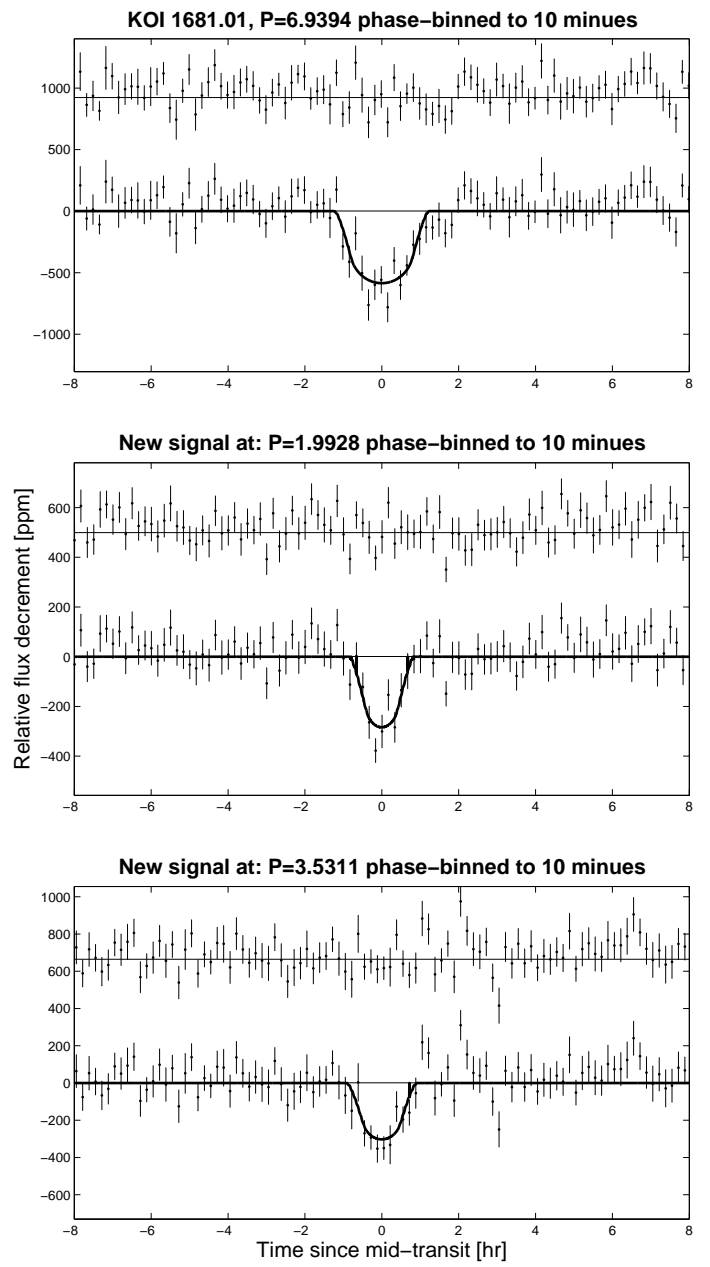


Fig. A.44. Similar to Figure 3.

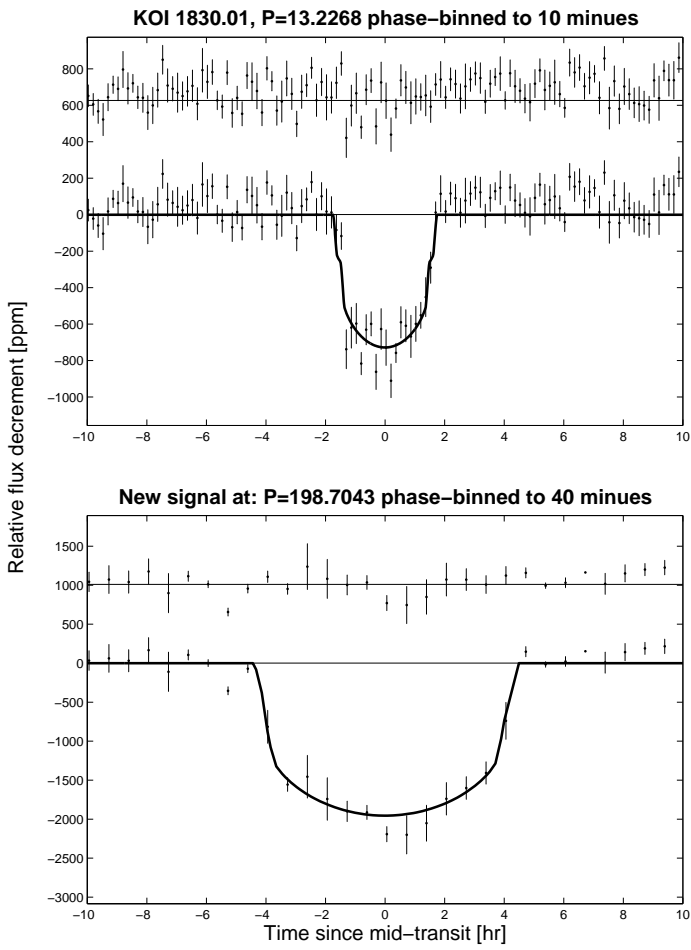


Fig. A.45. Similar to Figure 3.

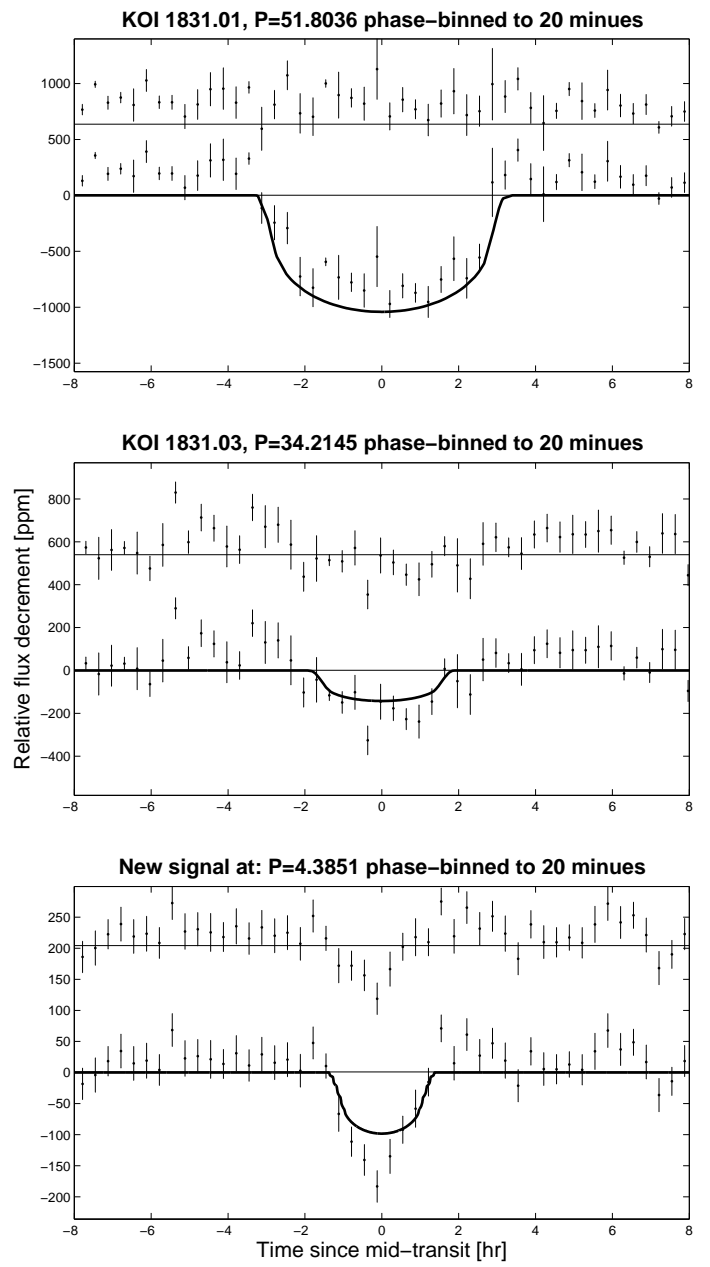


Fig. A.46. Similar to Figure 3.

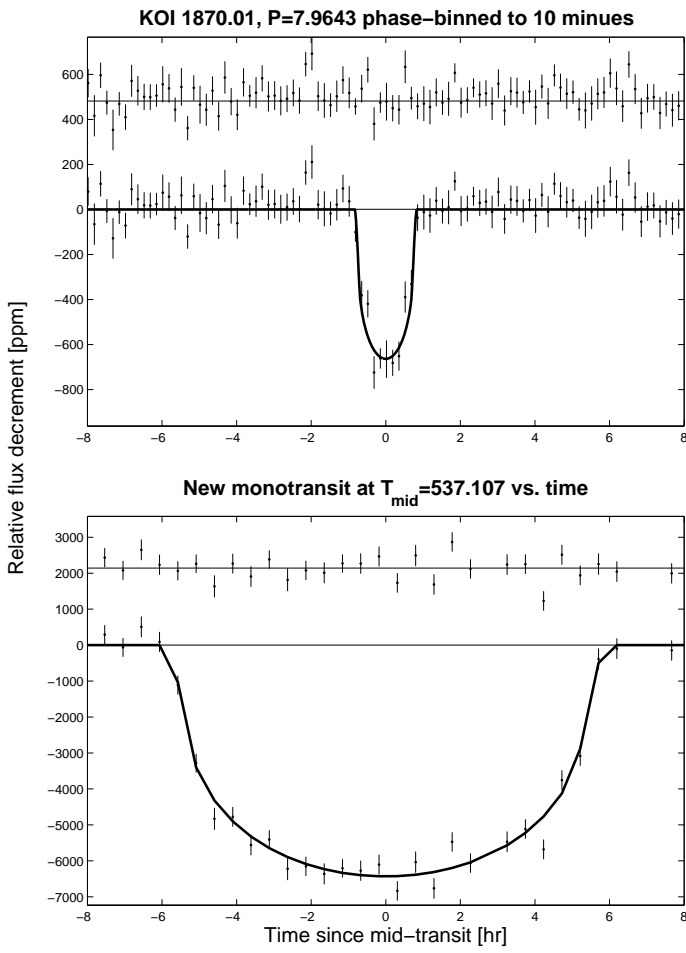


Fig. A.47. Similar to Figure 3.

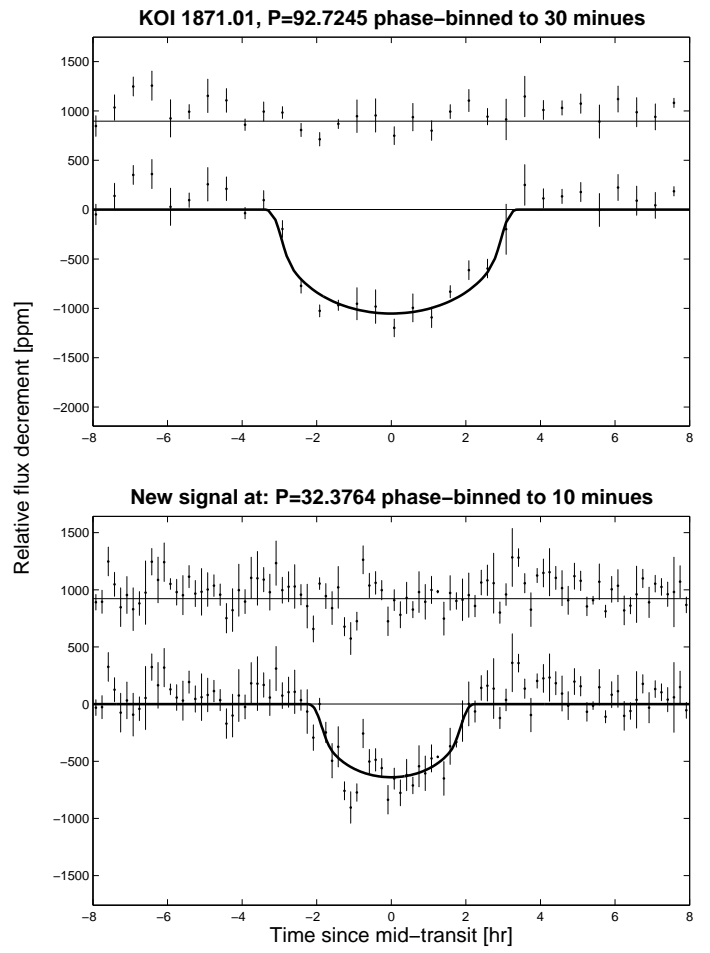


Fig. A.48. Similar to Figure 3.

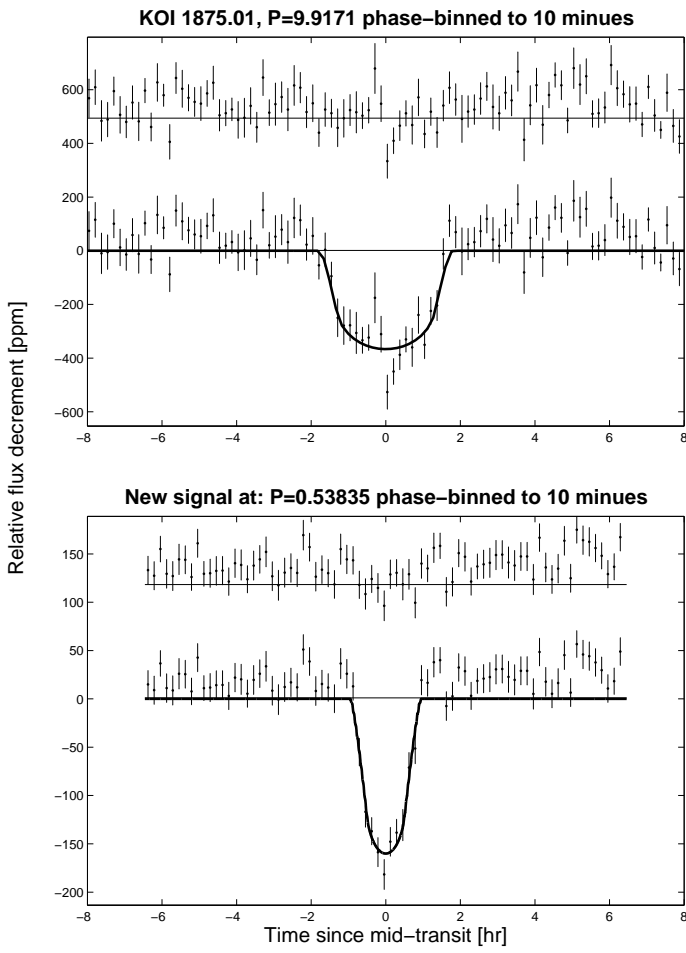


Fig. A.49. Similar to Figure 3.

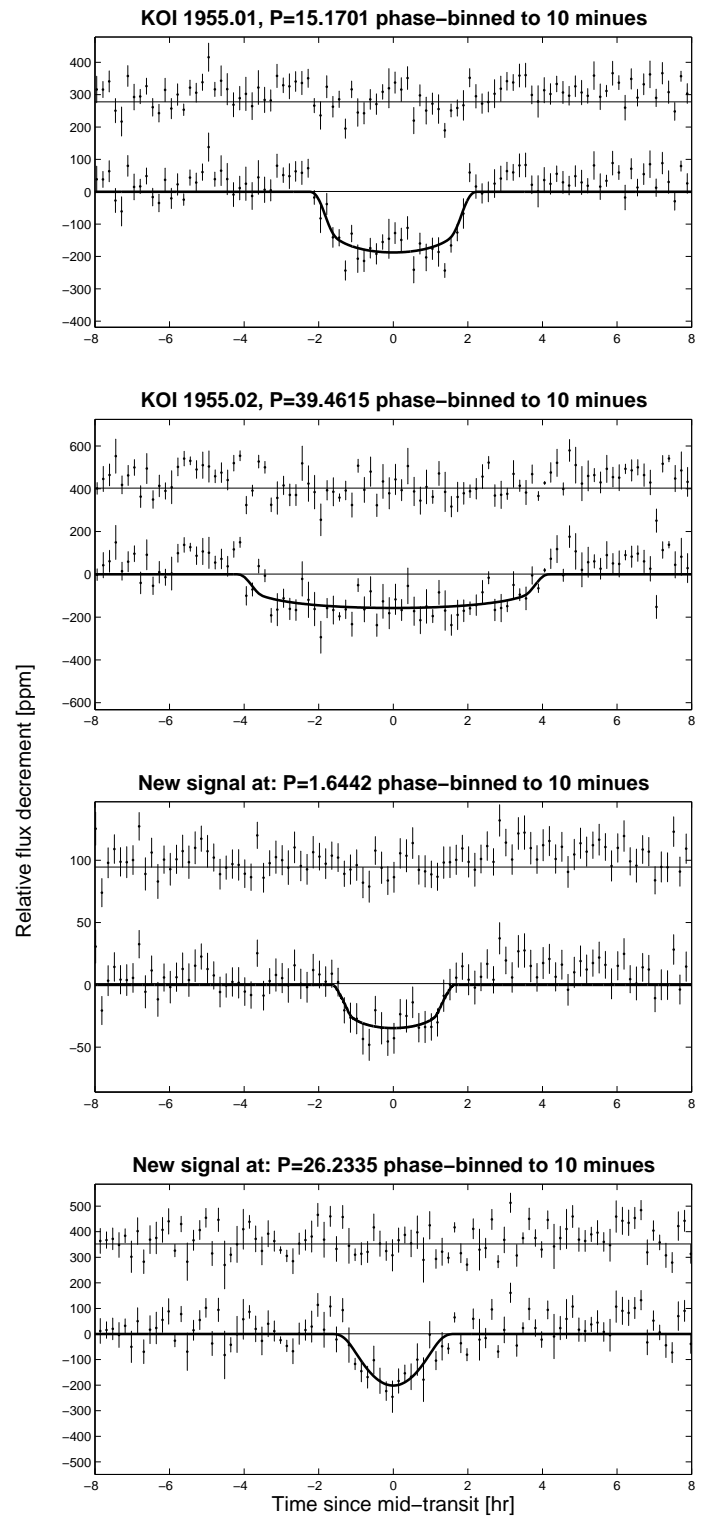


Fig. A.50. Similar to Figure 3.

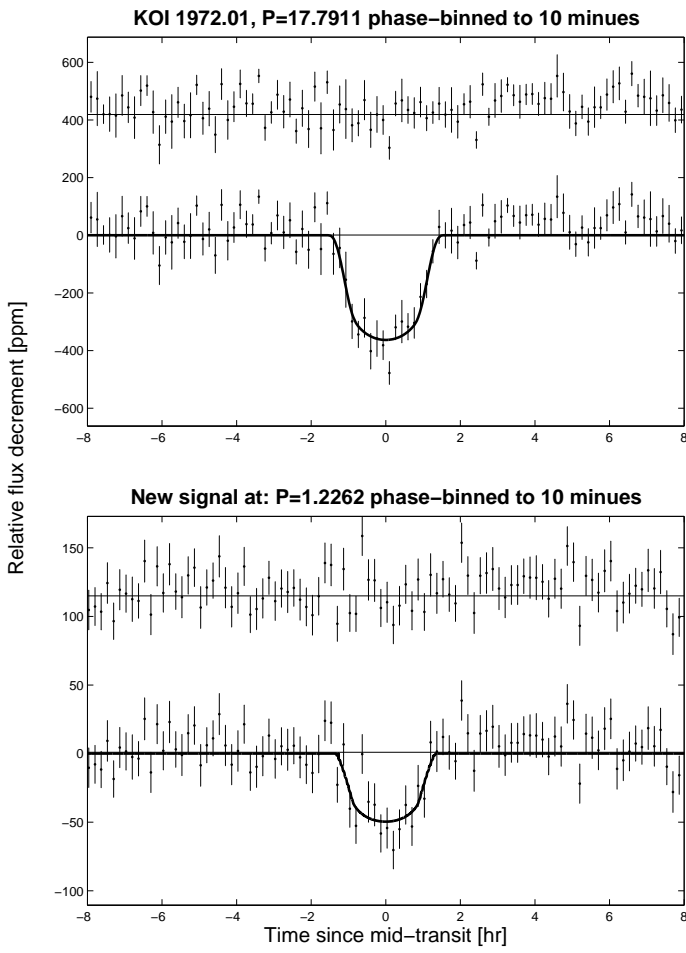


Fig. A.51. Similar to Figure 3.

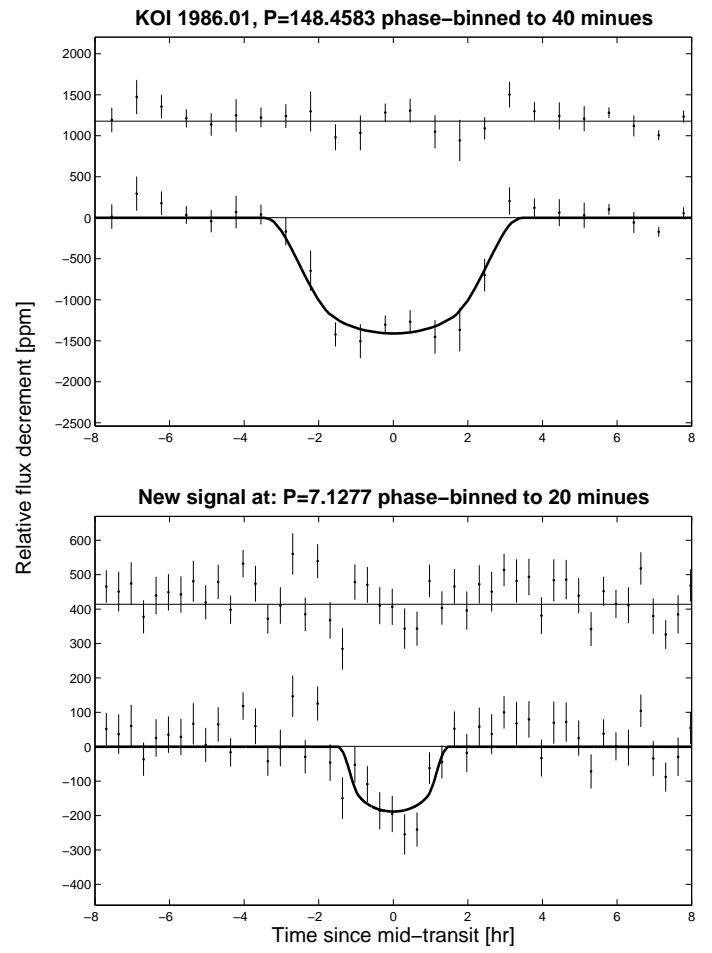


Fig. A.52. Similar to Figure 3.

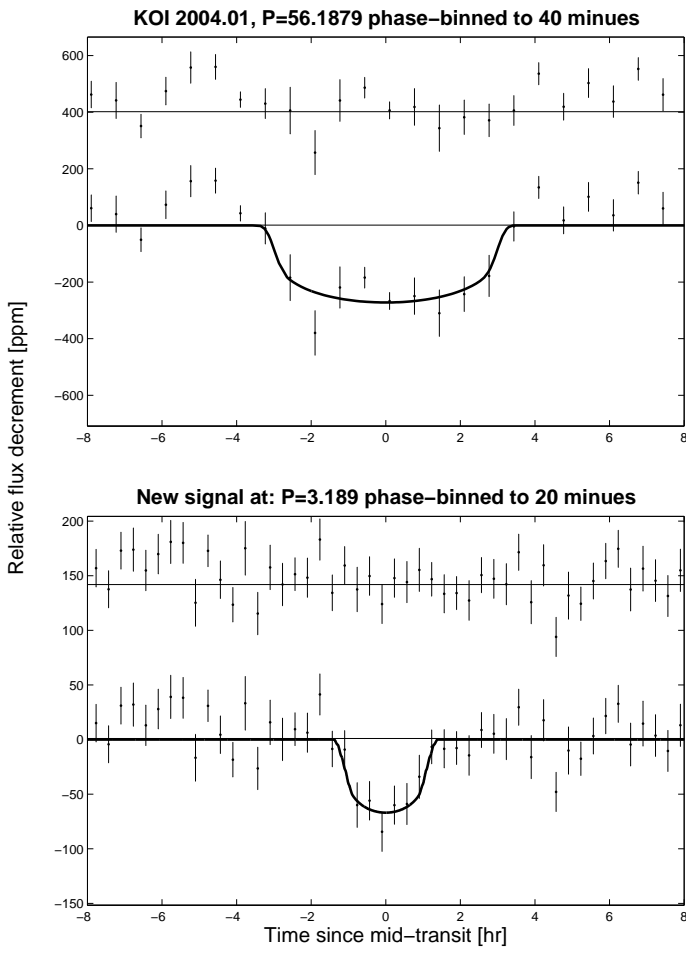


Fig. A.53. Similar to Figure 3.

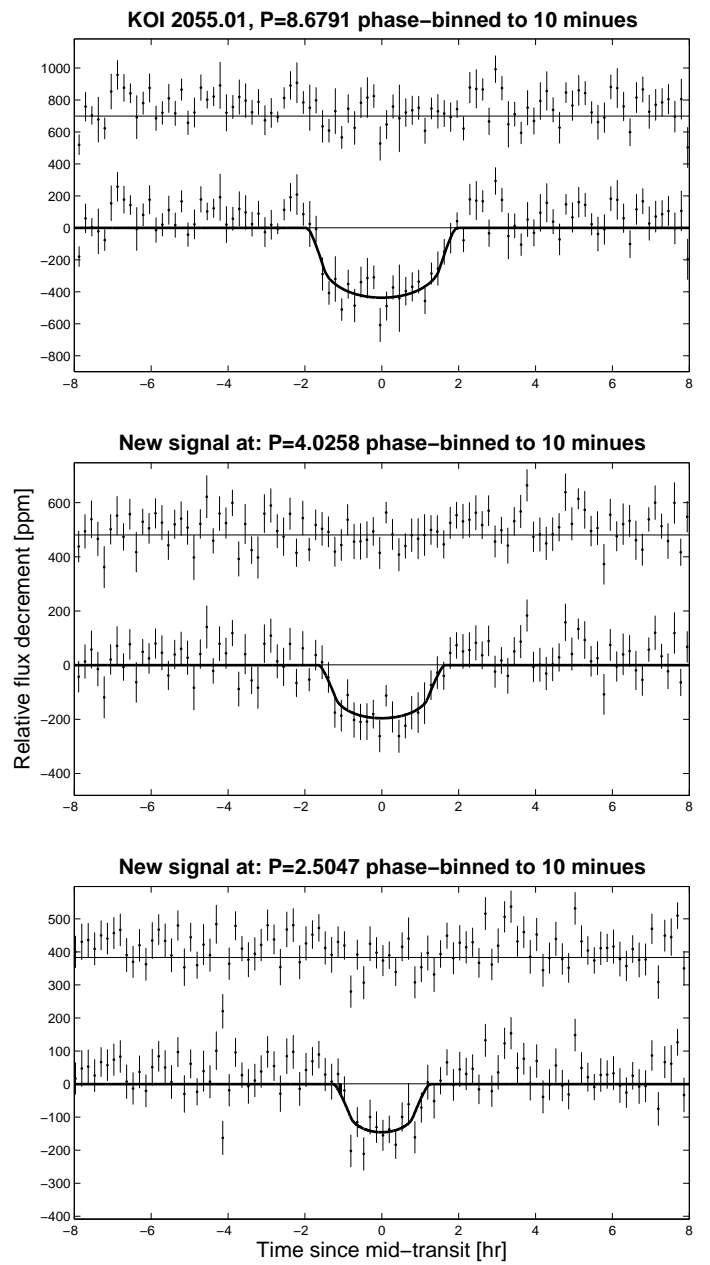


Fig. A.54. Similar to Figure 3.

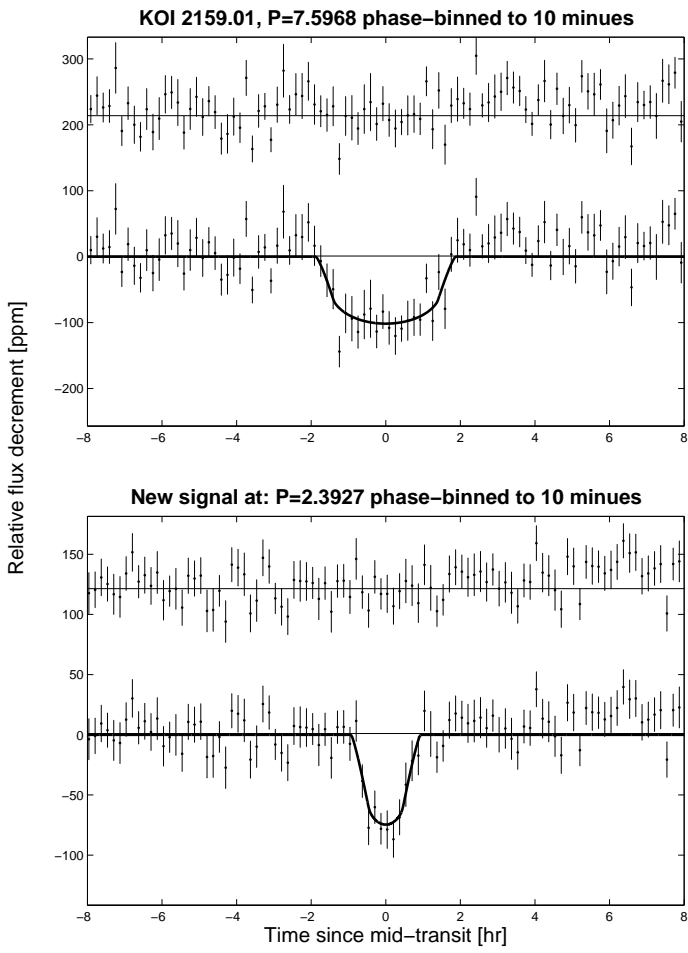


Fig. A.55. Similar to Figure 3.

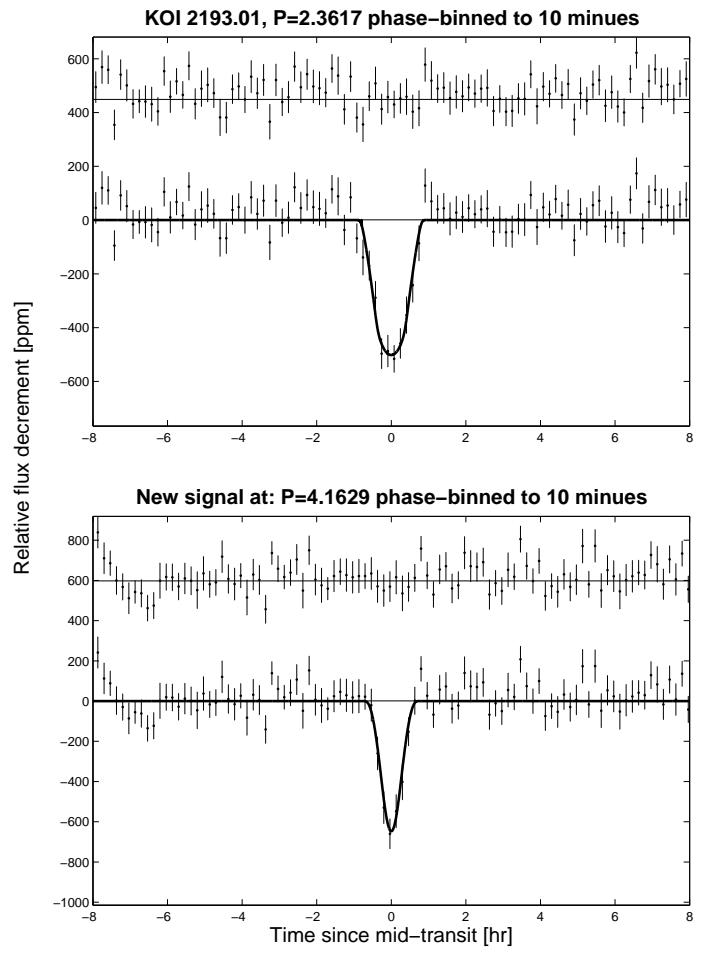


Fig. A.56. Similar to Figure 3.

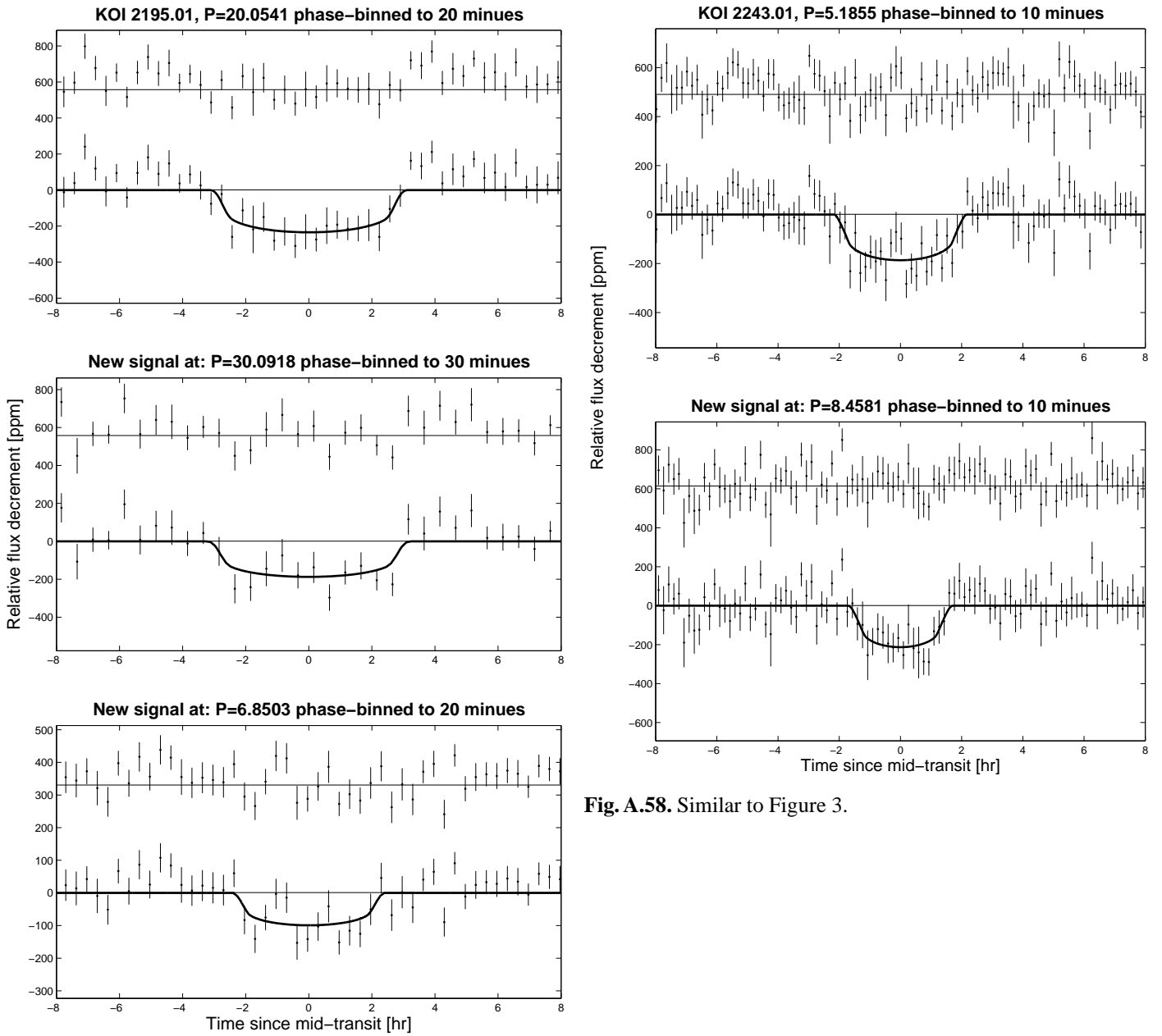


Fig. A.57. Similar to Figure 3.

Fig. A.58. Similar to Figure 3.

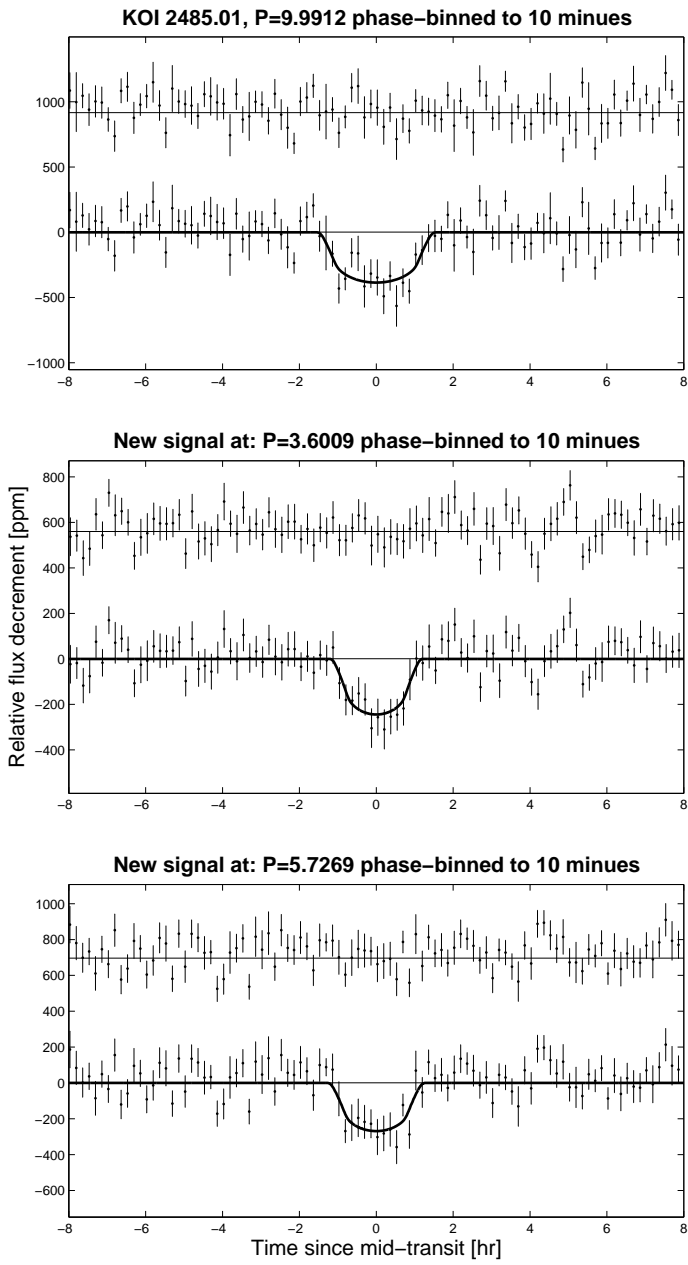


Fig. A.59. Similar to Figure 3.

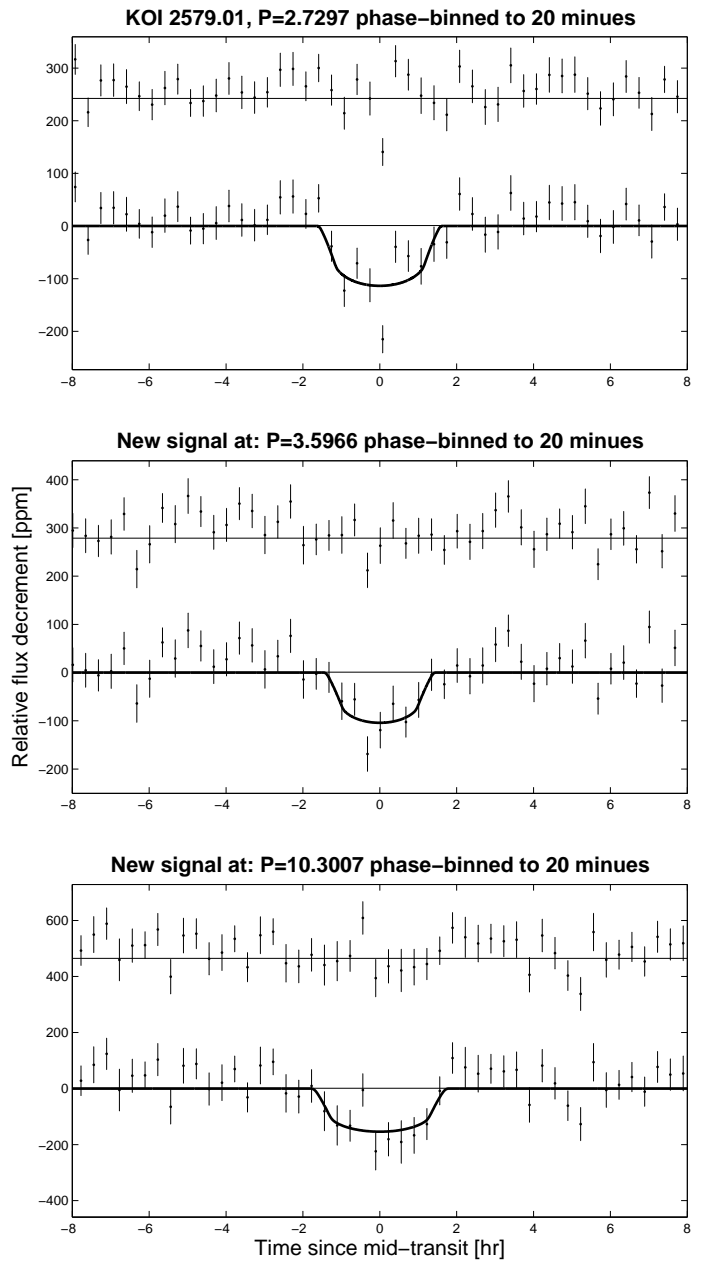
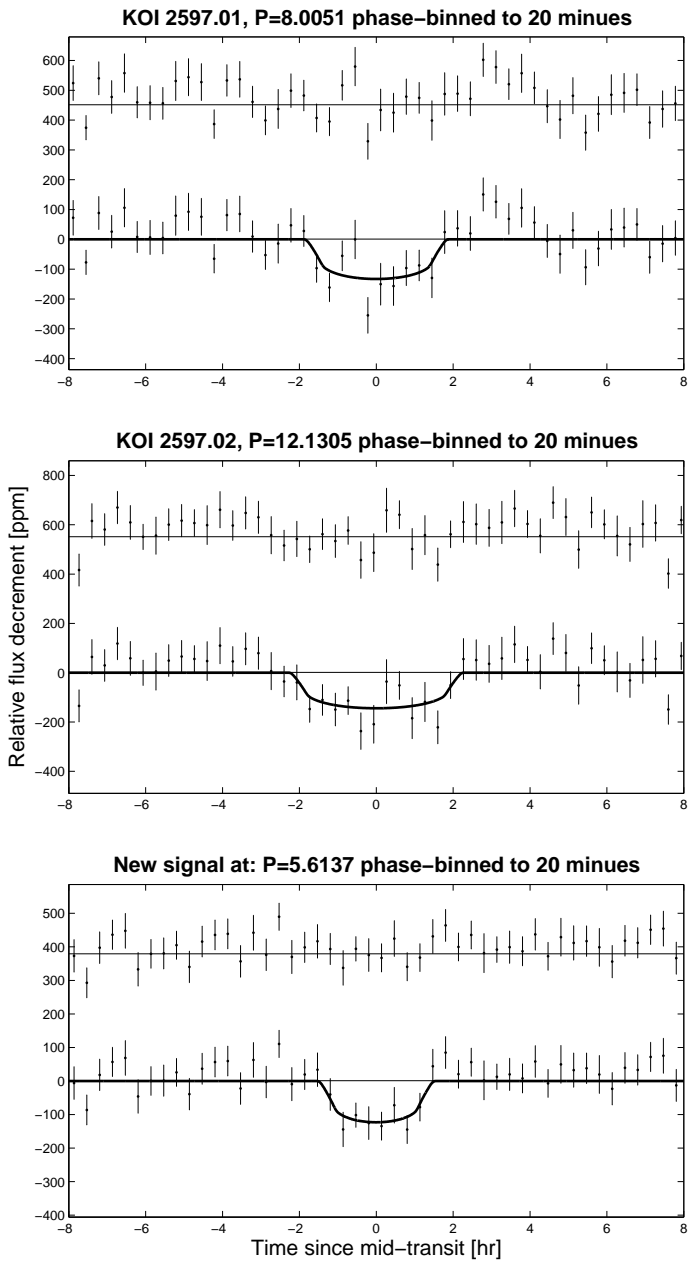
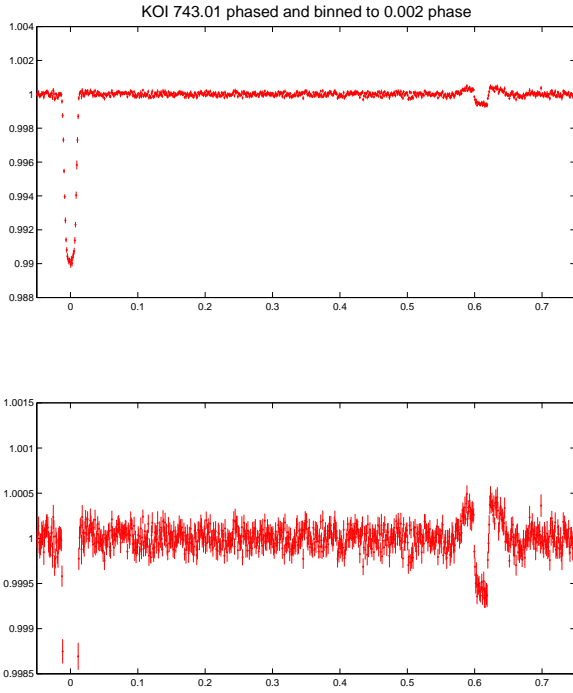


Fig. A.60. Similar to Figure 3.



**Fig. A.61.** Similar to Figure 3.



**Fig. B.1.** Phase folded and binned LC of KOI 743.01. Top: showing the 743.01 signal at phase 0. Bottom: expanded scale of the same data, showing a secondary eclipse near phase 0.61.

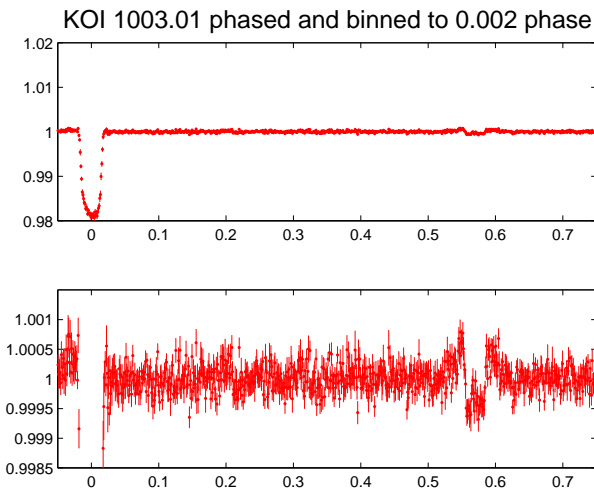


**Fig. B.2.** Phase folded and binned LC of KOI 1003.01. Top: showing the 1003.01 signal at phase 0. Bottom: expanded scale of the same data, showing a secondary eclipse near phase 0.57.

**Appendix B: Appendix B**

This appendix contain figures which have strong similarity to other appearing on the main text that are related to identification of KOIs as EBs or otherwise dicussion of KOIs with no new detections.

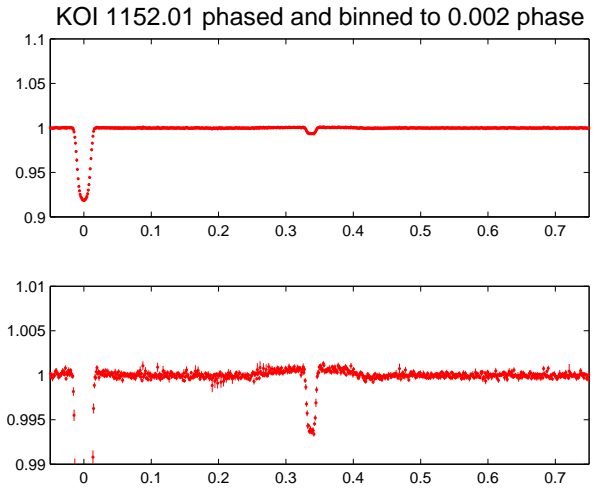


**Fig. B.3.** Phase folded and binned LC of KOI 1152.01. Top: showing the 1152.01 signal at phase 0. Bottom: expanded scale of the same data, showing a secondary eclipse near phase 0.338.

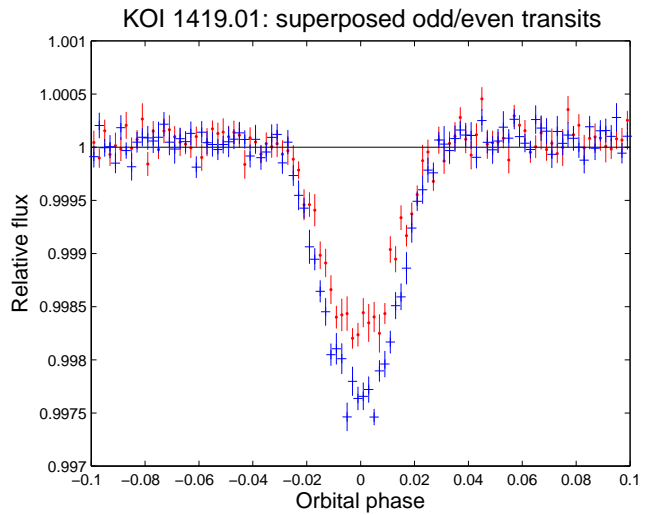


**Fig. B.4.** Similar to Figure 8.

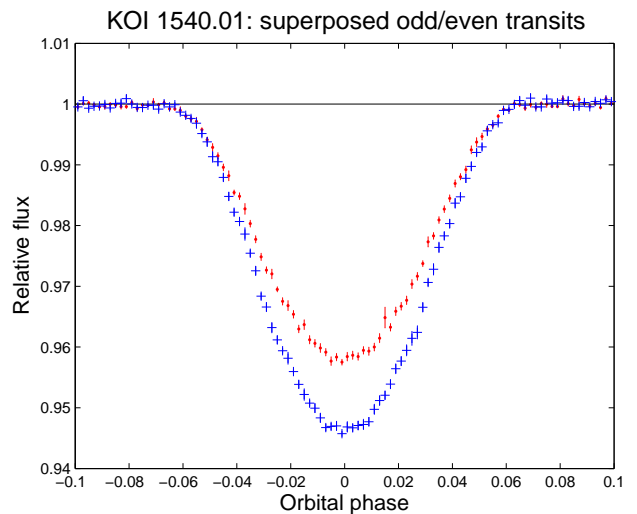


**Fig. B.5.** Similar to Figure 8

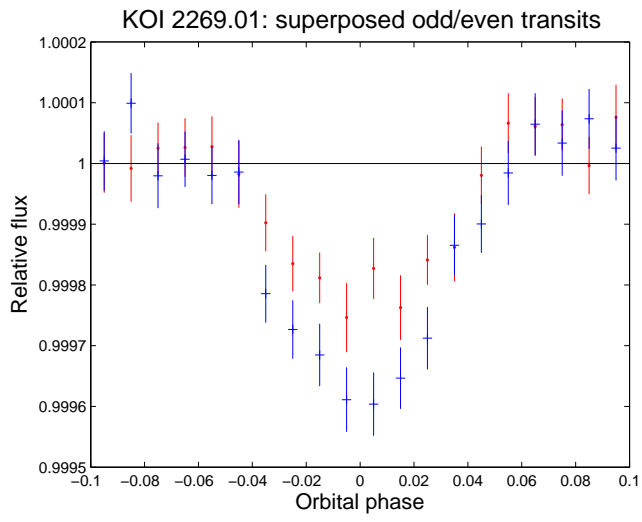


**Fig. B.6.** Similar to Figure 8, heavily binned to 0.01 phase.

KOI 1152.01 phased and binned to 0.002 phase

